

2016 BMI

Biomedical Molecular Imaging & Molecular Imaging Center Symposium

分子生醫影像國際學術研討會

時間 | 2016年11月11日至13日
地點 | 宜蘭礁溪捷絲旅 / Just Sleep Jiaoxi

Organizers



Academic Sponsors



Industry Sponsors



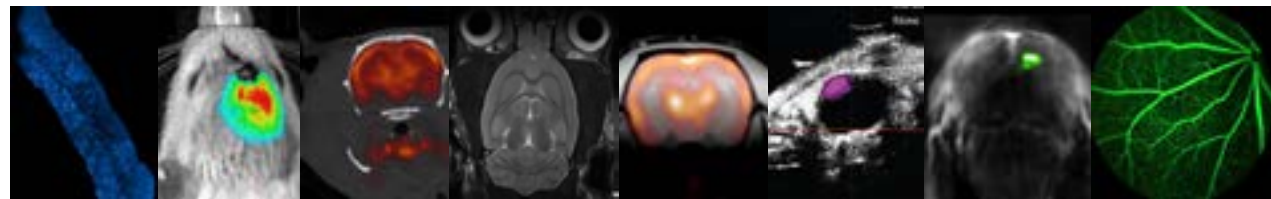
Photo Credit
Jiaosi Township Office, Taiwan
Molecular Imaging Center, NTU

多樣化臨床前造影設備 提供整體的解決方案

Optical Micro PET/CT Micro MRI Micro PET/MR Ultrasound MSOT

Probe Based Confocal Ophthalmology

從分子、代謝、功能性生理生化到全組織解剖影像，冷泉港生技提供您整體完善的分子影像解決方案。



MR SOLUTIONS 小動物磁共振複合影像的領航者

- 免液氦超導磁體技術 高場且無需建置射頻屏蔽與氣氦排放管
- Simultaneously PETMR造影 與臨床同步多模態解決方案
- Conversion Kit Gradient Insert 與臨床搭配使用解決方案

MR Solutions的多樣性磁共振造影解決方案，除傳統磁共振軟組織結構影像，並可提供功能性與細胞代謝如**血流灌注**、**水分子擴散影像**、**頻譜分析**等相關資訊。獨家提供的**3T/7T同步磁共振與正子造影**技術，大幅度提升研究與應用範圍，與臨床貼近**特別適合於轉譯醫學研究與新藥開發**。



冷泉港生物科技股份有限公司
Cold Spring Biotech Corporation

台北：(02) 2695-9990
www.csbiotech.com.tw

2016 BMI

Biomedical Molecular Imaging & Molecular Imaging Center Symposium

分子生醫影像國際學術研討會

Welcome message



Wen-Yih Isaac Tseng, MD, PhD
Director
National Taiwan University
Molecular Imaging Center



Contents

Dear Colleagues and Friends,

Welcome to the 2016 International Workshop on Holography (IWH) & Biomedical Molecular Imaging (BMI)! We are very glad to have you with us in the famous hot spring city of northeastern Taiwan, Jiaoxi, and share with us your recent progress in research.

The conference is organized jointly by the IWH and the National Taiwan University Molecular Imaging Center (NTU MIC). The aim of the conference is to create networking opportunities for exchanging research results and to stimulate new ideas. Every year, we hold the meeting in a resort area because we believe that novel ideas come from free interactions among relaxed minds.

There are 173 people attending the Conference of 2016 IWH & BMI. We have 69 keynote and invited speakers coming from China, Japan, Korea, Singapore, USA and Taiwan. The speakers are world-leading scientists in a wide spectrum of disciplines including holography, biomedical imaging, optical imaging, microscopy and spectroscopy.

I would like to thank all of you for your participation and sincerely hope that you will enjoy this three-day-event. I look forward to seeing you during the meeting to further strengthen our ties for future collaboration.

Welcome Message..... 3
Program of BMI 2016..... 7
BMI Lunch Session..... 30
Title of Abstracts for Poster Session in BMI 2016..... 51

Committee

Chair

Wen-Yih Isaac Tseng
Director, Molecular Imaging Center, National Taiwan University

Program Committee

Hiro-o Hamaguchi
Chair Professor, College of Science, National Ciao Tung University
Chi-Kuang Sun
Distinguished Professor, Department of Electrical Engineering, National Taiwan University
Jyh-Horng Chen
Professor, Department of Electrical Engineering, National Taiwan University
Chung-Ming Chen
Professor, Institute of Biomedical Engineering, National Taiwan University
Ling-Wei Hsin
Associate Professor, School of Pharmacy, National Taiwan University
Ruoh-Fang Yen
Associate Professor, College of Medicine, National Taiwan University
Hospital
Wei-Fang Su
Distinguished Professor, Department of Materials Science and Engineering, National Taiwan University
Chih-Yu Chao
Professor, Department of Physics, National Taiwan University
Pai-Chi Li
Distinguished Professor, Department of Electrical Engineering, National Taiwan University

Conference Secretary

Jiashing Yu
Associate Professor, Department of Chemical Engineering, National Taiwan University
Yuan Luo
Associate Professor, Institute of Medical Devices and Imaging, National Taiwan University

Organization Committee

Shi-Wei Chu
Professor, Department of Physics, National Taiwan University
Tzu-Ming Liu
Associate Professor, Institute of Biomedical Engineering, National Taiwan University
Hwan-Ching Tai
Assistant Professor, Department of Chemistry, National Taiwan University
Kung-Bin Sung
Professor, Department of Electrical Engineering, National Taiwan University

Academic Sponsors

Ministry of Education, Taiwan
Ministry of Science and Technology, Taiwan
Instrument Technology Research Center, NAR Labs

Industrial Sponsors

Coherent Taiwan
Cold Spring Biotech Corp.
GE Healthcare
Jasper Display Corp.
Onset Electro-Optics Co., LTD
Siemens Taiwan
SouthPort Corporation
Tayhwa Technology Co., LTD
Unice E-O Services Inc.

Organizer

National Taiwan University
Molecular Imaging Center, NTU
College of Medicine, NTU
Institute of Medical Device and Imaging, NTU
Taiwan Photonics Society

Program of BMI 2016

Fri., November 11 th , 2016			
Time	Schedule		
13:20-14:00	Opening Ceremony		
Time	Title	Speakers	Chair
14:00-14:30	Keynote Speaker I Brain Connectomics Imaging and Its Implications in Schizophrenia	TSENG, Wen-Yih Isaac National Taiwan University	YEN, Ruoh-Fang
14:30-14:50	Invited Speaker 1 A new method to capture sunaptic terminals derived from mammalian brains for super-resolution immunofluorescence imaging	TAI, Hwan-Ching National Taiwan University	
Break			
15:40-16:00	Invited Speaker 2 Machenisms of Amphetamine Action Illuminated through Optical Monitoring of Dopamine Synaptic Vesicles in Drosophila Brain	HSIN Ling-Wei National Taiwan University	YEN, Chen-Tung
16:00-16:20	Invited Speaker 3 Visualize pain fiber and terminals directly in vivo and ex vivo in self-fluorescent mice	YEN, Chen-Tung National Taiwan University	
16:20-16:40	Invited Speaker 4 Pet Radiotracers for Imaging Alzheimer's Disease	SHIUE, Chyng-Yann National Taiwan University Hospital	
16:40-17:00	Invited Speaker 5 Molecular PET Imaging in dementia	YEN, Ruoh-Fang National Taiwan University	
17:00-17:20	Invited Speaker 6 Brain FDOPA-PET imaging five years after gene therapy for aromatic L-amino acid decarboxylase deficiency	HWU, Wuh-Liang National Taiwan University	
17:20-17:40	Invited Speaker 7 Advanced Biomedical Applications of Focused-Ion-Beam	LIN, Po-Kang Taipei Veterans General Hospital	
18:00-21:00	Banquet (Invited)		
Sat., November 12 th , 2016			
Time	Title	Speakers	Chair
08:30-09:10	Keynote Speaker II Molecular Mechanism Underlying the Establishment of Neuronal Connectivity	KOLODKIN, Alex Leo Johns Hopkins University	SO, Peter
09:10-09:30	Invited Speaker 8 Electrospun Poly (benzyl glutamate)-r-Poly (glutamic acid) Scaffold for PC-12 Neurite Outgrowth	SU, Wei-Fang National Taiwan University	
09:30-09:50	Invited Speaker 9 The eyes as a window to the brain: the value of optical coherence tomography in neurodegenerative diseases	CHEN, Ta-Ching National Taiwan University Hospital	
09:50-10:10	Invited Speaker 10 Toward an ideal platform for functional brain study	CHU, Shi-Wei National Taiwan University	

Time	Title	Speakers	Chair
10:50-11:10	Invited Speaker 12 Whole embryo 3D deformation map during Zebrafish early development	BHATTACHARYA, Dipanjan Centre for Bioimaging Sciences	YAMAMOTO, Tatsuyuki
11:10-11:30	Invited Speaker 13 Nonlinear Optical Imaging of Cornea Development and Pathology: Current State and Future Development	DONG, Chen-Yuan National Taiwan University	
11:30-11:50	Invited Speaker 14 Optical imaging and focusing inside scattering biological tissues	MA, Cheng Tsinghua University, Beijing	
11:50-12:10	Invited Speaker 15 Application of Electron Microscopy for Vaccine Development of MERS-CoV Virus-like Particles	CHANG, Ming-Fu National Taiwan University	
Lunch Session & Break			
13:20-13:50	Keynote Speaker III Detection of Eosinophils for the Development of a New Raman Diagnostic Technique for Eosinophilic Esophagitis	YAMAMOTO, Tatsuyuki Shimane University	LIU, Tzu-Ming
13:50-14:10	Invited Speaker 16 Human microcephaly proteins: Roles in centriole duplication, neural stem cell division, and neurodevelopmental disorders	TANG, Tang Academia Sinica	
14:10-14:30	Invited Speaker 17 Copper-Based Nanoparticles and the Application to Photothermal Therapy	YU, Jiashing National Taiwan University	
14:30-14:50	Invited Speaker 18 Introduction to Electrical Stimulation for Tissue Engineering	LUO, Shyh-Chyang National Taiwan University	
Poster Session & Break			
15:40-16:00	Invited Speaker 19 An Infrared System for Detection of Breast Cancer Based on Single Visit	CHEN, Chung-Ming National Taiwan University	CHANG, Ming-Fu
16:00-16:20	Invited Speaker 20 Imaging Macrophages in vivo with Hemoglobin Fluorescence	LIU, Tzu-Ming National Taiwan University University of Macau	
16:20-16:40	Invited Speaker 21 Hyperspectral Imaging in Thick Tissues via Optical Sectioning Microscopy	CHEN, Szu-Yu National Central University	
16:40-17:00	Invited Speaker 22 Electric Cell-substrate Impedance Sensing for Real Time Investigation of Epithelial-Mesenchymal Interactions	CHEN, Min-Huey National Taiwan University	
17:00-17:20	Invited Speaker 23 Quantitative Susceptibility Mapping and its applications	CHEN, Jyh-Horng National Taiwan University	
Dinner			
Sun., November 13 th , 2016			
Time	Title	Speakers	Chair
08:30-09:30	Oral Presentations for Best Paper Award Competition		SU, Wei-Fang LUO, Shyh-Chyang
Break			
09:50-10:30	Keynote Speaker IV The Application of Quantitative Interferometric Imaging in Sickle Cell Disease	SO, Peter Mechanical Engineering and Biological Engineering	TSENG, Wen-Yih Isaac
10:30-11:50	IWH & BMI Academic Exchange		
11:50-12:10	Closing Ceremony		
Departure (Shuttle Service from JiaoXi JustSleep Hotel to Taipei NTU Campus)			

Brain Connectomics Imaging and Its Implications in Schizophrenia

Wen-Yih Isaac Tseng, MD, PhD

¹*Molecular Imaging Center, National Taiwan University, Taipei, Taiwan*

1. Summary

Schizophrenia is a debilitating mental disorder of which the biological underpinning is still unclear. Increasing evidence in neuroscience has indicated that schizophrenia arises from abnormal connections within or between networks, hence called dysconnectivity syndrome. Recently, we established an automatic method to analyze integrity of the white matter tracts over the whole brain based on diffusion MRI data, named tract-based automatic analysis (TBAA), and used this method to study white matter connection in patients with schizophrenia. We found that alteration of tract integrity is hereditary and inherent; it is found in siblings and in patients in the early phase of disease. Moreover, patients with good treatment outcome and those with poor outcome show distinctly different patterns of alterations, suggesting that these two groups of patients might be distinguishable based on the difference in tract alteration. In summary, the altered tracts revealed by TBAA might become potential biomarkers or trait markers for schizophrenia.

2. Introduction

Brain is a giant network composed of billions of axons and trillions of synapses acting as basic units of connection. It is believed that consciousness and cognitive functions arise from signal conduction between neurons via this network, and that comprehensive description of brain connections, called connectomics, is the key to understanding how brain works. In the past ten years, connectomics imaging has been an area of intense research, ranging from microscopic (synapse imaging), mesoscopic (cell imaging) to macroscopic (in vivo neuroimaging) levels. Recent advance in neuroscience also emphasizes the neural network (or circuitry) as the target of cognitive function, and ascribes many mental disorders to abnormal connections within or between the networks, hence called dysconnectivity syndrome. Recently, we established an automatic method to analyze integrity of the white matter tracts over the whole brain based on diffusion MRI data, named tract-based automatic analysis (TBAA)[1]. The output of the method is a standardized 2D array of tract integrity for each person, and so it can be considered as personalized connectomics. Using this automatic method, we are able to analyze a large amount of image data efficiently and investigate relevant hypotheses about schizophrenia as follow. First, tract alteration presents hereditary trait of schizophrenia. Second, tract alteration exists early in the course of disease. Third, different patterns of tract alteration can predict different treatment outcomes. In this talk, I will introduce TBAA and show how we perform TBAA to investigate three hypotheses listed above.

3. Methods

Participants were recruited under the approval of the ethics committee of the National Taiwan University Hospital. Patients with schizophrenia were diagnosed by psychiatrists according to

Diagnostic and Statistical Manual of Mental Disorders, Fourth Edition (DSM IV) for schizophrenia. Healthy control subjects were assessed by Diagnostic Interview for Genetic Studies (DIGS) to rule out major mood and psychotic disorders. All participants received MRI scans of the head on a 3-Tesla magnetic resonance imaging (MRI) system. The MRI pulse sequences included T1-weighted and T2-weighted images for brain structures, and diffusion spectrum imaging (DSI) for white matter microstructures. MRI data processing involves creation of a study-specific template by registering all the image data, followed by registering the study-specific template to a DSI template (NTU-DSI-122)[2]. TBAA was performed by transforming the coordinates of 76 major tract bundles which were predefined in the template to individual's native space in DSI. The standardized 2D array of tract integrity was obtained for each person by sampling the tract integrity index (called generalized fractional anisotropy, GFA) along each tract bundle. ANCOVA was used for the comparison of the tract integrity among patients with schizophrenia, siblings and healthy controls (hypothesis 1), among first episode patients, chronic patients and healthy controls (hypothesis 2), and among patients with good treatment outcome (remission), patients with poor treatment outcome (non-remission) and healthy controls (hypothesis 3).

4. Results and Discussion

For hypothesis 1, 10 tracts were found to exhibit significant differences between the groups with a linear, stepwise order from controls to siblings to patients. Posthoc between group analyses revealed that the GFA of the right arcuate fasciculus was significantly decreased in both the patients and unaffected siblings compared to the controls (Fig. 1). The GFA of the right arcuate fasciculus exhibited a trend toward positive symptom scores [3]. Our findings suggest that the right arcuate fasciculus may be a candidate trait marker and deserves further study to verify any genetic association. For hypothesis 2, 7 tracts were found to exhibit significant difference between the groups. Post-hoc between-group analyses revealed that the connection of the callosal fibers to the bilateral DLPFC was significantly decreased in chronic patients but not in first-episode patients. In a stepwise regression analysis, the decline of the tract connection was significantly predicted by the duration of illness. In contrast, the remaining six tracts showed significant alterations in both first-episode and chronic patients and did not associate with clinical variables [4]. Our findings suggest that reduced white matter connectivity of the callosal fibers to the bilateral DLPFC may be a secondary change that degrades progressively in the chronic stage, whereas alterations in the other six tracts may be inherent in the disease. For hypothesis 3, patients with non-remission showed significantly decreased tract integrity in the bilateral uncinata fasciculi, bilateral fornices, and callosal fibers to bilateral hippocampal poles, as compared with patients with remission and healthy controls. Our findings suggest that remitted and non-remitted patients might present two different groups of patients who showed distinctly different patterns of tract alteration. In summary, alterations of tract integrity in specific tracts imply the heredity of the microstructural abnormality, and implicate potential biomarkers for treatment outcome.

Reference:

- [1] Y.J. Chen et al., *Human Brain Mapping*, 36(9):3441-58, 2015.
- [2] Y.C. Hsu et al., *Human Brain Mapping*, 36(9):3528-41, 2015.
- [3] C.H. Wu et al., *Human Brain Mapping*, 36(3):1065-76, 2015.
- [4] C.H. Wu et al., *Schizophrenia Research*, 169(1-3):54-61, 2015.

Invited Speaker 1

A new method to capture synaptic terminals derived from mammalian brains for super-resolution immunofluorescence imaging

Hwan-Ching Tai¹, Jia-Feng Jhou¹, Fan-Ching Chien²

¹ *Department of Chemistry, National Taiwan University, Taipei, Taiwan*

² *Department of Optics and Photonics, National Central University, Taoyuan, Taiwan*

The study of neurological disorders, such as Alzheimer's disease, depression, and autism, has become one of the most important areas in current biomedical research. The synapse, which is associated with neurotransmission, signal transduction, network plasticity, as well as learning and memory, has always been the central focus in brain function investigations, neuropathological studies, and neuropharmacological development. Although various isolation strategies of synaptic terminals from brain tissues, called synaptosomes, have been developed over the decades, there still lack suitable sample preparation techniques for imaging studies of synaptosomes. We therefore devised a simple and facile method for the efficient capture of brain synaptosomes over coverglasses, which greatly reduced aggregation artifacts and improved immobilization efficiency compared to conventional methods based on formaldehyde crosslinking. We discovered a chemical fixative that ensured proper dispersion and devised a capturing strategy based on electrostatic interaction.

Synaptosomes captured by our method were well suited for super-resolution imaging studies including direct stochastic optical reconstruction microscopy (dSTORM), which allowed us to visualize tau protein and synaptic markers at ~30 nm resolution. In contrast, the diffraction-limited resolution of conventional optical microscopy at ~200 nm was inadequate for resolving the spatial distribution of proteins within synaptic terminals, which were ~500 nm in diameter. This technique will be applied to the study of tau pathology within cortical synapses of Alzheimer's disease model mice and postmortem patient tissues.

Invited Speaker 2

Mechanisms of Amphetamine Action Illuminated through Optical Monitoring of Dopamine Synaptic Vesicles in Drosophila Brain

Z. Freyberg^{1,2}, M. S. Sonders^{1,2,3}, J. I. Aguilar^{1,2}, T. Hiranita⁴, C. S. Karam^{1,2}, J. Flores⁵, A. B. Pizzo^{1,2}, Y. Zhang^{1,2}, Z. J. Farino^{1,2}, A. Chen⁶, C. A. Martin⁷, T. A. Kopajtic⁴, H. Fei⁶, G. Hu⁸, Y.-Y. Lin⁹, E. V. Mosharov³, B. D. McCabe^{10,11,12}, R. Freyberg¹³, K. Wimalasena¹⁴, L.-W. Hsin⁹, D. Sames⁸, D. E. Krantz⁶, J. L. Katz⁴, D. Sulzer^{1,2,3,15} and J. A. Javitch^{1,2,15}

¹ *Department of Psychiatry, College of Physicians & Surgeons, Columbia University.*

² *Division of Molecular Therapeutics, New York State Psychiatric Institute.*

³ *Department of Neurology, College of Physicians & Surgeons, Columbia University.*

⁴ *Psychobiology Section, IRP, DHHS, NIDA, NIH.*

⁵ *Department of Biochemistry and Molecular Biophysics, Howard Hughes Medical Institute, College of Physicians & Surgeons, Columbia University.*

⁶ *Department of Psychiatry and Biobehavioral Sciences and Semel Institute for Neuroscience and Human Behavior, Hatos Center for Neuropharmacology, David Geffen School of Medicine UCLA.*

⁷ *UCLA Interdepartmental Program in Molecular Toxicology, UCLA.*

⁸ *Department of Chemistry, Columbia University.*

⁹ *Molecular Imaging Center, National Taiwan University.*

¹⁰ *Center for Motor Neuron Biology and Disease, College of Physicians & Surgeons, Columbia University.*

¹¹ *Department of Pathology and Cell Biology, College of Physicians & Surgeons, Columbia University.*

¹² *Department of Neuroscience, College of Physicians & Surgeons, Columbia University.*

¹³ *Department of Psychology, Stern College for Women, Yeshiva University.*

¹⁴ *Department of Chemistry, Wichita State University.*

¹⁵ *Department of Pharmacology, College of Physicians & Surgeons, Columbia University.*

Amphetamines elevate extracellular dopamine, but the underlying mechanisms remain uncertain. Here we show in rodents that acute pharmacological inhibition of the vesicular monoamine transporter (VMAT) blocks amphetamine-induced locomotion and self-administration without impacting cocaine-induced behaviours. To study VMAT's role in mediating amphetamine action in dopamine neurons, we have used novel genetic, pharmacological and optical approaches in *Drosophila melanogaster*. In an ex vivo whole-brain preparation, fluorescent reporters of vesicular cargo and of vesicular pH reveal that amphetamine redistributes vesicle contents and diminishes the vesicle pH-gradient responsible for dopamine uptake and retention. This amphetamine-induced deacidification requires VMAT function and results from net H⁺ antiport by VMAT out of the vesicle lumen coupled to inward amphetamine transport. Amphetamine-induced vesicle deacidification also requires functional dopamine transporter (DAT) at the plasma membrane. Thus, we find that at pharmacologically relevant concentrations, amphetamines must be actively transported by DAT and VMAT in tandem to produce psychostimulant effects.

Reference:

[1] *Nature Communications*, 2016, 7, 10652.

Invited Speaker 3

Visualize pain fiber and terminals directly in vivo and ex vivo in self-fluorescent mice

Chen-Tung Yen¹, Jye-Chang Lee¹ and Chi-Kuang Sun²

¹Department of Life Science, National Taiwan University

²Graduate Institute of Photonics and Optoelectronics, National Taiwan University, Taiwan

Skin is the largest sensory organ in our body. There are numerous sensory endings in the skin that report to our somatosensory nervous system. Nociceptors (pain fibers) are the sensory fibers sensing noxious mechanical, thermal, and chemical stimuli. In normal subject, nociceptor activation produces painful sensation which helps us avoiding further injury and serves an important adaptive function. On the other hand, under disease conditions, patients suffer from chronic intractable spontaneous pain and evoked pains. Sensitization of the peripheral nociceptors may underlie many neuropathic pain conditions. In this talk, I will present our preliminary results on the use of two-photon microscopic methodologies to longitudinally following changes of nociceptor fibers and terminals under the skin of transgenic mice that express fluorescent reporters. The quantitatively measured results were compared with ex vivo imaging of the same fibers in situ in CLARITY cleared transparent tissue. We are utilizing harmonic microscopic methodologies to examine the same tissue of the mice. This may help us to see nerve fibers and endings in human subjects.

Invited Speaker 4

PET RADIOTRACERS FOR IMAGING ALZHEIMER'S DISEASE

Chyng-Yann Shiue¹⁻⁴

¹PET Center, Department of Nuclear Medicine, National Taiwan University Hospital, Taipei, 10002, Taiwan

²Molecular Imaging Center, National Taiwan University, Taipei, 10617, Taiwan

³PET Center, Department of Nuclear Medicine, Tri-service General Hospital, Taipei, 11490, Taiwan

⁴Institute of Nuclear Energy Research, Taoyuan, Taiwan

Alzheimer's disease (AD) is one of the most frequent causes of death and disability worldwide and has a significant clinical and socio-economic impact. It is the most common form of dementia in the elderly and in individuals over 65 y and accounts for 50-60% of cases of dementia. Dementia with Lewy bodies (DLB) and frontotemporal dementia (FTD) account for approximately 15%-25% of cases. Alzheimer's disease (AD) is characterized by the degeneration of neurons in the hippocampus and cortex, and the appearance of neuritic plaques and neurofibrillary tangles 1-3. Although the precise cause of AD remains unclear, it is most likely due to multiple etiologies such as neuronal apoptosis, inflammatory responses, and alterations in various receptors and enzymes. Over the past several years, a consensus has emerged that a cocktail of drugs influencing multiple mechanisms may be required to effectively treat AD. Thus, PET imaging agents that target multiple mechanisms such as β - amyloids, tau proteins and various receptors and enzymes will be useful for monitoring the response of AD drug therapy non-invasively and facilitating AD drugs development.

Over the past forty years, several PET tracers have been developed for AD imaging ranging from [18F]FDG, various neurotransmitters radioligands to β -amyloids plaque, tau proteins and histone deacetylases (HDACs) inhibitors 4,5.

In this presentation, I will focus on the status of PET radiotracers development for AD imaging which include [11C]PiB 6, [18F]T-8077, [18F]FEPP8 and [18F]Fluoroethyl-INNER15779 at the PET Center of National Taiwan University Hospital and Institute of Nuclear Energy Research.

Reference:

- [1] Goedert, M; Spillantini, M. G. A century of Alzheimer's disease. *Science* 314, 777-781 (2006).
- [2] Roberson, E. D; Mucke, L. 100 years and counting: prospects for defeating Alzheimer's disease. *Science* 314, 781-784 (2006).
- [3] Huang, Y. & Mucke, L. Alzheimer Mechanisms and Therapeutic Strategies. *Cell* 148, 1204-1222 (2012).
- [4] Näggen, K; Halldin, C; Rinne, JO. Radiopharmaceuticals for positron emission tomography investigations of Alzheimer's disease. *Eur J Nucl Med Mol Imaging* 37(8):1575-93 (2010).
- [5] Vallabhajosula, S. Positron emission tomography radiopharmaceuticals for imaging brain Beta-amyloid. *Semin Nucl Med.* 41:283 (2011).
- [6] Tzen, K-Y; Yang, S-Y; Chen, T-F; Cheng, T-W; Horng, H-E; Wen, H-P; Huang, Y-Y; Shiue, C-Y; Chiu, M-J. Plasma A β but not tau related to brain PiB retention in early Alzheimer's disease. *ACS Chemical Neuroscience.* 5(9):830-6 (2014).
- [7] Huang, Y-Y; Tsai, C-L; Chou, T-K; Hsieh, H-Y; Hsin, L-W; Cheng, C-Y; Tzen, K-Y; Shiue, C-Y. An Improved Radiosynthesis of [18F]T807 and Its Biodistribution in Mice and Monkeys, SNMMI 2015 Annual Meeting, Baltimore, MD, USA. #2204221.
- [8] Huang, Y-Y; Huang, W-S; Wu, H; Kuo, Y; Chang, Y; Lin, P; Wu, C; Yen, R; Shiue, C-Y. Automated Production of [18F] FEPPA as a Neuroinflammation Imaging Agent. SNMMI 2016 Annual Meeting, San Diego, Calif, USA. #1036.
- [9] Li, M; Shiue, C-Y., Chang, H; Chu, H. Synthesis of [18F]Fluoroethyl-INNER1577 as Histone Deacetylase (HDACs) Imaging Agent. SNMMI 2016 Annual Meeting, San Diego, Calif, USA. #2664.

Invited Speaker 5

Molecular PET Imaging in dementia

Ruoh-Fang Yen

Department of Nuclear Medicine, National Taiwan University Hospital, Taipei, Taiwan

Department of Radiology, National Taiwan University College of Medicine, Taipei, Taiwan

Abstract

Dementia has been a growing health problem worldwide. An estimated 46.8 million people worldwide living with dementia in 2015. In Taiwan, a nationwide survey showed population aged 65 years and above, the age adjusted prevalence of mild cognitive impairment (MCI) was 18.76% (95% CI 17.91-19.61) (MCI), and prevalence of all-cause dementia was 8.14% (95% CI 7.47-8.61), including a 3.25% prevalence of very mild dementia (VMD). The total estimated worldwide cost of dementia is US\$818 billion in 2015, which represents 1.09% of global GDP. The annual costs exceed the market values of companies such as Apple (US \$742 billion) and Google (US \$368 billion).

The diagnoses of dementia rely on clinical examinations including various neuropsychological tests. Recently, brain imaging has been playing a more and more important role. CT and MRI provide detail structure changes of brain, which can exclude treatable causes of dementia, such as tumor or hydrocephalus.

By using specific targeting radiotracers and imaging with PET, molecular imaging provide information of brain biochemistry, including, metabolic, neurotransmitters, enzymes, transporters, receptors, abnormal intracellular or extracellular proteins, etc. It has become surrogate biomarker of dementia and provides information about pathophysiological process of dementia.

¹⁸F-FDG, a glucose analog, can demonstrate patterns of glucose hypometabolism observed in different type of dementia. Dopaminergic neuronal imaging is helpful in the investigation of the pathogenesis and pathophysiologic process of Parkinson's disease. Since 2003, Amyloid PET imaging has been used to image the amyloid distribution in the brain, and has become mainstay of drug trials that intend to treat the disease by eliminating the plaques. In addition, tau, another key protein of Alzheimer's dementia (AD), imaging has been developed and is opening up new possibilities for research into the pathogenesis of AD.

Invited Speaker 6

Brain FDOPA-PET imaging five years after gene therapy for aromatic L-amino acid decarboxylase deficiency

Wuh-Liang Hwu

Department of Pediatrics and Medical Genetics, National Taiwan University Hospital

Aromatic L-amino acid decarboxylase (AADC) is an enzyme responsible for the final step of the synthesis of neurotransmitters dopamine and serotonin. AADC deficiency is a rare genetic disorder causing motor and autonomic dysfunction and early death in children. We conducted a human gene therapy trial with local injection of recombinant adeno-associated virus (AAV) serotype 2 CMV promoter-driven human AADC (AAV2-hAADC) in 18 children with AADC deficiency since 2010. FDOPA-PET signal intensity over putamen increased and cerebrospinal fluid neurotransmitter levels rose in all treated patients currently completed the trial, and all treated patients improved in their motor function. The first few patients have been 5 years after gene therapy, and their clinical benefits from the gene therapy were maintained. In four patients who has conducted a fifth-year PET study, positive signals over bilateral putamen can still be visualized.

Reference:

[1] Hwu WL, Muramatsu S, Tseng SH, Tzen KY, Lee NC, Chien YH, Snyder RO, Byrne BJ, Tai CH, Wu RM. Gene therapy for aromatic L-amino acid decarboxylase deficiency. *Sci Transl Med.* 2012 May 16;4(134):134ra61.

Advanced Biomedical Applications of Focused-Ion-Beam

Po-Kang Lin^{1,2}, Meng-Jiun Sui², Chieh-Hsiung Kuan¹

¹ Graduate Institute of Biomedical Electronics and Bioinformatics, National Taiwan University;

Room 410 Bo-Li building, No 1 Sec 4 Roosevelt Rd., Taipei, Taiwan

² School of Medicine, National Yang Ming University / Department of Ophthalmology, Taipei

Veterans General Hospital, No 201 Sec 2 Shih-Pai Rd., Taipei, Taiwan

1. Purpose

Focused-Ion-Beam (FIB) is a powerful tool and has been widely used in semiconductor research and industry. It mills semiconductor substance with focused ion and views the cross section with a co-installed scanning electron microscope. It bears potential to be a powerful tool in biomedical study, though seldom reported. This study is to develop biological applications of FIB.

2. Methods

In the past researches, we had established special technology to apply FIB on botanical cells study. We had endeavored to simplify the instruments and procedures of FIB to make it a useful tool. Efforts were made to decrease the noises. In the succeeding researches, we further extended the technology on animal cells study. We further advanced it on tissues study. Even more advanced, we established FIB immuno-electron microscopy (IEM) through employing quantum dots.

3. Results

Biological samples could be milled and viewed by FIB. Intracellular ultrastructure could be exposed. The resolution is similar to transmission electron microscopy. FIB-IEM with quantum dots could clearly depict subcellular organelles, for example, mitochondria and specific molecules such as beta-actin.

4. Conclusion

Through the studies, we had developed several critical technologies for FIB to perform biomedical researches. Among them, FIB-IEM with quantum dots might be a major advancement, which might have wide applications in biomedical researches.

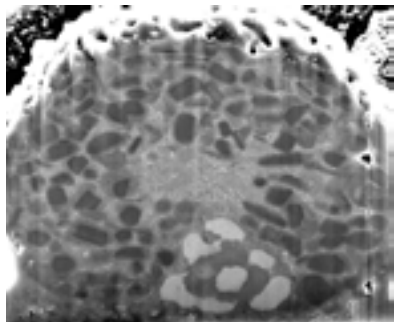


Fig. 1. FIB shows cross-section of a WBC from a mitochondrial diseased patient. Numerous intracellular aggregations are demonstrated.

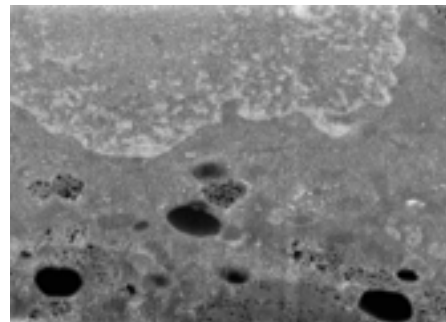


Fig. 2. Beta-actin molecules are denoted as clusters of tiny electron dense dots in an ARPE-19 cell. Processed through FIB-IEM with quantum dots.

References:

- [1] D Drobne, M Milani, V Leser, F Tatti. Surface damage induced by FIB milling and imaging. *Microscopy Research and Technique*. 70:895–903. (2007)
- [2] V Leser, D Drobne, Z Pipan, M Milani, F Tatti. Comparison of different preparation methods of biological samples for FIB milling and SEM investigation. *J Microscopy*. 233, Pt 2:309–319. (2009)

Molecular Mechanisms Underlying the Establishment of Neuronal Connectivity

Alex L. Kolodkin, Ph.D.

Charles J. Homcy and Simeon G. Margolis Professor

Department of Neuroscience,

Howard Hughes Medical Institute

The Johns Hopkins University School of Medicine

Baltimore, MD, USA

Directing neuronal processes to their appropriate targets during neural development involves the action of extrinsic guidance cues. We have addressed distinct cellular contexts in which a large family of guidance cues, the semaphorins, regulates neural circuit assembly. In our present work, we investigate how developing neural circuits achieve fidelity and specificity, including how laminar organization of neuronal processes is achieved, how select sensory afferent targeting occurs within the CNS, the underlying mechanisms that govern pruning of neural connections, and how classical guidance cue signaling regulates synapse organization and function. The molecular mechanisms that direct these processes are likely conserved across a wide range of neuronal and non-neuronal subtypes, and they are also utilized by many distinct ligand-receptor signaling systems. Therefore, our work serves as a model for understanding the diverse contexts in which guidance cues establish neural connections, defining extrinsic and intrinsic contributions to the elaboration of neuronal connectivity during embryonic and postnatal development.

Invited Speaker 8

Electrospun Poly(benzyl glutamate)-r-Poly(glutamic acid) Scaffold for PC-12 Neurite Outgrowth

Zhen-Hua Wang, Yen-Yu Chang, Shyh-Chyang Luo and Wei-Fang Su*

Department of Materials Science and Engineering

National Taiwan University, Taipei, Taiwan

We investigate the effect of polymer scaffold containing neuron stimulate: glutamic acid on the neurite outgrowth of PC-12 neuron cells. The poly(benzyl glutamate) (PBG) was synthesized from γ -benzyl glutamate-N-carboxy anhydride via ring opening polymerization using sodium methoxide initiator in anhydrous benzene. Then the PBG was partially hydrolyzed to obtain glutamic acid containing copolymer of poly(benzyl glutamate)-r-poly(glutamic acid) (PBGA) using an acid catalyst (33 wt% HBr in acetic acid). The ratio of glutamic acid on the polymer was controlled by hydrolysis time. The chemical structures of monomer and polymers were confirmed FTIR and NMR. The molecular weight of either PBG or PBGA was >200,000 measured by GPC. The polymers were fabricated into fibrous scaffolds by electrospinning using 20 wt. % of solution in a mixed solvent of tetrahydrofuran (THF) and dimethylacetamide (DMAc) (9:1 wt. ratio). Both PBG and PBGA are biodegradable and biocompatible. The effect of glutamic acid ratio in the polymer on the proliferation and neuron differentiation of PC-12 cells was investigated. Three kinds of samples were evaluated: pure PBG, PBGA20 and PBGA30. The latter two contain 20% and 30% molar of glutamic acid in the polymer respectively. The biocompatibility and neuron differentiation can be improved by increasing the amount of glutamic acid in polymer. The PBGA30 exhibited the best biocompatibility and the longest nerve outgrowth. The scaffold made from aligned fibers can guide the nerve outgrowth along the fibers with longer length of neurite (>100 micron) as compared with the scaffold made from random fibers. Thus, the aligned electrospun PBGA scaffold has better properties toward the application in nerve regeneration.

1. Keywords

poly(benzyl-glutamate)-r-poly(glutamic acid), electrospinning, PC-12 culture, optic nerve regeneration

Invited Speaker 9

The eyes as a window to the brain: the value of optical coherence tomography in neurodegenerative diseases

Ta-Ching Chen, MD

¹ *Department of Ophthalmology, College of Medicine, National Taiwan University, Taipei, Taiwan*

² *Molecular Imaging Center, National Taiwan University, Taipei, Taiwan*

It is widely recognized that optical coherence tomography (OCT) has a transformative impact in the field of ophthalmology and vision research, contributing to fundamental understanding of disease pathogenesis and daily clinical decision making. As a non-invasive diagnostic technique, spectral-domain OCT (SD-OCT) can provide us an in vivo cross-sectional view of the retina and optic nerve head with very high resolution (<7 μ m). Enhanced-depth imaging OCT (EDI-OCT) demonstrated good penetration of choroidal tissue, further broadening the clinical applications. In recent years, increasing evidences have shown that OCT imaging also benefits in several neurodegenerative diseases, such as multiple sclerosis, Alzheimer disease, Parkinson's diseases, cerebral vascular accidents, intracranial tumors, and traumatic brain injuries. It can help the early diagnosis, monitoring progression, and prognostic judgment. In this talk, we would like to share our clinical experiences and scientific findings in recent years. Retrograde degeneration of retinal neurons has been a valuable index of the intracranial pathology. With the advanced data processing methodology, we further proved that peripapillary choroidal circulation, to some extent, could mimic the hemodynamic change of intracranial circulation and become a highly accessible and non-invasive model.

Toward an ideal platform for functional brain studyShi-Wei Chu^{1,2}¹ *Department of Physics, National Taiwan University, 1, Sec 4, Roosevelt Rd, Taipei 10617, Taiwan.*² *Molecular Imaging Center, National Taiwan University, 1, Sec 4, Roosevelt Rd, Taipei 10617, Taiwan.*

In recent years, brain imaging emerges to be one of the most significant scientific topics worldwide, for example, the BRAIN initiative in USA and the HBP project in EU. When considering optical imaging for brain, with a special emphasis for in vivo observation, there are several key aspects to improve, including contrast, resolution, imaging speed, imaging depth, and the capability to control the neuron firing. Our lab has been concentrated to develop an ideal platform that improves all the above aspects, and I would like to share our recent progresses in this meeting.

In terms of contrast, we are working with calcium indicators GCaMP1 and voltage sensors ASAP22 to capture the dynamics of neuron firing in the brain. For resolution, we developed a new algorithm to enhance 3D spatial resolution specifically suitable for deep brain tissue imaging³. We have also innovatively introduced a new contrast based on nanoparticle scattering to the field of superresolution^{4,5}. For imaging depth, other than the standard two-photon approaches, we have accomplished three-photon fluorescence imaging for GFP, and found 50% improvement in depth performance⁶. For imaging speed, by incorporating a high-speed axial scanning lens, we have achieved volumetric imaging for a whole drosophila brain in vivo with ~100 ms temporal resolution. In this meeting, we will show our recent efforts to push the volumetric imaging speed down to millisecond regime by the strategy of multifocus imaging⁶. For the control of neuron signaling, an extra scanner is integrated into the platform to provide an activation beam for a red-color channel rhodopsin (ReaChR) in the brain⁶. Combining the above efforts, the new imaging platform will facilitate brain studies toward the mapping of live functional connectome.

Reference:

- [1] Chen, T. W. et al. Ultrasensitive fluorescent proteins for imaging neuronal activity. *Nature* 499, 295-300 (2013).
- [2] St-Pierre, F. et al. High-fidelity optical reporting of neuronal electrical activity with an ultrafast fluorescent voltage sensor. *Nature Neuroscience* 17, 884-889 (2014).
- [3] Su, I. C., Hsu, K.-J., Shen, P.-T., Lin, Y.-Y. & Chu, S.-W. 3D resolution enhancement of deep-tissue imaging based on virtual spatial overlap modulation microscopy. *Opt. Express* 24, 16238-16246 (2016).
- [4] Chu, S. W. et al. Measurement of a saturated emission of optical radiation from gold nanoparticles: application to an ultrahigh resolution microscope. *Phys. Rev. Lett.* 112, 017402 (2014); please also refer to the reports in the BMI conference by Deka Gitanjal "Plasmonic SAX microscopy in deep tissue" and by Hou-Xian Ding "Sub-20-nm spatial resolution based on saturation excitation (SAX) microscopy with an appropriate nonlinear response".
- [5] Wu, H.-Y. et al. Ultrasmall all-optical plasmonic switch and its application to superresolution imaging. *Scientific Reports* 6, 24293 (2016).
- [6] Manuscripts in preparation. Please refer to the reports in the BMI conference by Kuo-Jen Hsu "Deep brain imaging in Drosophila by 3-photon excitation"; Chih-Wei Liu "High Speed 3D Functional Imaging of Living Brain"; Chih-Huan Chiang "Automated Analysis of Functional Connectome Images"; Chiao Huang "All-Optical Physiology based on Fast Volumetric Imaging".

Monitoring of the Depigmentation Therapy of Hyperpigmentary Disorders on Female Face by Using Label-free Noninvasive Optical Biopsy ImagingChi-Kuang Sun,¹ Yu-Hsiang Su¹, Ming-Liang Wei¹, and Yi-Hua Liao²¹ *Molecular Imaging Center, National Taiwan University, Taipei 10617, Taiwan*² *Department of Dermatology, National Taiwan University Hospital and National Taiwan University Medical School, Taipei 10048, Taiwan*

In this talk, we will focus on reporting our recent noninvasive virtual biopsy diagnosis and post-therapy evaluation of hyperpigmentary disorders on female face, including melasma and solar lentigines (SL), with a histopathological accuracy. These evaluations are subjective, quantitative, and can be with a molecular specificity for melanin. Without our recent developed harmonic generation microscopy (HGM), none of these studies were possible before.

These two types of hyperpigmentary disorders have high prevalence. For melasma, it is up to 40% in females of some Asian populations [1], while SL can be observed in as many as 90% of whites older than 60 years [2] and in more than 70% of Asians older than 50 years [3]. They are of great concern for mid-aged women and thus have brought a huge therapeutic demand in clinics. Our studies aim at performing high-resolution quantitative and molecular diagnosis on the exact same site of lesions during both pre- and post- therapeutic periods and at providing microscopic information impossible for traditional biopsies to reach.

33 Asian women, between 30 to 65 years old and having symmetrically distributed melasma on the cheeks, were recruited. All facial lesions were treated with topical agents once at night for 3 months. At week 5 and 7, low-fluence Nd:YAG laser was performed on the same selected side. The volunteers were asked to come for HGM image acquisition both before and after the treatment process (12 weeks). For SL, 18 Asian women, between 40 to 80 years old and having solar lentigines on the face, were recruited. Lentiginous lesions were treated with ruby laser after clinical examination. The volunteers were asked to come for image acquisition three times, that is before the laser treatment, approximately 3 weeks after the treatment, and 6 to 8 weeks after the treatment, respectively. The experimental protocol was approved by the National Taiwan University Hospital Research Ethics Committee.

For facilitate computer-assisted diagnosis, several image analysis programs were developed by Prof. Guo-Gwin Lee of National Cheng-Kung University. HGM is also the only technique capable of providing the absolute mass density of melanin value with a sub-femtoliter 3D spatial resolution for quantitative molecular imaging of melanin distribution beneath human face.

In this annual report, we will present our analysis results on this diagnosis study. Our study first provides histopathological evidence on the long-debating origin of these two hyperpigmentary disorders: melasma is due to UV- or hormone- induced hyperactivation of melanocytes while SL is due to UV-induced gene mutation on keratinocytes [4,5]. Our study then provides a new angle to look into the laser-based therapy, which actually does not cure these diseases at all. Our study provides the following quantitative items: melanocyte density, melanophage density, average depth of dermal papilla zone (DPZ), average melanin mass density (MMD) in the cytoplasm of a specific

cell, melanin-rich keratinocyte density, thickness of stratum corneum (SC), average nucleus size of basal cells, average cell size of basal cells, NC ratio of basal cells. For melasma, the change in the DPZ depth was observed for the first time. It could be attributed to dissolution of collagen fiber due to activation of matrix metalloproteinases (MMPs) by keratinocytes. The change in the MMD in SL lesions was distinguished as a novel characteristic that differentiates SL from normal skin. Thicker SC in the SL lesions indicates interfered desquamation as well as keratinocytic proliferation, which relates to the pathogenesis of SL. The depigmenting effect from the laser treatments is mainly attributed to reduction of melanin-rich cells. On the other hand, the decrease in MMD after treatment is only close to borderline significant, implying a rather subtle influence on melanin production from the laser treatment. More details statistical results will be presented.

To sum up, HGM is capable of providing unprecedented information on origin of different hyperpigmented lesions and treatment effects and is with a high potential to serve as a novel diagnosis tool for hyperpigmentary disorders and their therapeutic monitoring. Our study also indicates the necessity of new clinic diagnosis and therapy strategy for the treatment of hyperpigmentary disorders. This study is supported by NHRI, NTU MIC, NCKU, and NTUH.

Reference:

- [1] Sivayathorn A., "Melasma in Orientals," *Clinical Drug Investigation* 10 (suppl 2), pp 34-40 (1995).
- [2] Ber Rahman S, Bhawan J, "Lentigo," *International Journal of Dermatology* 35 (4), pp 229-304 (1996).
- [3] Nip J, Pottery S. B, Rocha S et al., "The New Face of Pigmentation and Aging," *Text Book of Aging Skin*, Farage, M.A. and Maibach, H.I. ed., Springer Science & Business Media, pp 509-521(2009).
- [4] Shin J, Park J Y, Kim S J, et al. "Characteristics of keratinocytes in facial solar lentigo with flattened rete ridges: comparison with melasma," *Clinical and Experimental Dermatology* 40 (5), pp 489-494 (2015).
- [5] Cario-André M, Lepreux S, Pain C et al. "Perilesional vs. lesional skin changes in senile lentigo," *Journal of Cutaneous Pathology* 31 (6), pp 441-447 (2004).

Invited Speaker 12

Whole embryo 3D deformation map during Zebrafish early development

Dipanjan Bhattacharya^{1,2,3}, Jun Zhong^{1,2,3}, Alexandre Kabla⁴ and Paul Matsudaira^{2,3}

¹*Singapore-MIT Alliance for Research and Technology Center, Singapore.*

²*Center for Bioimaging Sciences, DBS, NUS.*

³*MechanoBiology Institute, NUS.*

⁴*Department of Engineering, University of Cambridge.*

1. Introduction

The function of an animal organ is strongly dependent on its ability to control its shape, size and patterns at different length-scales, ranging from few nanometers to tens of millimeter. These multilevel organization and functionality from individual molecules to large tissues are governed by physical laws. When misregulated, these processes are the leading cause of developmental defects, diseases such as cancer or organ malfunction. Cell migration and tissue regeneration are the keys for tissue-patterning, tissue reorganization and wound healing processes to determine and maintain tissue in its local microenvironment. In this article we will be describing our imaging and innovative image analysis method to understand the tissue mechanics during Zebrafish embryogenesis. In cellular level, every animal develops differently; causing diversity within same species but the structure and function of each tissues of the animal remain conserved. Any genetic-physical abnormality during development deviates from normal developmental process and breaks the normal structure-function relationship of the developmental cues. Large-scale and coordinated morphogenetic movements organize cells into the embryonic axis and form the primitive embryonic tissues. These movements are guided by morphogen gradients and cell-cell interactions but the role of mechanical forces in organizing and folding the embryonic tissues is very poorly understood [1,2,3,4]. The main challenge to understand these large scale tissue mechanics lies in imaging 3D thick tissues, image processing and quantitation. Towards this, we have developed a 'Digital Scanned Light Sheet Microscope (DSLM)' with structured illumination capability for 3D live tissue imaging and developed an application specific high end image processing algorithms [5]. This enables the quantitative analysis at the whole tissue in real time during development. Organs in the body develop by a systematic growth of the underlying tissue which then undergoes a regulated change in shape and pattern at precise developmental times. These morphogenetic movements would require coordinated forces acting on the tissue. It is hence important to measure the direction and magnitude of these forces leading to large scale tissue reorganization during developmental process. But measuring force is difficult in such a multi-cellular tissue system with no prior information about local three-dimension stiffness of the developing tissue. Deformation is the direct outcome of the effective forces locally driving the reorganization and pattern formation of the tissue structure, and hence can be used to measure the effects of forces involved in the developmental process.[6,7]

2. Results

Although people have clear idea of different developmental stages of embryogenesis, but the

mechanical cues of its specific structure formation at a specific time point of development is poorly understood. In my approach, we have experimentally obtained a time evolution of 3-D tissue deformation-map during Zebrafish embryogenesis to understand the tissue regeneration and reorganization process. To understand the fundamental mechanism of this tissue deformation and consequent neuronal tube formation (neurulation) from a layer of cells during zebra fish embryogenesis, different biomechanical parameters such as velocity-maps, strain-maps of the whole embryo along polar, azimuthal and radial directions at each time point of development were computed at different time points from the trajectories of individual cells obtained by 3D imaging.

In my approach, I have experimentally obtained a time evolution of 3-D tissue deformation-map to understand the tissue regeneration and reorganization process. The model system I use is formation of the neural tube during early development in zebra fish embryos. To understand the fundamental mechanism of this tissue deformation and consequent neuronal tube formation (neurulation) from a layer of cells during zebra fish embryogenesis, different biomechanical parameters such as velocity-maps, strain-maps and shear-maps were computed at different time points from the trajectories of individual cells obtained by 3D imaging. From the 3D time-trajectories of the individual nuclei, I obtained the strain maps of the whole embryo in polar, azimuthal and radial directions at each time point of development.

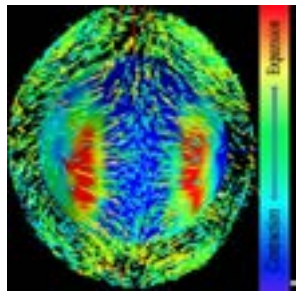


Fig. 1. Representative image of ‘three dimensional strain-map’ at a time-point during neurulation of whole Zebrafish embryo in the ‘Polar direction’ (Dorsal view).

3. Discussion

Our analysis is providing us a novel deformation and tissue reorganization map of Zebrafish embryo during the neurulation. In this process I experimentally obtain changes in shape-pattern and cell clustering of the whole embryo during neurulation process. Large scale 3D tissue imaging and the time evolution of 3D tissue deformation pattern of the whole embryo, in each stages of development, provides us with a unique tool to understand the biomechanics of tissue deformation during embryogenesis

Reference:

- [1] Roszko I, Sawada A, Solnica-Krezel L. (2009). Regulation of convergence and extension movements during vertebrate gastrulation by the wnt/pcp pathway. *Seminars in cell & developmental biology* 20:986-997.
- [2] Schoenwolf G, Smith J. (1990). Mechanisms of neurulation: traditional viewpoint and recent advances. *Development* 109:243-270.
- [3] Topczewski J, et al. (2001). The zebrafish glypican knypek controls cell polarity during gastrulation movements of convergent extension. *Developmental Cell* 1:251-264.
- [4] Kimura K, et al. (1996). Regulation of myosin phosphatase by rho and rho-associated kinase (rho-kinase). *Science* 273:245-248.
- [5] Bhattacharya D, et al. (2012). Three dimensional HiLo-based structured illumination for a digital scanned laser sheet microscopy (DSLIM) in thick tissue imaging. *Opt. Express*. 20:27337-27347.
- [6] Blanchard GB, et al. (2009). Tissue tectonics: morphogenetic strain rates, cell shape change and intercalation. *Nat Meth* 6:458-464.
- [7] Behrndt M, et al. (2012). Forces driving epithelial spreading in zebrafish gastrulation. *Science*. 338:257-260.

Invited Speaker 13

Nonlinear Optical Imaging of Cornea Development and Pathology: Current State and Future Development

Chen-Yuan Dong^{1,2}

¹ Department of Physics, National Taiwan University, Taipei 106, Taiwan

² Molecular Imaging Center, National Taiwan University, Taipei 100, Taiwan

Abstract

Due to the high degree of corneal transparency, standard optical microscopy examination is of limited use in imaging superstructure in normal and pathological corneas. However, since the cornea is composed primarily of type I collagen, a combination nonlinear optical phenomena such as multiphoton-induced fluorescence and second harmonic generation (SHG) has been shown to be effective in visualizing three-dimensional superstructure and pathological changes in corneal specimens. In this presentation, I will show our results in investigating cornea development and pathology. I will also discuss future research directions and potential development in the clinical setting.

1. Introduction

The cornea is the outermost layer of the human eye. Since refractive index change is the largest at the cornea-air interface, therefore, the cornea is also the most refractive element of the eye. Due to its importance in image formation, various techniques such as LASIK and PRK have been developed to alter cornea structure in order to improve vision. In addition, for successful image formation, the cornea is also highly transparent, with well over 90% transmittance in the visible spectrum. Due to its high transparency, standard optical microscopic examination is of limited value in revealing detailed structural information within the cornea. However, since type I collagen is the main molecular component of cornea, therefore, nonlinear optical microscopy can be used for effective examination of cornea superstructure for physiological and pathological studies.

2. Results and Discussion

In this presentation, I will show various results on normal and pathological corneas in different species such as porcine, chicken, and ex vivo human specimens. These results will show that multiphoton microscopy is an effective tool for cornea imaging.

Reference:

- [1] Tan, H. Y., Chang, Y. L., Lo, W., Hsueh, C. M., Chen, W. L., Ara A. Ghazaryan, A. A., Hu, P. S., Young, Y. H., Chen, S. J. & Dong, C. Y. Characterizing the morphological change of collagen crosslinked-treated corneas by Fourier transform-second harmonic generation imaging. *Journal of Cataract & Refractive Surgery* 39, 779–788 (2013).
- [1] Lo, W., Chen, W. L., Hsueh, C. M., Ghazaryan, A. A., Chen, S. J., Ma, D. H. K., Dong, C. Y. & Tan, H. Y. Fast Fourier transform based analysis of second-harmonic generation image in keratoconic cornea. *Investigative Ophthalmology & Visual Science* 53(7), 3501-3507 (2012).

Optical imaging and focusing inside scattering biological tissues

Cheng Ma¹, and Lihong V. Wang²

¹Department of Electronic Engineering, Tsinghua University, Beijing 100084, China

²Department of Biomedical Engineering, Washington University in St Louis, St Louis, MO 63139, USA

1. Introduction

In the entire electromagnetic spectrum, the near infrared wavelength range is one of three low absorption windows for biomedical imaging. At these low-absorbing wavelengths, light scattering plays a major role: For example, the optical absorption and scattering coefficients for tissue at 630 nm are about 0.3 cm⁻¹ and 10 cm⁻¹, respectively [1]. Unlike absorption, scattering does not dissipate energy, but it does scramble information. The propagation directions of photons are completely randomized in tissue regions deeper than 1 millimeter because photons are, on average, scattered more than ten times with a scattering anisotropy (average of cosine of the scattering deflection angle) of ~0.9 when they reach this depth. As a result, 1 millimeter is often referred to as the optical diffusion limit. It is extremely desirable to break through the optical diffusion limit and use light to image deep into biological tissue. In our lab, we tackle the challenging task of optical imaging inside scattering media using wavefront shaping (WFS) [2], which seeks to guide photons through the scattering medium to interact with the embedded target. In an ideal situation, wavefront shaping allows externally launched photons to be zigzagged to reach the target with optimized possibility.

2. Light scattering suppression using WFS

Despite its laboratory success, WFS must overcome several challenges before it can be made biomedically useful. First, since biological tissues are dynamic, WFS must be fast enough to adapt to tissue changes on the microscopic scale. A rule of thumb is the order of 1 millisecond for the entire process. Second, since the scattering process is complex, the complexity (i.e., degrees of freedom) supported by the wavefront control device must be scaled accordingly. Currently, due to a lack of control complexity, WFS quality is still poor for most meaningful in vivo applications. Third, to image or focus inside a scattering medium is more useful than to image or focus through it. In the former case, it is challenging to develop guide stars that are non-invasive. Last, in fluorescence imaging, even though a focus is formed and raster scanned inside the scattering medium, the fluorescence from the bulk background outside the focus can easily overwhelm the signal within the focus.

In our research, the first three problems have been intensively studied, and great progress has been made (To the best of our knowledge, the last problem has remained untouched so far). To speed up the WFS process, optical time reversal can be used [3]. Its validity rests on the time reversal symmetry of the wave equation governing the scattering process [4], and it offers the advantage of being able to determine the optimal wavefront at once rather than having to go through an iterative process. To further speed up WFS, we have developed a method of binary phase modulation which significantly reduces the wavefront calculation complexity and data throughput, while maintaining 40% of the focusing quality [5].

To address the second problem, using analog crystals is a better choice, since they support orders of magnitude more degrees of freedom than their digital counterparts. However, crystals suffer from poor energy efficiency, which significantly limits their widespread use. Digital spatial light modulators can typically support on the order of 10⁴ to 10⁵ degrees of freedom in an optical time reversal setting, which is barely enough for real applications.

To solve the third problem, we have developed two types of non-invasive guide stars. In the first approach [6], a focused ultrasound wave is introduced into the scattering medium, where the ultrasonic focus is employed as the guide star. The ultrasound guide star shifts the light frequency, and a time-reversed focus can be made by phase-conjugating the frequency-shifted light. Termed time reversed ultrasonically encoded (TRUE) optical focusing, this technology had been proven useful in forming images of fluorescent [7] and absorptive objects inside scattering media. In the second approach, termed time reversed adapted perturbation (TRAP) [8] optical focusing, dynamic objects inside a relatively stable scattering background are used as guide stars. Since most of these dynamic objects (such as flowing red blood cells) are non-emissive, we subtract the scattered field captured at different times to cancel out the contribution from the static background, exposing only the field scattered by such dynamic targets. Using the differential field, we then digitally synthesize a conjugate phase map which guarantees focusing of photons onto the objects. This method has been proven useful in tracking moving objects, condensing optical energy on vasculature, imaging time-variant objects, and measuring blood flow, all inside scattering media [5, 8, 9].

3. Conclusion

If we draw a “resolution versus depth” chart for optical imaging modalities, all high-resolution pure optical microscopies, such as two-photon, confocal, and OCT, lie within the bottom-left corner, where resolution is high (<1 micron) but penetration is shallow (<1 mm). The dream technology would lie on the lower right: deep penetration and high resolution. WFS is pushing into this territory. Among all optical imaging modalities, WFS is relatively new and is being actively developed. Once the major problems discussed in this paper are solved, widespread applications of WFS are expected.

Reference:

- [1] D. Razansky, "Multispectral opto-acoustic tomography of deep-seated fluorescent proteins in vivo." *Nat. Photon.* 3, 412-417 (2009).
- [2] Z. Merali, "Optics: Super vision." *Nature* 518, 158, 2015.
- [3] Z. Yaqoob, et al. "Optical phase conjugation for turbidity suppression in biological samples." *Nat. Photon.* 2, 110-115, 2008.
- [4] A. Mosk, et al. "Controlling waves in space and time for imaging and focusing in complex media." *Nat. Photon.* 6, 283-292, 2012.
- [5] C. Ma, et al. "Single-exposure optical focusing inside scattering media using binarized time-reversed adapted perturbation." *Optica* 2, 869-876, 2015.
- [6] X. Xu, H. Liu, and L. V. Wang. "Time-reversed ultrasonically encoded optical focusing into scattering media." *Nat. Photon.* 5, 154-157, 2011.
- [7] Y. Wang, et al. "Deep-tissue focal fluorescence imaging with digitally time-reversed ultrasound-encoded light." *Nat. Commun.* 3, 928, 2012.
- [8] C. Ma, et al. "Time-reversed adapted-perturbation (TRAP) optical focusing onto dynamic objects inside scattering media." *Nat. Photon.* 8, 931-936, 2014.
- [9] E. H. Zhou, et al. "Focusing on moving targets through scattering samples." *Optica* 1, 227-232, 2014.

Invited Speaker 15

Application of Electron Microscopy for Vaccine Development of MERS-CoV Virus-like Particles

Ming-Fu Chang¹, Yu-Pin Yeh¹, Ssu-Chia Chien¹, Wei-Ting Chen², Chih-Yu Chao², Rong-Huay Juang³ and Shin C. Chang⁴

¹*Institute of Biochemistry and Molecular Biology*

²*Department of Physics*

³*Department of Biochemical Science and Technology*

⁴*Institute of Microbiology, National Taiwan University, Taiwan*

Middle East respiratory syndrome (MERS), an atypical variant of pneumonia, emerged in June 2012 and spread to European, North America, and Asian countries including United Kingdom, France, Italy, USA, Malaysia and South Korea. Until June 2016, the MERS epidemic had been considered as a significant threat to human beings as its mortality rate was around 36% among 1,733 patients, which is more than 3 times the mortality rate associated with severe acute respiratory syndrome (SARS). Why the mortality rate of MERS is so high is unclear. Most patients with MERS had been in contact with dromedary camels. MERS coronavirus (MERS-CoV), a novel lineage C betacoronavirus classified as a member of the Coronaviridae family was identified as the causative pathogen of MERS. In addition to atypical pneumonia, MERS-CoV infection also causes a high risk of renal failure. The structural proteins translated from subgenomic mRNAs comprise a spike glycoprotein (S), a membrane glycoprotein (M), a small envelope protein (E), and a nucleocapsid protein (N). DPP4 (also known as CD26), a type II integral transmembrane protein, was identified to be the functional receptor for MERS-CoV. To date, no drugs and vaccines have been clinically approved to control MERS-CoV infection. One of the most promising tools in vaccine development is the use of recombinant-based virus-like particles (VLPs). VLPs are multiprotein structures closely resembling natural virions. VLPs that lack viral genetic materials are non-infectious and non-replicating particles. In addition, VLPs display intact and biochemically active antigens on their surface and thus, show high immunogenicity and antigenicity. Importantly, VLPs interact with the host immune system inducing humoral and cellular responses similarly to the native pathogen. In this study, MERS-CoV virus-like particles (MERS-VLPs) containing S, M, and E proteins were produced by baculovirus expression system and the molecular architecture was elucidated by electron microscopy (EM). Results showed that MERS-VLPs with diameters approximately 100 nm were detected, and spike protein appeared around the spherical particles. Immunofluorescence assay demonstrated that colocalization of the spike protein-incorporated VLPs with DPP4. In addition, BALB/c mice were vaccinated with the partially purified MERS-VLPs. MERS-VLPs induced host immune response and generated neutralizing antibodies. Humanized antibodies will be generated as a promising passive immunotherapy for MERS.

**BMI Lunch Session
GE Healthcare**

BIOGRAPHICAL SKETCH

Provide the following information for the Senior/key personnel and other significant contributors. Follow this format for each person. DO NOT EXCEED FIVE PAGES.

NAME: Albert P. Chen

POSITION TITLE: Senior Scientist

EDUCATION/TRAINING

(Begin with baccalaureate or other initial professional education, such as nursing, include postdoctoral training and residency training if applicable. Add/delete rows as necessary.)

INSTITUTION AND LOCATION	DEGREE (if applicable)	Completion Date MM/YYYY	FIELD OF STUDY
University of Washington	B.S.	06/2000	Chemical Engineering
University of California, San Francisco	Ph.D.	06/2006	Biomedical Engineering
University of California, San Francisco	Post Doctoral	04/2008	MR imaging and spectroscopy

A. Personal Statement

Since the start of my graduate study, I have been involved in research studies using magnetic resonance (MR) imaging and spectroscopy with the goal of obtaining more than just anatomical data from an MR exam. In particular, I have been focusing my efforts for more than a decade on acquiring MR data that reflects changes in tissue metabolism. With the development of Dynamic Nuclear Polarization (DNP) – dissolution technique in recent years to allow investigation of cellular metabolism in real time non-invasively, MR metabolic imaging has a real potential to provide valuable diagnostic information not available before. I have fortunately been involved in some of the early and pioneering work in this area of hyperpolarized ¹³C imaging at both UCSF and GE healthcare. Although I have transitioned from an academic environment to the industry, my role with GE healthcare has been primarily devoted to research collaborations with academia to bring this technology forward. During the process of conducting MR research with various colleagues and collaborators, I have also acquired a broad set of skills in biomedical research and molecular imaging. Most of my publications in peer reviewed scientific journals have been co-authored with researchers in academia, funded by various agencies in US and Canada.

- Chen AP, Albers P, Cunningham CH, Kohler SJ, Yen Y, Hurd RE, Tropp J, Bok R, Nelson SJ, J K, Vigneron DB. Hyperpolarized C-13 spectroscopic imaging of the TRAMP mouse at 3T-Initial experience. *Mag Res Med* 2007;58(6):1099-1106.
- Chen AP, Hurd RE, Schroeder MA, Lau AZ, Gu YP, Lam WW, Barry J, Tropp J, Cunningham CH. Simultaneous investigation of cardiac pyruvate dehydrogenase flux, Krebs cycle metabolism and pH, using hyperpolarized [1,2-(¹³C)(²) pyruvate in vivo. *NMR Biomed* 2012 Feb;25(2):305-11.

- Nelson SJ, Kurhanewicz J, Vigneron DB, Larson PE, Harzstark AL, Ferrone M, van Criekinge M, Chang JW, Bok R, Park I, Reed G, Carvajal L, Small EJ, Munster P, Weinberg VK, Ardenkjaer-Larsen JH, Chen AP, Hurd RE, Odegardstuen LI, Robb FJ, Tropp J, Murray JA. Metabolic imaging of patients with prostate cancer using hyperpolarized [1-¹³C]pyruvate. *JA.Sci Transl Med.* 2013 Aug 14;5(198).
- Cunningham CH, Lau JY, Chen AP, Geraghty BJ, Perks WJ, Roifman I, Wright GA, Connelly KA. Hyperpolarized 13C Metabolic MRI of the Human Heart: Initial Experience. *Circ Res* 2016, Sep 15; [Epub ahead of print]

B. Positions and Honors

Positions and employment

2008 – Senior Scientist, GE healthcare

Other Experiences and Memberships

2001-Present Member of International Society of Magnetic Resonance in Medicine

Honors and Awards

2004 UCSF Graduate Research Award

2006 Margaret Hart Surbeck Laboratory for Advanced Imaging scholar

2007 Pelican Cancer Foundation Post-doctoral Research Fellowship

C. Contribution to Science

1. My early research focused on MR imaging methods for multi-parametric imaging of the human prostate. Non-invasive characterization of prostate cancer is very important because it would allow patients and clinicians to better manage a disease that can stay indolent for years, yet can also be lethal in many patients. In the early 2000s, more powerful MR scanners (3T or above) were becoming available and hardware and software developments were needed to take advantage of the higher signal to noise and also to address the trade-offs associated with the higher magnetic field. Working with several PIs at the UCSF radiology departments and collaborating with scientists from electrical engineering department at Stanford, we contributed several novel data acquisition methods that have continued to be used today to image human prostate.

- Cunningham CH, Vigneron DB, Marjanska M, Chen AP, Xu D, Hurd RE, Kurhanewicz J, Garwood M, Pauly JM. Sequence design for magnetic resonance spectroscopic imaging of prostate cancer at 3 T. *Magn Reson Med* 2005;53(5):1033-1039.
- Chen AP, Cunningham CH, Kurhanewicz J, Xu D, Hurd RE, Pauly JM, Carvajal L, Karpodinis K, Vigneron DB. High-resolution 3D MR spectroscopic imaging of the prostate at 3 T with the MLEVPRESS sequence. *Magn Reson Imaging* 2006;24(7):825-832.
- Chen AP, Cunningham CH, Ozturk-Isik E, Xu D, Hurd RE, Kelley DA, Pauly

JM, Kurhanewicz J, Nelson SJ, Vigneron DB. High-speed 3T MR spectroscopic imaging of prostate with flyback echo-planar encoding. *J Magn Reson Imaging.* 2007 Jun;25(6):1288-92.

2. With the development of Dynamic Nuclear Polarization (DNP) – dissolution technique in recent years, it became feasible to acquire MR data that reflect real time cellular metabolic processes, by injecting a hyperpolarized 13C metabolic substrate that has more than 10,000 fold higher MR sensitivity. MR imaging is then performed to detect the signal from the injected substrate as well as its down stream metabolic products, in real time. Since the pre-polarized signal is only available for a very limited time (1-2 minutes), and it is desirable to obtain as much of the information as possible (chemical, spatial, temporal), MR imaging techniques needed to be drastically modified or re-developed to perform such studies. I was involved in some of the earliest research efforts to apply DNP-dissolution technique to image metabolic changes in cancer noninvasively. These efforts include developments of novel and advanced MR imaging techniques to improve spatial-temporal resolutions of hyperpolarized 13C imaging, as well as applications of these techniques to animal models of cancer. I have also made significant contributions as a scientist at both UCSF and later at GE towards the successful first in man MR imaging study with this emerging metabolic imaging modality.

- Chen AP, Albers P, Cunningham CH, Kohler SJ, Yen Y, Hurd RE, Tropp J, Bok R, Nelson SJ, J K, Vigneron DB. Hyperpolarized C-13 spectroscopic imaging of the TRAMP mouse at 3T-Initial experience. *Magn Reson Med* 2007;58(6):1099-1106.
- Patent US7795868 B2. Hyperpolarized dynamic chemical shift imaging with tailored multiband excitation pulses. Larson PE, Pauly JM, Vigneron DB, Chen A, Kerr, AB. Publication date: Apr 8, 2010.
- Albers M, Bok R, Chen AP, Cunningham CH, Zierhut ML, Zhang VY, Kohler SJ, Tropp J, Hurd RE, Yen Y, Nelson SJ, Vigneron DB, Kurhanewicz J. Hyperpolarized 13C Lactate, Pyruvate, and Alanine: Noninvasive Biomarkers for Prostate Cancer Detection and Grading. *Cancer Res* 2007;68(20):8607-8615.
- Nelson SJ, Kurhanewicz J, Vigneron DB, Larson PE, Harzstark AL, Ferrone M, van Criekinge M, Chang JW, Bok R, Park I, Reed G, Carvajal L, Small EJ, Munster P, Weinberg VK, Ardenkjaer-Larsen JH, Chen AP, Hurd RE, Odegardstuen LI, Robb FJ, Tropp J, Murray. Metabolic imaging of patients with prostate cancer using hyperpolarized [1-¹³C]pyruvate. *JA.Sci Transl Med.* 2013 Aug 14;5(198).

3. While hyperpolarized 13C MR metabolic imaging has shown great potential to provide valuable diagnostic information in the field of oncology, it is also possible to use this technique to probe tissue metabolism noninvasively in other tissues and pathologies such as cardiology. To explore the use of hyperpolarized 13C imaging in various applications, I have been conducting research in all aspects of metabolic imaging, including probe developments, MR pulse sequence developments and

testing in pre-clinical models. These works will help bring this promising imaging technology forward into more clinical research studies and ultimately making a positive impact in healthcare.

- Chen AP, Hurd RE, Gu YP, Wilson DM, Cunningham CH. (13)C MR reporter probe system using dynamic nuclear polarization. *NMR Biomed* 2011;24(5):514-520.
- Chen AP, Hurd RE, Schroeder MA, Lau AZ, Gu YP, Lam WW, Barry J, Tropp J, Cunningham CH. Simultaneous investigation of cardiac pyruvate dehydrogenase flux, Krebs cycle metabolism and pH, using hyperpolarized [1,2-(13) C(2) pyruvate in vivo. *NMR Biomed* 2012 Feb;25(2):305-11.
- Chen AP, Lau JY, Alvares RD, Cunningham CH. Using [1-13C]lactic acid for hyperpolarized 13C MR cardiac studies. *Magn Reson Med* 2015;73(6):2087-93.
- Lau AZ, Chen AP, Ghugre NR, Ramanan V, Lam WW, Connelly KA, Wright GA, Cunningham CH. Rapid multislice imaging of hyperpolarized 13C pyruvate and bicarbonate in the heart. *Magn Reson Med* 2010;64(5):1323-1331.

Complete List of Published Work in MyBibliography:

<https://www.ncbi.nlm.nih.gov/sites/myncbi/10Slc0oWDs52/bibliography/47435573/public/?sort=date&direction=ascending>

D. Research Support

None

Keynote Speaker III

DETECTION OF EOSINOPHILS FOR THE DEVELOPMENT OF A NEW RAMAN DIAGNOSTIC TECHNIQUE FOR EOSINOPHILIC ESOPHAGITIS

Tatsuyuki Yamamoto^{1,2}, Suguru Uemura¹, Hemanth Noothalapati², Naoki Oshima^{2,3}, Yoshikazu Kinoshita^{2,3}, Masahiro Ando⁴, Hiro-o Hamaguchi^{4,5}

¹*Faculty of Life and Environmental Science, Shimane University, 1060 Nishikawatsu-cho, Matsue, Japan,*

²*Raman Project Center for Medical and Biological Applications, Shimane University, 1060 Nishikawatsu-cho, Matsue, Japan,*

³*Faculty of Medicine, Shimane University, 89-1 Enya-cho, Izumo, Japan,*

⁴*Research Organization for Nano & Life Innovation, Waseda University, 513 Wasedaturumaki-cho, Shinjuku, Tokyo, Japan,*

⁵*Institute of Molecular Science and Department of Applied Chemistry, National Chiao Tung University, 1001 University Road, Hsinchu, Taiwan*

We are working on developing a new non-biopic diagnostic technique for detecting Eosinophilic esophagitis (EoE) using Raman spectroscopy in Raman Project Center for Medical and Biological Applications, Shimane University. We have already succeeded in detecting eosinophils in the esophageal tissue from EoE model mice (EoE induced by administering Interleukin-33) using Raman spectroscopy [1]. We have also succeeded in differentiating eosinophils from neutrophils in a concentrated granulated leukocytes separated from human blood. The granulated leukocytes were separated by a standard method, using a blood separation solution (Polymorphprep™, Cosmobio Co., Ltd) and a Red blood cell hemolysis solution (Red blood Cell Lysis Solution(10x), and Miltenyi Biotec K.K.) to obtain a white pellet. The pellet thus obtained was diluted with a PBS(-) buffer solution (1 ml) to obtain a sample solution for Raman measurements. In the prepared sample solution, neutrophils are abundant and in fact outnumber eosinophils. Although overall Raman spectrum of neutrophil resembles to that of eosinophil, characteristic Raman bands of eosinophil peroxidase at 1614, 1547 and 757 cm⁻¹ unambiguously indicate the existence of eosinophil in a straightforward manner. We are now trying to detect these Raman bands due to eosinophil peroxidase on the esophageal tissue of mouse using a new fiber based Raman spectrometer, which will automatically measure Raman spectra of tissues and obtain Raman molecular distribution images. This spectrometer is supposed to be highly useful in developing Raman endoscope for the diagnosis of Eosinophilic esophagitis in the near future.

Reference:

[1] H. Noothalapati et al., *Vibrational Spectroscopy*, 85, 7-10(2016).

Invited Speaker 16

Human microcephaly proteins: Roles in centriole duplication, neural stem cell division, and neurodevelopmental disorders

Tang K. Tang (唐堂)

Institute of Biomedical Sciences, Academia Sinica, Taipei, Taiwan

Centrioles are microtubule-based cylinders that form centrosomes, which are the major microtubule organizing centers of animal cells, and are vital for many cellular and developmental processes. Primary microcephaly (MCPH) is an autosomal recessive congenital disorder characterized by smaller brain size with mild to severe mental retardation. Currently, at least twelve MCPH genes have been identified. Interestingly, most MCPH gene-encoding proteins are located at the centrioles/centrosomes and the roles of these MCPH proteins are incompletely understood. We previously showed that overexpression of STIL/MCPH7 induces centriole amplification (EMBO J 2011), excess CPAP/MCPH6 induces extra-long centrioles (Nat Cell Biol 2009), and phosphorylation of CPAP by Aurora-A kinase could cohere PCM proteins and maintain spindle pole integrity during mitosis (Cell Report 2016). Interestingly, CEP135/MCPH8 directly interacts with SAS6 and CPAP, and serves as a linker protein that connects the cartwheel to the outer microtubules for centriole duplication (EMBO J 2013). Our results firstly link three MCPH proteins CPAP, STIL, and CEP135 into a common pathway in centriole duplication. Furthermore, we also found that the interaction between CEP120 and CPAP (J Cell Biol 2013), and CEP295 and microtubules (J Cell Sci 2016) are required for centriole elongation. To study the role of CPAP protein in brain development, we have generated Cpap conditional knockout mice. Our results showed that homozygous Cpap knockout mice are embryonic lethal, while the Nestin-cre-mediated Cpap conditional knockout mice showed the loss of neocortex and cerebellum in E18.5 embryos. Surprisingly, we found that p53 deficiency can rescue Cpap knockout-induced neural cell death, implying a p53-mediated apoptotic pathway. In addition, we also found that a newly identified human microcephaly protein RTTN binds to STIL and is required for building full-length centrioles. Together, we provide a molecular basis for a model of how four microcephaly proteins (CPAP, STIL, CEP135, RTTN) participate in centriole duplication and propose that interference in this pathway may activate a p53-mediated neuronal cell death in microcephaly patients.

Invited Speaker 17

Copper-Based Nanoparticles and The Application to Photothermal Therapy

Yu-Wei Tai¹, Jiasheng Yu² and Chih-Chia Huang³

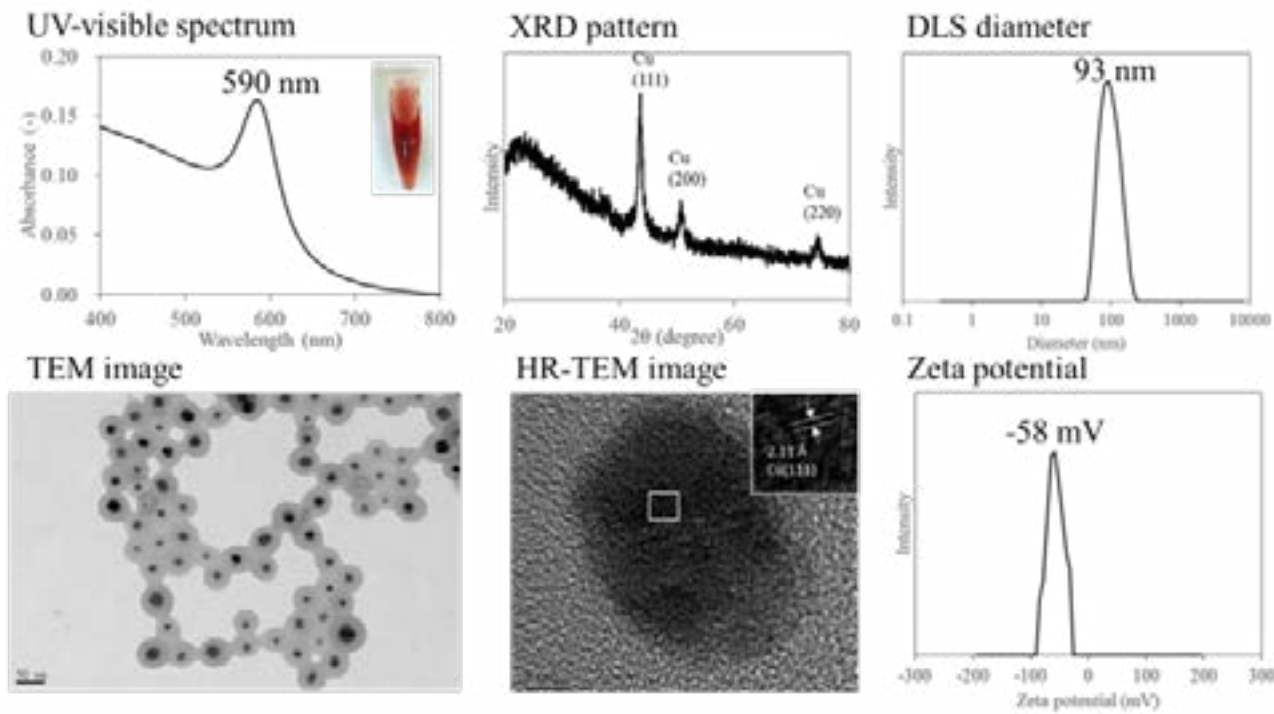
¹ *Department of Chemical Engineering, National Taiwan University, Taipei, Taiwan*

² *Center for Molecular Imaging Research, National Taiwan University, Taipei, Taiwan*

³ *Department of Photonics, National Cheng Kung University, Tainan, Taiwan*

Photothermal therapy (PTT) is a new technique combining nanotechnology and biomedical engineering for cancer treatment. As other metallic nanoparticles (NPs), copper nanoparticles (CuNPs) have unique optical characteristics. An adsorption peak of CuNPs was observed in adsorption spectra, indicating that CuNPs will exhibit localized surface plasmon resonance (LSPR) effect, which means energy of photon at a wavelength of 590 nm can be transferred to the free electron on NPs, leading the oscillation of electronic field. The energy of the resonance subsequently transfer to heat and cause a temperature elevation. This phenomenon can be used as a way to kill cancer cells by targeting and partial heating in tumor tissue with light stimulation. However, due to the instability, CuNPs were not widely used as a PTT agent because they may induce reactive oxygen species (ROS) generation and cause cytotoxicity. This drawback is needed to be controlled if we want to introduce CuNPs to biomedical application.

In the work, we synthesized CuNPs with polymer shell via one-step hydrothermal reduction reaction. The formation of Cu@polymer NPs is sensitive to the presence of halide ions in the reaction. Next, we developed a smooth oxidation process of Cu@polymer NPs to fabricate polymer surface coating-Cu₂O shell-Cu core nanocomposite. UV-visible spectra determined the as-prepared Cu@Cu₂O@polymer NPs with absorption band covered from red to near infrared (NIR) wavelengths. It indicates that the LSPR effect of Cu@Cu₂O@polymer NPs can be stimulated by NIR light, which has higher penetration to tissue and is more appropriate for light-induced therapy. Also, these nanoparticles exhibited optical and physical stability in the aqueous solution. Moreover, compared with Cu@polymer NPs, less ROS generation and cytotoxicity were induced while cells were incubated with Cu@Cu₂O@polymer NPs. The cell death pathway attributed to NP-cell interaction was also studied. Finally, the photothermal effect was examined by light stimulation. As exposure to red light, an obvious photon-to-thermal conversion was obtained for 20-50 ppm of Cu@Cu₂O@polymer NPs and 300-650 mW/cm² of laser power. In contrast, pure Cu@polymer NPs plus red light received less significant PTT effect. In vitro PTT studies also showed that viability of cells incubated with Cu@Cu₂O@polymer NPs was significantly decreased after light exposure. The results indicated that Cu@Cu₂O@polymer NPs are more appropriate to be applied in PTT therapy than Cu@polymer NPs.



Reference:

- [1] Liu, X., et al., Enhanced retention and cellular uptake of nanoparticles in tumors by controlling their aggregation behavior. *ACS Nano*, 2013. 7(7): p. 6244-57.
- [2] Duan, X. and Y. Li, Physicochemical characteristics of nanoparticles affect circulation, biodistribution, cellular internalization, and trafficking. *Small*, 2013. 9(9-10): p. 1521-32.

Invited Speaker 18

Introduction to Electrical Stimulation for Tissue Engineering

Shyh-Chyang Luo, Min-Han Tsai, Chia-Hsuan Lin, Zhen Hua-Wang and Wei-Fang Su
Department of Materials Science and Engineering, National Taiwan University, No. 1, Sec. 4, Roosevelt Road, Taipei, 10617 Taiwan

Abstract

Electrical stimulation is a critical technique in treating neurological diseases, disorders or injuries. Deep brain stimulation can effectively reduce tremor associated with Parkinson's disease. Cochlear implants can provide a sense of sound to people who are deaf or severely hard-of-hearing. Functional electrical stimulation be used to generate muscle contraction to produce functions such as grasping. More recently, gastric electrical stimulation has received approval from the U.S. Food and Drug Administration (FDA) to treat patients with chronic nausea and vomiting associated with gastroparesis. In the first part of this presentation, I would like to give an overview of the study focused on using electrical stimulation as cues to manipulate cellular responses, such as neurite outgrowth. This information is important for applying electrical stimulation for regeneration of neural tissue. The application of electrical stimulation on other non-neuronal cells will also be shortly mentioned. In the second part of the presentation, I will then introduce our setup and methods to conduct the electrical stimulation on cells, including the biomaterials we are interested and the prospect of this project.



Reference:

- [1] Zhu, B.; Luo, S. -C.; Zhao, H.; Lin, H. -A; Sekine, J.; Nakao, A.; Chen, C.; Yamashita Y.; Yu, H. -h. "Large Enhancement of Neurite Outgrowth on a Cell-Membrane Mimicking Conducting Polymer" *Nature Communications*, 2014, 5, 4523.
- [2] Su, Wei-Fang; Ho, Chun-Chih; Shih Tzu-Hsiang, Wang, Chen-Hua, Yeh, Chun-Hao, "Exceptional Biocompatibility of 3D Fibrous Scaffold for Cardiac Tissue Engineering Fabricated from Biodegradable Polyurethane Blended with Cellulose" *International Journal of Polymeric Materials and Polymeric Biomaterials*, 2016, 65, 703-711.

An Infrared System for Detection of Breast Cancer Based on Single Visit

Chung-Ming Chen¹, Ruo-Jhen Lin¹, Chi-En Lee¹ and Ching-Yen Lee¹

¹ Institute of Biomedical Engineering, National Taiwan University, #1, Sec. 1, Jen-Ai Road, Taipei 100, 3366-5274, Taiwan

1. Introduction

Screening is a commonly used approach for early detection of breast cancers, which has been generally believed to be an effective way to increase the survival rate. Although mammogram and breast sonogram have been widely employed for screening nowadays, both of them provide structure information only for breast cancers. On the other hand, breast infrared (IR) images, also known as breast thermogram, has been longtime considered as a potential functional imaging modality for breast cancers. Nevertheless, the role of breast thermogram remains controversial because of its high false positive rate and difficulty in interpretation.

To serve as an adjunct imaging modalities of mammogram and breast sonogram in breast cancer screening, in this paper, a dual-spectrum IR system was proposed to provide functional information for early detection of breast cancer. The unique idea of the proposed method was to characterize the existence of breast cancers based on the thermal information of the high-temperature tissue estimated from a long-wave IR (LIR) and a middle-wave IR (MIR) images, rather than based on the thermal patterns revealed by a single IR camera only.

2. Patients and Methods

With the approval of the Institutional Review Board of NTU hospital, 292 subjects were involved in this study, including 153 benign cases and 139 malignant cases with biopsy confirmation. All subjects were examined either by mammogram or breast sonogram following a routine protocol. In addition, an LIR and an MIR images were simultaneously captured for each subject by the dual-spectrum IR imaging system.

For each subject, the LIR and the MIR images were aligned based on the Thin-Plate Spline method. Following that, two feature maps were derived, namely, vascular map and qH map. The vascular map, which was computed from the LIR image based on the eigenvalues of the Hessian matrix of each pixel, characterized the structure and temperature information of breast vessels. The qH map, which was calculated from both LIR and MIR images using the Dual-Spectrum Heat Pattern Separation (DS-HPS) algorithm, revealed the heat pattern and energy distribution of the high-temperature tissue of a breast. Tens of descriptors had been devised from these two maps to distinguish the cancer subjects from the non-cancer subjects. The Support Vector Machine was used as the classifier.

3. Results and Discussions

Figure 1 demonstrated the vascular map derived by using the Hessian matrices of the LIR image, including the warped LIR image aligned to the MIR image, the vascular structure marked on the

LIR image, and the vascular structure alone.

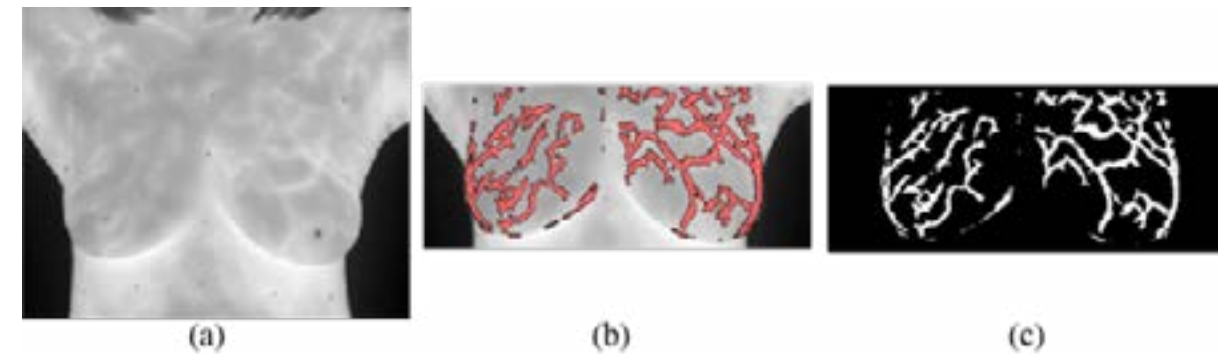


Fig. 1. Vascular map: (a) Warped LIR image; (b) vascular structures on the warped LIR image; (c) vascular structures of breast. Figure 2 showed the qH map derived by the DS-HPS algorithm. Specifically, Figs. 2(a) and 2(b) were the cropped ROIs of the registered LIR and MIR images. Figures 2(c) and 2(d) gave the qH and qN maps, which represented the heat contributions from the high-temperature and normal-temperature tissues, respectively.

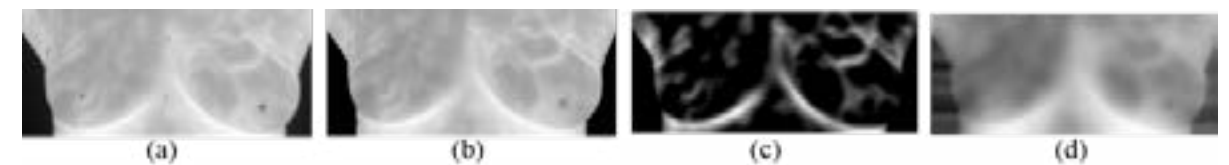


Fig. 2. Results of DS-HPS algorithm; (a) LIR image after registration; (b) MIR image after registration; (c) qH map; (d) qN map.

Based on the vascular map and qH map, varieties of features have been developed to describe the difference between the breasts of the cancer and non-cancer subjects. These features were basically designed to quantify the 7 types of information as illustrated in Fig. 3. The first one (Fig. 3(a)) was the heat distribution revealed by the LIR and MIR images. The second one (Fig. 3(b)) was the heat distribution enclosed by the qH mask, which was a binary representation of the qH map with a threshold of 0.02. The third one (Fig. 3(c)) was the heat distribution on the vascular structure defined by the vascular map. The fourth one (Fig. 3(d)) was the heat distribution of the vascular structure with the qH mask. The fifth one (Fig. 3(e)) was the qH mask. The sixth one (Fig. 3(f)) was the qH map. The seventh one (Fig. 3(g)) was the qH values on the vascular structure.

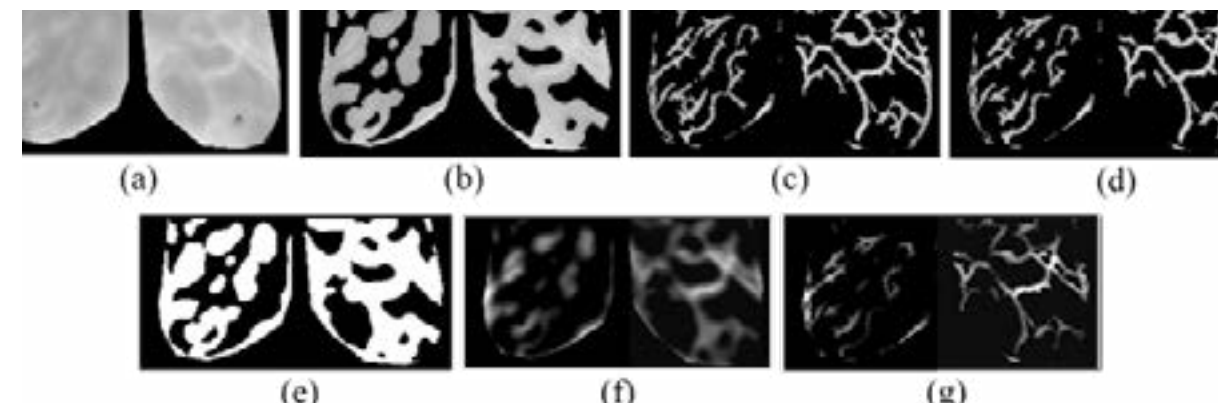


Fig. 3. (a) The heat distribution revealed by the LIR image; (b) the heat distribution enclosed by the qH mask; (c) the heat distribution on the vascular structure defined by the vascular map; (d) the heat distribution of the vascular structure with the qH mask; (e) the qH mask; (f) the qH map; (g) the qH values on the vascular structure.

To avoid the curse of dimensionality problem, feature selection has been carried out in this study based on the leave-one-out method. Three features were selected, including the maximum of the areas of the qH mask on both breasts, the difference of the mean values of both breasts in Fig. 3(c), and the difference of the mean values of both breasts in Fig. 3(g). By using SVM as the classifier, the AUC of the ROC curve was 0.91 and the best accuracy 86.3%. The sensitivity and specificity at the best accuracy were 77.0% and 94.8%, respectively. When specificity was 85.0%, the accuracy was 83.2% and the sensitivity 81.2%. When sensitivity was 85.0%, the accuracy was 82.9% and the specificity 81.4%. Compared to the conventional breast thermography, the proposed features are inherently more robust because derivation of the qH values has taken into account the physiological and environmental influences on the estimation of the heat emitted from the cancers.

Reference:

- [1] Bookstein FL. Principal warps: Thin-plate splines and the decomposition of deformations. *IEEE Trans PAMI* 1989; 11(6): 567-585.
- [2] Lee CY, et al. Dual-spectrum heat pattern separation algorithm for assessing chemotherapy treatment response and early detection. U.S. Patent No. 8,295,572, 2012.

Invited Speaker 20

Imaging Macrophages in vivo with Hemoglobin Fluorescence

Pei-Chun Wu^{1,2}, Yu-Fang Shen^{2,3}, Ming-Rung Tsai² and Tzu-Ming Liu^{1,2}

¹ Faculty of Health Sciences, University of Macau, Taipa, Macao SAR, China

² Institute of Biomedical Engineering & Molecular Imaging Center, National Taiwan University, 10617 Taipei, Taiwan

³ 3D Printing Medical Research Center, China Medical University Hospital, Taichung City 40447, Taiwan

1. Introduction

Macrophages are sentinels and regulators of the immune system. They play pivotal roles in attacking foreign insult and maintaining organismal homeostasis. Upon tissue damage or infection, they can engulf apoptotic cells and pathogens, produce immune effector molecules and regulate the immune dynamics for wound healing. At steady state, they are strategically located throughout the body for tissue surveillance. The absence or dysfunction of certain sub-types of macrophages may lead to tissue injury, auto-immune diseases, neurodegeneration¹, metabolic syndrome², or tumor metastasis^{3,4}. Therefore, understanding the mechanism how macrophages are recruited, infiltrate, and how they function in different contexts may provide useful insight to develop diagnosis methods and treatment strategies^{4,5}. To achieve this goal, the macrophages need to have fluorescence contrast to be observed in microscopy. For pre-clinical study, people can use transgenic mice and fluorescence labeling on surface markers of monocytes or phagocytic lysozyme to observe and track the activated macrophages. For clinical studies, a label free method is required. Except for protein markers, metabolic status could serve as alternative functional phenotypes to characterize macrophages. For example, people used multiphoton NADH/FAD fluorescence lifetime imaging microscopy (FLIM) to reveal the glucose metabolism in mitochondria and correlate them with the stage of cancer cells⁶. In the tumorigenesis process, the squamous cells underwent a metabolic switch from oxidative phosphorylation to glycolysis (Warburg's effect). Similar metabolic dynamics have been exploited to observe M1 macrophages.⁷ The activated macrophages exhibited increased glycolysis, accompanied by decreased oxygen consumption. Recently, the glucose metabolism of tumor-associated macrophages was characterized in vivo by multiphoton NADH/FAD FLIM⁸. Here we proposed another method to image macrophages through the hemoglobin they scavenged. The contrast came from the two-photon red fluorescence of hemoglobin. The macrophage can actively scavenging hemoglobin and keep them within for a long time. This can be used to observe the macrophage in bleeding environment.

2. Results

In a preliminary study, we found the hemoglobin red fluorescence ($\lambda = 620$ nm) can be selectively excited at 1100 nm [Fig. 1(a)]. At this wavelength, the two-photon excitation of most endogenous pigments like NADH or FAD can be greatly suppressed. Using this contrast, we have confirmed that cultured macrophage can scavenge the broken red blood cells and store the red fluorescent

hemoglobin, thus achieve the labeling of macrophages [Fig. 1(b)]. In an in vivo test of bleeding, we can also find these red fluorescence cells in the bleeding microenvironment [Fig. 1(c)]. These cells were resident for more than one week after bleeding. We believe they are macrophages taken up hemoglobin. Details about the validation will be reported in the presentation.

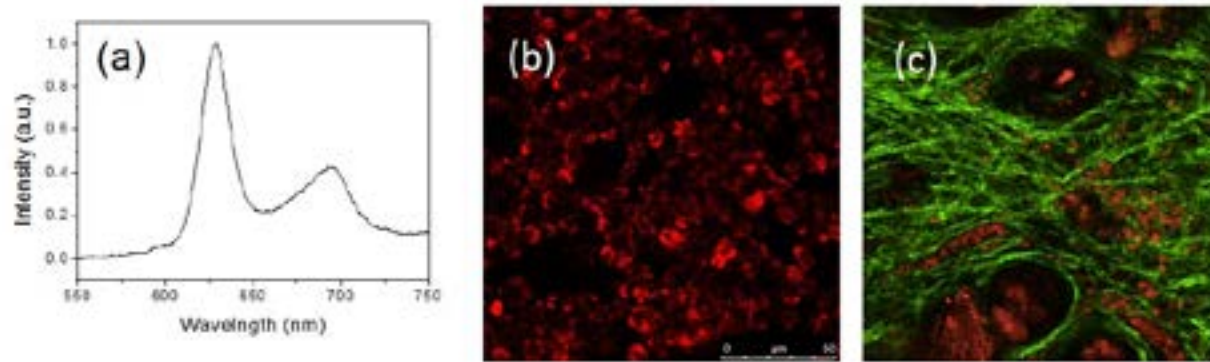


Fig. 1. (a) Two-photon fluorescence spectra of the hemoglobin excited at 1100 nm. (b) Two-photon red fluorescence microscopy of hemoglobin uptake by macrophages (RAW cell lines). (c) The in vivo imaging of bleeding microenvironment. Lots of red fluorescent cells reside in collagen networks (green). Fields of view of (c) : $240 \times 240 \mu\text{m}$.

Reference:

[1] H. Noseworthy, C. Lucchinetti, M. Rodriguez et al. "Multiple Sclerosis," *New England Journal of Medicine* 343, 938-952 (2000).
 [2] A. Chawla, K. D. Nauyen and Y. P. Sharon Goh. "Macrophage-mediated inflammation in metabolic disease," *Nature Review Immunology* 11, 738-749 (2011).
 [3] J. B. Wyckoff et al. "Direct visualization of macrophage-assisted tumor cell intravasation in mammary tumors," *Cancer Research* 67, 2649-2656 (2007).
 [4] A. Mantovani and P. Allavena, "The interaction of anticancer therapies with tumor-associated macrophages," *The Journal of Experimental Medicine* 212, 435-445 (2015).
 [5] Y. Luo et al. "Targeting tumor-associated macrophages as a novel strategy against breast cancer," *The Journal of Clinical Investigation* 116, 2132-2141 (2006).
 [6] M. C. Skala et al. "In vivo multiphoton microscopy of NADH and FAD redox states, fluorescence lifetimes, and cellular morphology in precancerous epithelia," *Proceeding of the National Academy of Sciences of the United States of America* 104, 19494-19499 (2007).
 [7] B. Kelly and L. A. J. O'Neill. "Metabolic reprogramming in macrophages and dendritic cells in innate immunity," *Cell Research* 25, 771-784 (2015).
 [8] J. M. Szulczewski et al. "In Vivo Visualization of Stromal Macrophages via label-free FLIM based metabolite imaging," *Scientific Reports* 6, 25086 (2016).

Invited Speaker 21

Hyperspectral Imaging in Thick Tissues via Optical Sectioning Microscopy

Szu-Yu Chen^{1*}, Yu John Hsu¹, Chih-Chiang Chen² and Chien-Hsiang Huang¹

¹Department of Optics and Photonics, National Central University, 300 Zhongda Road, Zhongli, Taoyuan, Taiwan, R.O.C

²Department of Dermatology, Taipei Veterans General Hospital, No.201, Sec. 2, Shipai Rd., Taipei, Taiwan, R.O.C.

Abstract

To eliminate the off-focus fluorescence signals, the concept of structured illumination optical sectioning microscopy is combined with line-scanning hyperspectral microscopy. With this system, the hyperspectral information of thick turbid specimens such as an intact leaf and mouse skin can be obtained with high axial contrast.

1.Index Terms

Fluorescence microscopy, Multispectral and hyperspectral imaging, Scanning microscopy.

2.INTRODUCTION

Hyperspectral microscopic studies have been flourishing in recent years, not only it has been used in geological observations such as earth science, but has also been widely utilized in material science, physics, semiconductor industries, and biomedical studies. By applying hyperspectral microscopy in biological researches, it provides the ability to obtain spectral information of molecular structures in tissues. The concept of hyperspectral imaging can be implemented in various microscopic systems, such as wide-field, confocal, or two-photon microscopy. Being compared to a scanning-based hyperspectral microscopy, the wide-field hyperspectral microscopy provides a much higher acquisition rate. However, the applications of wide-field hyperspectral microscopy are limited in thick specimens due to the lack of the axial resolution. To compromise the acquisition rate and the axial resolution, in this research, a structured illumination optical sectioning microscopy based on digital light processor (DLP) [1] was combined with a parallel-recording hyperspectral detection system. The hyperspectral imaging of intact leaves was successfully demonstrated to show the ability of this system for thick specimen applications.

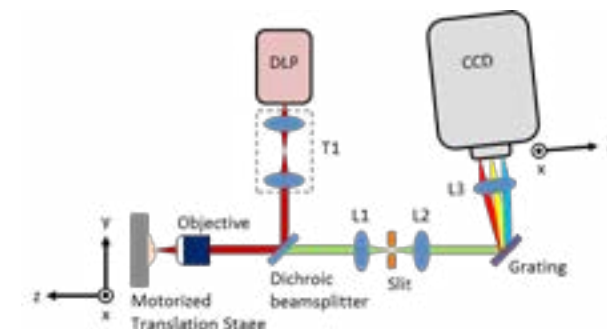


Fig. 1. DLP-projector-based structure illumination optical sectioning microscopic system.

3.RESULTS AND CONCLUSIONS

The system setup is shown in Fig.1. Utilizing a parallel-recording detection system, the DLP projects a line-shape structured illumination light onto the specimen along the x-direction. The line-shape excited fluorescence signals are first gathered by an objective and by utilizing a grating afterwards, the spectra (λ) of the fluorescence signals are unfolded through an imaging system, the 2-dimensional image of x-axis spatial information and λ -axis spectral information are then obtained by a 2-D sCMOS, and by scanning the specimen in the y-direction using a translation stage, an x-y- λ hyperspectral image can then be accomplished. To apply the structured illumination optical sectioning for the reduction of off-focus signals, a sequenced hyperspectral images I1, I2, and I3 with structured illumination patterns of three equally-spaced phases, 0, $2\pi/3$, and $4\pi/3$ should be acquired [1]. By continuously repeating the above procedure at various depths inside the specimen, a reconstruction of a four dimension hyperspectral image, consisting 3D spatial information and a single dimension of spectral information is therefore achieved. Using an intact leaf as specimen, an x- y image with illumination pattern is shown in Fig. 3(a). After image reconstruction, the optical sectioning image of the mesophyll cells at 685 nm is shown in Fig. 3(b). Combined with structured illumination, the off-focus fluorescence signals are shown to be reduced.

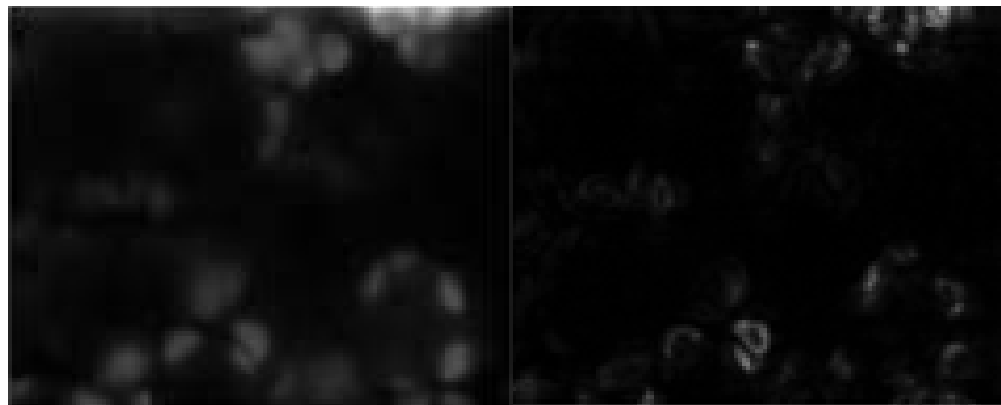


Fig. 3. (a) Image of x-y with illumination pattern (b) Reconstructed optical sectioning image

In contrast to the wide-field hyperspectral microscopy [3], this system shows its capability for thick-specimen applications based on its high axial resolution. Compared to the laser scanning hyperspectral microscopy [4], parallel recording geometry provides the benefit of increasing the acquisition rate.

Reference:

- [1] Chen, S. Y., Hsu, Y. J., Yeh, C. H., Chen, S. W., & Chung, C. H. "Pico-projector-based optical sectioning microscopy for 3D chlorophyll fluorescence imaging of mesophyll cells." *Journal of Optics*, 17(3), 035301. (2015)
- [2] Dan, D., Lei, M., Yao, B., Wang, W., Winterhalder, M., Zumbusch, A. & Zhao, W. "DMD-based LED-illumination Super-resolution and optical sectioning microscopy." *Scientific reports* 3 (2013).
- [3] Roger A. Schultz, Thomas Nielsen, Jeff R. Zavaleta, Raynal Ruch, Robert Wyatt, & Harold R. Garner. "Hyperspectral Imaging: A Novel Approach For Microscopic Analysis." Wiley-Liss, Inc. (2001).
- [4] Michael D. Malik, Patrick J. Cutler, Jason M. Byars, & Keith A. Lidke "Multicolor Super-Resolution Imaging using a Laser Line Scanning Hyperspectral Microscope." *Biophysical Journal* (2011).

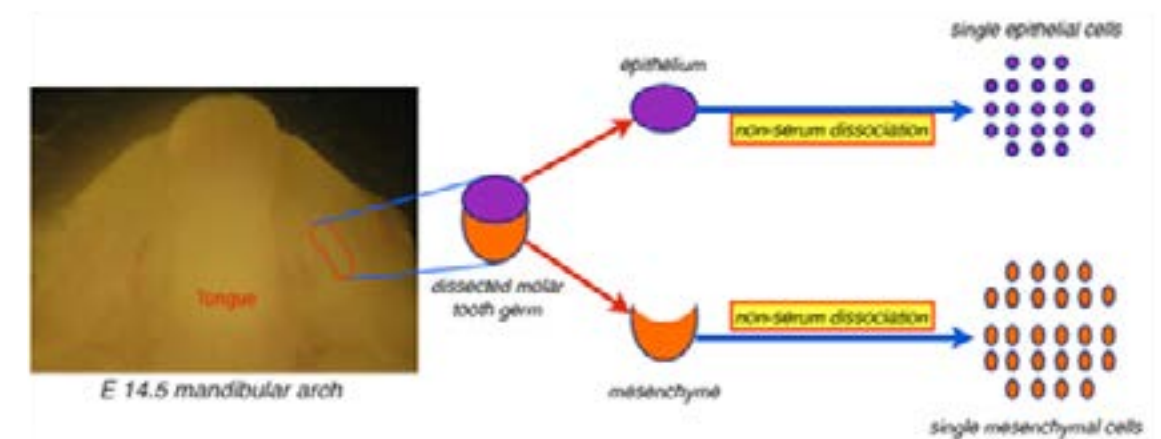
Invited Speaker 22

Electric Cell-substrate Impedance Sensing for Real Time Investigation of Epithelial-Mesenchymal Interactions

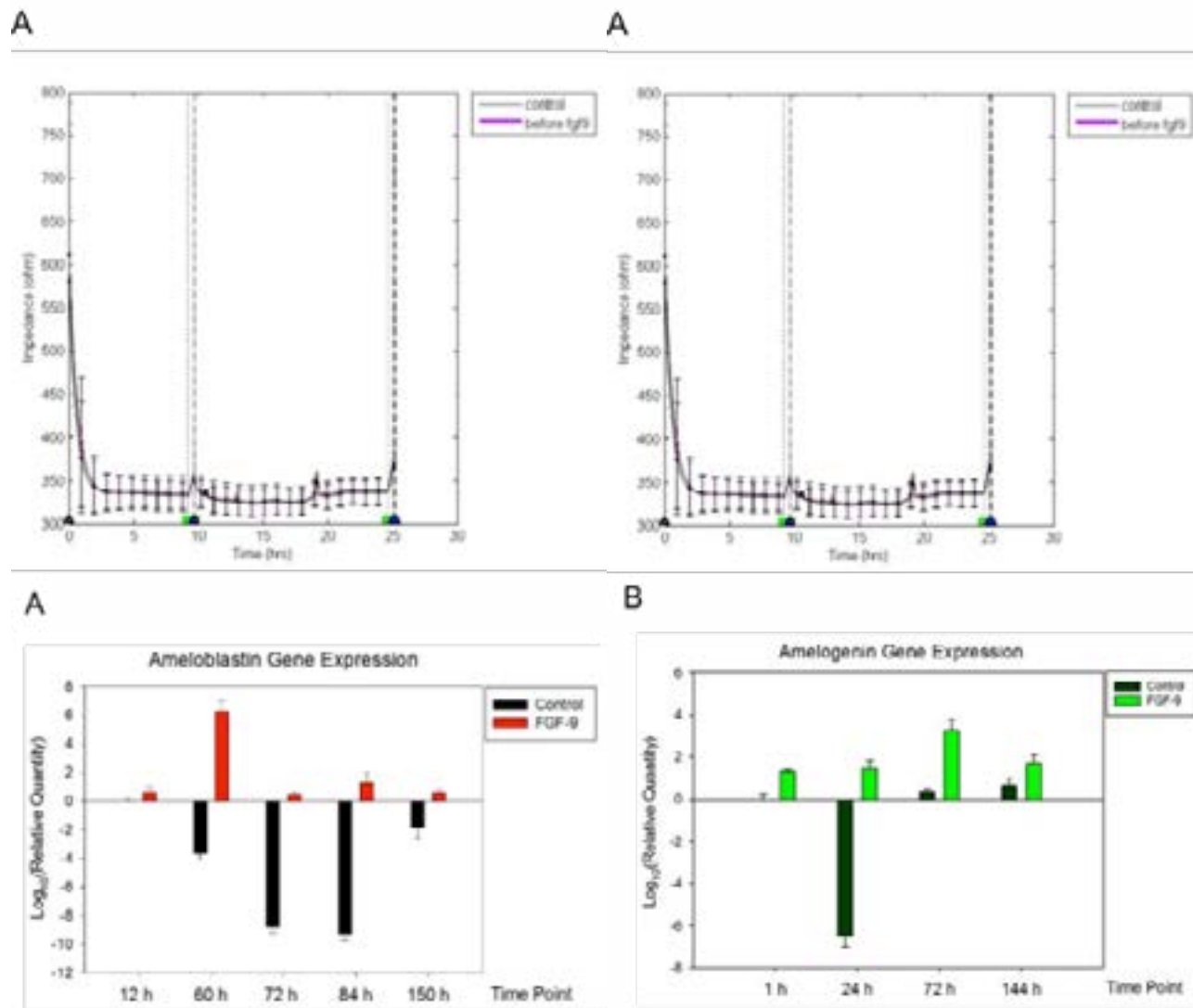
Min-Huey Chen

Graduate Institute of Clinical Dentistry, School of Dentistry, National Taiwan University, Taiwan R.O.C.

Tooth development is originated from the cross-talk between embryonic epithelial cells and mesenchymal cells which is similar to other organs. Therefore, the most meaningful goals of tooth regeneration is to find the important mechanism of interactions between epithelial cells and mesenchymal cells and to build up the study model for other organ regeneration. Electric cell-substrate impedance sensing (ECIS) is a real-time, label-free, impedance-based method to study the activities of cells grown in tissue culture previously. Objectives: The purposes of this study is to set up a dynamic model for investigating epithelial-mesenchymal interactions (time for epithelial invagination) during tooth development by using ECIS and also investigate and the effects of FGF-9. Methods: The epithelium and mesenchymal cells were separated from the tooth germs and seeded in the transwells. ECIS was used for investigating these epithelial-mesenchymal interactions and the effects of FGF-9 on the time for epithelial invagination. The odontogenic genes expressions were also investigated. Results: Our results demonstrated that by using ECIS, epithelial-mesenchymal interactions can be observed and the time for epithelial invagination can be identified. We also found that by adding FGF-9, the time for epithelial invagination was reduced. Our results also showed the effects of FGF-9 in increasing the odontogenic gene expression in dental mesenchymal cells. Conclusion: This study demonstrated that ECIS is a good system for real time investigation of epithelial-mesenchymal interactions. The effects of FGF-9 in promoting tooth development and differentiation of dental mesenchymal cells were also confirmed. ECIS is a good system for investigating the factors in promoting epithelial-mesenchymal interactions and can be applied for further studies in tooth regeneration and ectodermal organogenesis.



Tooth germs were dissected from E14.5 mouse embryos and dissociated into single cells using non-serum protocol

**Reference:**

- [1] Pispá J, Thesleff I: Mechanisms of ectodermal organogenesis. *Dev. Biol* 2003, 262:195–205.
- [2] Hu B, Nadiri A, Küchler-Bopp S, Perrin-Schmitt F, Lesot H: Dental epithelial histomorphogenesis in vitro. *J. Dent. Res.* 2005, 84:521–525.
- [3] Honda MJ, Tsuchiya S, Sumita Y, Sagara H, Ueda M: The sequential seeding of epithelial and mesenchymal cells for tissue-engineered tooth regeneration. *Biomaterials* 2007, 28:680–689.
- [4] Nakao K, Morita R, Saji Y, Ishida K, Tomita Y, Ogawa M, Saitoh M, Tomooka Y, Tsuji T: The development of a bioengineered organ germ method. *Nature Methods* 2007, 4:227–230.
- [5] Oshima O, Ogawa M, Yasukawa M, Tsuji T: Generation of a Bioengineered Tooth by Using a Three-Dimensional Cell Manipulation Method (Organ Germ Method). In *Odontogenesis: Methods and Protocols, Methods in Molecular Biology*. Volume 887. Edited by Kioussi C. Springer Science+Business Media, LLC; 2012:149–165.
- [6] Pispá J, Thesleff I: Mechanisms of ectodermal organogenesis. *Dev. Biol.* 2003, 262:195–205.
- [7] Tucker AS, Sharpe PT: The cutting-edge of mammalian development; How the embryo makes teeth. *Nat. Rev. Gen.* 2004, 5:499–508.
- [8] Kettunen P, Thesleff I: Expression and function of FGFs-4, -8, and -9 suggest functional redundancy and repetitive use as epithelial signals during tooth morphogenesis. *Dev. Dyn.* 1998, 211:256–268.
- [9] Keese CR, Bhawe K, Wegener J, Giaever I: Real-time impedance assay to follow the invasive activities of metastatic cells in culture. *Biotechniques* 2002, 33:842–844, 846, 848–850.

The Application of Quantitative Interferometric Imaging in Sickle Cell Disease

Peter T. C. So, Poorya Hosseini, Sabia Abidi, E Du, Dimitrios Papageorgiou, Youngwoon Choi, YongKeun Park, John Higgins, Gregory Kato, Subra Suresh, Ming Dao, and Zahid Yaqoob

Hydroxyurea (HU) has been used clinically to reduce the frequency of painful crisis and the need for blood transfusion in sickle cell disease (SCD) patients. However, the mechanisms underlying such beneficial effects of HU treatment are still not fully understood. Studies have indicated a weak correlation between clinical outcome and molecular markers, and the scientific quest to develop companion biophysical markers have mostly targeted studies of blood properties under hypoxia. Using a common-path interferometric technique, we measure biomechanical and morphological properties of individual red blood cells in SCD patients as a function of cell density, and investigate the correlation of these biophysical properties with drug intake as well as other clinically measured parameters. Our results show that patient-specific HU effects on the cellular biophysical properties are detectable at normoxia, and that these properties are strongly correlated with the clinically measured mean cellular volume rather than fetal hemoglobin level. The development of next generation interferometric imaging with molecular specificity that can quantify hemoglobin concentration in sickle red blood cells will be discussed.

Poster Presentation Titles

1. Non-scanning In-vivo three-dimensional structured illumination microscopy

Chen-Yen Lin

2. Nano patterning control human adipose stem cell (hASC) differentiation

Chen-Yen Lin

3. Evaluation of Adhesion, Proliferation and Differentiation of Human Adipose-derived Stem Cells on Keratin Biomaterials

Che-Wei Lin

4. All-Optical Physiology Based on Fast Volumetric Imaging

Chiao-Huang

5. Neural Tissue Engineering through Modulated Magnetic Field and Aligned Neurotransmitted Scaffold

Chia-Yu Lin

6. Altered microstructural integrity in patients with tuberous sclerosis complex revealed by whole brain tract-specific analysis

Chien-Feng Huang

7. 3D Imaging of Hematoxylin and Eosin Stained Thick Tissues with a Sub-Femtoliter Resolution by Using Cr:forsterite-laser-based Nonlinear Microscopy

Chien-Ting Kao

8. Altered microstructural integrity of the white matter tracts in children with aromatic L-amino acid decarboxylase: A systematic tract-specific analysis using diffusion MRI

Chih-Hsien Tseng

9. Automated Analysis of Functional Connectome Images

Chi-Huan Chiang

10. Human Adipose Stem Cell Spheroid Forming on Glycol Chitosan and Gelatin Hydrogel

Ching-Cheng Tsai

11. High Speed 3D Functional Imaging of Living Brain

Chi-Wei Liu

12. Combining Magnetic Nanoparticles with Monocyte Chemoattractant Protein-1 (MCP-1) as the Targeting Tool for Atherosclerosis

Chung-Wei Kao

13. Plasmonic SAX microscopy in deep tissue

Gitanjal Deka

14. Sub-20-nm spatial resolution based on saturation excitation (SAX) microscopy with an appropriate nonlinear response

Hou-Xian Ding

15. To Reveal the Recognition between C-Reactive Protein and Phosphorylcholine by Quartz Crystal Microbalance

Jhih-Guang Wu

16. A new method for synapse capture by electrostatic interaction for epifluorescence and super-resolution microscopy

Jia-Fong Jhou

17. Comparison of Cell Behaviour on Nanofibrous Surface with Different Orientation Properties

Kao-Chun Tang

18. Fabrication of Uniform Pore Size Scaffolds And Its Influence Toward Adipose-Derived Stem Cells Chondrogenic Ability

Kuan-Han Wu

19. Deep brain imaging in Drosophila by 3-photon excitation

Kuo-Jen Hsu

20. Optical Biopsy of Melasma for Diagnosis Decision Using in Vivo non-invasive Harmonic Generation Microscopy

Ming-Liang Wei

21. Polyimide/amino-silica mixed matrix membranes for gas separation

Po-Hsiu Cheng

22. Cu@polymer Nano-template for the Preparation of Drug Nano-vesicle as a Promising Photodynamic Therapeutic

Po-Ting Wu

23. CREATION OF CELL-DERIVED EXTRACELLULAR MATRIX OF BOTH RANDOM AND ALIGN ECM SCAFFOLD AS A TEMPLATE FOR VASCULAR TISSUE ENGINEERING

Shing-Tak Li

24. Whole brain tract-based automatic analysis of white matter changes in anisometropic amblyopia

Su Edward

25. In Vivo Deep-tissue Super-resolution Imaging of Motor Axon with Two-Photon SAX Microscopy

Tian You Cheng

26. Endoscopy Embedded with Focus Tunable Dielectric Liquid Lens

Wei-Min Cheng

27. Biomaterial Scaffolds for Neurogenesis

Yen-Yu Chang

28. High Spatio-Temporal-Resolution Detection of CF Dynamics from a Single Chloroplast with Confocal Imaging Fluorometer

Yi-Chin Tseng

29. Synthesis of Four Stereoisomers of 4-(3-Fluoropropyl)-glutamate for Quality control of 18F-FSPG in Clinical Trials

Yun-Ning Tseng

#1

Non-scanning In-vivo three-dimensional structured illumination microscopy

Chen Yen Lin^{1,2}, Ju-Hsuan Chien² and Yuan Luo^{2,4}

¹Department of Electrical Engineering and Graduate Institute of Photonics and Optoelectronics, National Taiwan University, Taipei 10617, Taiwan

²Institute of Medical Device and Imaging, National Taiwan University, Taipei, 10051, Taiwan R.O.C

³School of Medicine, National Taiwan University, Taipei, 10051, Taiwan R.O.C

⁴Molecular Imaging Center, National Taiwan University, Taipei, Taiwan 100

Abstract

Structured illumination microscopy equipped with a physical grating provides an optically sectioned image through wide field approach. In term of acquisition time, the speed has become a limitation. In order to investigate in vivo sample, a non-scanning structured illumination microscope with the optical sectioning capability is implemented with a digital micro device and a focus tunable lens to structure the illumination pattern and conduct an optical scanning by shifting focal plane of the objective lens across the sample. The digital micro-mirror device (DMD) and the focus tunable lens (FTL) both have the fast frame rate and quick response time. The focus tunable lens is conjugate to the aperture stop of a microscope objective to ensure a fixed magnification, contrast and resolution during an axial scanning. By utilizing a DMD and a focus tunable lens, the microscopic system can provide a quick 3D imaging of the biological specimen and acquire optically sectioned images by using HiLo principle in image reconstruction [1-2]. In this work, a three dimensional optical sectioning imaging modality is evaluated and characterized through a 3D imaging of the mixed pollen grain and *Caenorhabditis elegans* as shown in Fig. 1.

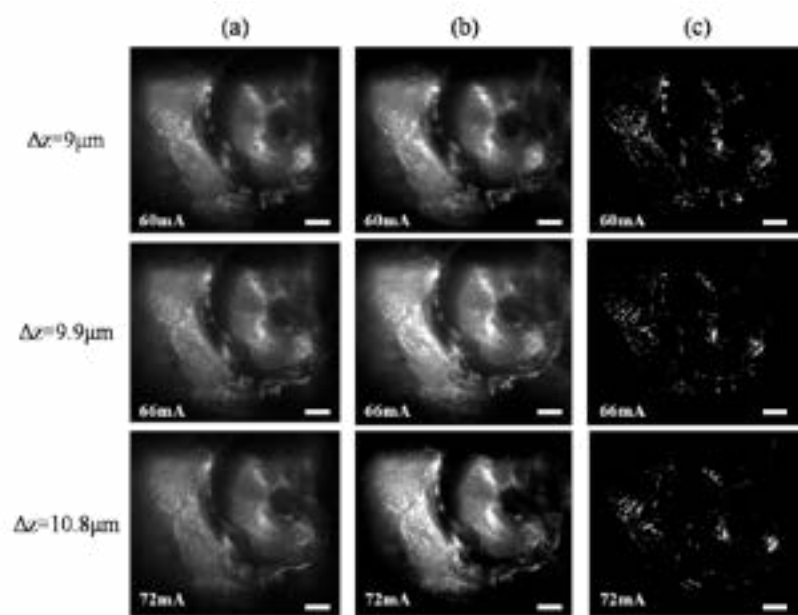


Fig. 1. (a) multiple uniform illumination image planes at different depths within a *C. elegans*. (b) corresponding structured illumination image. (c) processed images at three different depth, $\Delta z = 9, 9.9\mu\text{m}$, and $10.8\mu\text{m}$ within a sample. Column figure (c) shows the growth cone and nervous fiber inside the worm is clearly resolved.

We demonstrate the advantages of adopting the DMD and FTL into a conventional wide field experiment. The DMD provides a flexible way to adopt a suitable structured illumination pattern for the biological sample and change the pattern without any moving part. The focus tunable lens offers a rapid scanning along the axial direction and causes no disturbance to the sample. A relay lens in our system maps the aperture stop of the objective lens onto the FTL so that the system magnification becomes constant during the full scanning range.

Reference:

- [1] T. N. Ford, C. Hourtoule, A. C. Bartoo, S. K. Singh, and J. Mertz, "Optically sectioned fluorescence endomicroscopy with hybrid-illumination imaging through a flexible fiber bundle," *J. Biomed. Opt.* 14(3), 030502 (2009).
- [2] C. Y. Lin, W. T. Lin, H. H. Chen, J. M. Wong, V. R. Singh, and Y. Luo, "Talbot multi-focal holographic fluorescence endoscopy for optically sectioned imaging," *Opt. Lett.* 41, 344-347 (2016)

Nano patterning control human adipose stem cell (hASC) differentiation

Chen-Yu Tsai¹, Zhi-Wei Zhao¹ and Jia-Shing Yu¹

¹ Department of Chemical Engineering, National Taiwan University, Taipei, Taiwan.

Abstract

Biophysical cues (e.g., patterns, flexibility and porosity of the cell culture substrates) have been seen as a potential approach to control the modulation of cell behavior. Topography on the substrate like grooves can guide stem cells fate and lead to various cell types. This study devoted to investigating the potential of topography on the differentiation of human adipose-derived stem cells (hASCs) into osteogenic lineage. Different patterns were fabricated on the silicon wafer by lithography, and stamped on the soft substrates such as gelatin. Most of previous work used synthetic materials like PS or PDMS. It was not bio-friendly and may cause some problems on cell adhesion. However, gelatin was chosen as our substrate for its good biocompatibility and biodegradability. Otherwise, hydroxyapatite (HAp) nanoparticles were also added into gelatin to enhance osteogenic differentiation, a core-shell nanostructure as the core and organic alginate as the shell (HAp@Alg) was synthesized due to its good dispersion in aqueous solution. [4] We could further control its degradation by regulating degree of cross-linking with different cross-linker. Hence, our patterned gelatin could be used to guide cell growth and naturally degraded.

1. INTRODUCTION

In tissue engineering field, regulation of cell behavior in a predictable way is desired. One approach to achieve it is to modulate the extracellular conditions by controlling biomaterial surface characteristics. Topographic cues of micro or nano pattern is attractive in many applications, especially for guiding stem cells differentiation. [1]

With the trend of aesthetic medicine, more and more people had various surgeries to make them more slim and appealing. Among those surgical operations, liposuction was one of the most well-developed and popular operations. However, those lipoaspirates contained abundance of hASCs and supplied a sufficient source of adult stem cells. Hence, stem cells related studies have become increasingly popular. [2]

In this work, to fabricate topography on the substrates, we take advantage of gelatin to construct patterns due to its good biocompatibility and biophysical properties. With such topographic cues, we can efficiently control the modulation of osteogenic differentiation of hASCs.

2. MATERIALS AND METHODS

Preparation of patterned surfaces

Pattern such as groove width/depth (nm): 400/400 was fabricated on silicon wafer primarily by lithography. Silicon substrates were cleaned in piranha solution (H₂O/H₂SO₄), silanized using 1% (v/v) octadecyltrichlorosilane/isooctane, and used as a template to replicate PDMS molds. PDMS mold was fixed on the petri dish. 5% gelatin aqueous solution was added and submerged the mold. After air-drying it at R.T. overnight to solidify, gelatin film was immersed in the ethanol-water

mixture (8:2), which containing 50mM ethyl(dimethylaminopropyl) carbodiimide (EDC) and 10mM N-Hydroxysuccinimide (NHS) for 96 hr. Finally, release the mold and rinse the gelatin film with DI water, patterned gelatin films were made. Surface topography of grooved substrates was characterized by atomic force microscope (AFM) using a tapping model with scanning rate of 0.5 Hz and scanning area of 5 x 5 μm. To improve the dispersion of HAp in aqueous solution, we synthesize HAP@Alg to cover HAp nanoparticles with negative charged alginate. Hence, HAP@Alg will disperse well in aqueous solution due to electrostatic force.

Culture and differentiation of hASCs

All related medium were prepared according to the human adult stem cell manual from ZenBio, Inc. [3] To cryopreserve hASCs, place approximately 6.7 x 10⁵ cells in T-75 culture flasks using PM-1. Incubate cells until they are 85-90% confluent. Aspirate medium and wash adult stem cells 4-5 times using sterile PBS to remove all traces of serum. Remove the PBS and release the cells from the flask bottom by adding 2 mL/T-75 flask of 0.25% trypsin/ 2.21mM EDTA solution. Allow cells to trypsinize for 5 min at 37°C. Neutralize the trypsin using 7 ml PM-1 per T-75 flask. Place in a humidified incubator at 37°C and 5% CO₂. For differentiation of hASCs into osteoblasts, remove cells from liquid nitrogen and place immediately into a 37°C water bath and agitate while in bath. Upon thawing, transfer the cells to a sterile conical bottom centrifuge tube containing 10 ml of Preadipocyte Medium (PM-1). Centrifuge: 1,200 rpm (282 x g) / 20°C / 5 min. Aspirate the supernatant. Plate approximately 3,000 cells / cm² and place in a humidified 37°C incubator with 5% CO₂. Add the appropriate volume of Osteoblast Differentiation Medium (OB-1) to the wells. Incubate cells at 37°C and 5% CO₂. Feed cells every 3 days with Osteoblast Differentiation Medium (OB-1).

3. RESULTS

Patterned gelatin films

The AFM image of patterned gelatin film was showed in Fig. 1. Patterns on silicon wafer were successfully stamped to the substrate surface. Due to the fragile property of gelatin, PDMS molds had better be thinner to release easily.

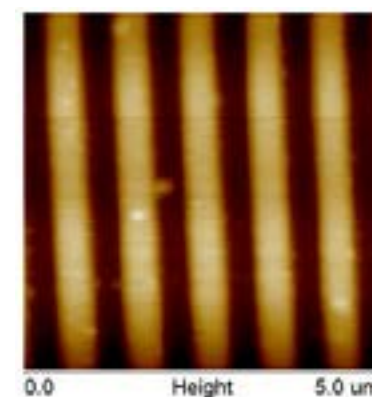


Fig. 1. AFM image of patterned gelatin film

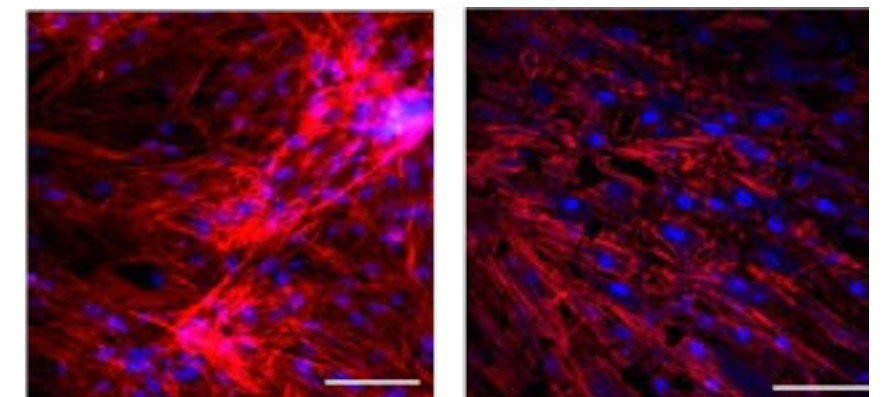


Fig. 1. 2D and 3D images of osteoblasts morphology after 14 days culturing. Scale bar = 100 μm

Osteogenic differentiation of hASCs

The expected differentiation results were showed in Fig. 2. hASCs were affected by topographic cues from patterned gelatin films and HAp and differentiated into osteoblasts. However, the actual results were to be done.

4. CONCLUSIONS

The importance of topographic cues on cell behavior has been recognized. While related studies focused on other stem cells such as mesenchymal stem cell (MSC), this study chose hASCs as cell source. The other point is that gelatin films offered a cell-friendly environment to cells, prevented cells from toxic chemicals. The results suggested that the differentiation of hASCs was associated with the patterns on substrates and the lineage destination.

Reference:

- [1] Peng-Yuan Wang, Wen-Tyng Li, Jia-Shing Yu, Wei-Bor Tsai (2012) Journal of Materials Science: Materials in Medicine 23:3015-3028
- [2] Ammar T. Qureshi, Cong Chen, Forum Shah, Caasy Thomas-Porch, Jeffrey M. Gimble, Daniel J. Hayes (2014) Methods in Enzymology Volume 538, pp.67-88
- [3] ZenBio, Inc. Human Adult Stem Cell Manual ZBM0015.01
- [4] Yung-He Liang et al. (2012) ACS Appl. Mater. Interfaces 4, 6720-672

#3

Evaluation of Adhesion, Proliferation and Differentiation of Human Adipose-derived Stem Cells on Keratin Biomaterials

Che-Wei, Lin¹ and Jia-Shing, Yu²

¹Institute of Biotechnology, National Taiwan University, Taipei, Taiwan

²Department of chemical engineering, National Taiwan University, Taipei, Taiwan

Abstract

Controlled adhesion and continuous growth of human adipose stem cells (hASCs) are essential to the delivery of hASCs on films in tissue engineering applications. The main goal of this study is to develop keratin substrates to actively control adhesion and proliferation of hASCs. Keratin, isolated from human hair, gained researchers' interests due to its intrinsic ability to interact with different cells. Keratin has the potential to serve as a controllable extracellular matrix protein and can be used to demonstrate cell mechanism and cell matrix interaction. However, the effects of keratin on stem cells have not been reported. In the present study, the effects of keratin on human adipose-derived stem cells (hASCs) were demonstrated. Relative to untreated culture plates, results showed that keratin coating substrates promoted cell adhesion and proliferation to above cell lines. Keratin also improved hASCs adhesion, proliferation, and enhanced cell viability. Evaluation of gene markers and protein levels showed that adipogenic, osteogenic and chondrogenic differentiations of hASCs can be successfully induced, which revealed that keratin did not influence the stemness of hASCs. In addition, keratin improved adipogenic differentiations in terms of up-regulations in lipoprotein lipase, peroxisome proliferator-activated receptor gamma and CCAAT-enhancer binding protein alpha. The osteogenic markers: type I collagen, runt-related transcription factor 2, and vitamin D receptor were also up regulated on keratin substrates. The chondrogenic marker SOX9 was also up-regulated on keratin coating. Therefore, keratin can serve as a biologically derived material for surface modification for biomedical purposes. The combination of keratin with stem cells may be a potential candidate for tissue repair in the field of regenerative medicine.



Fig. 1. Preparation of keratin solution extracted from human hair

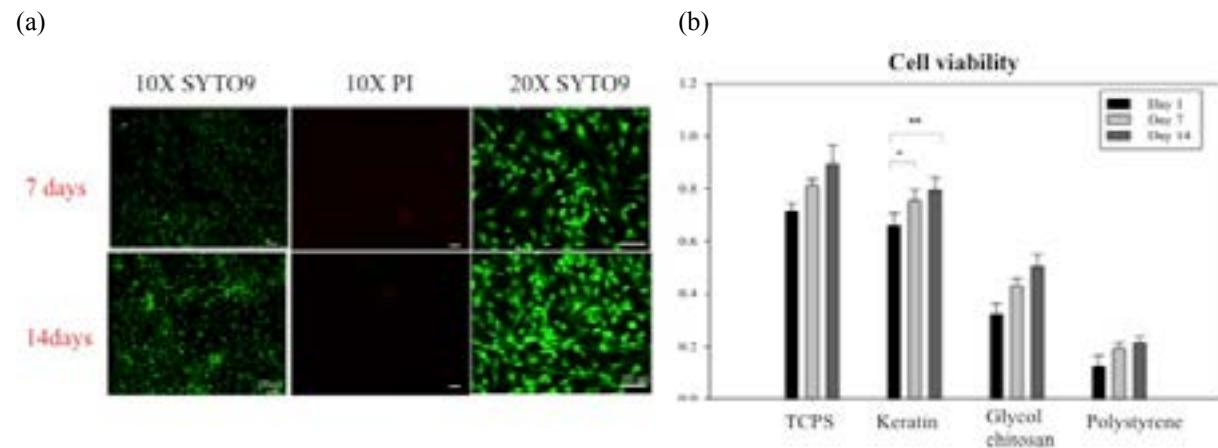


Fig. 2. (a) Fluorescence images of LIVE/DEAD assay on day 7 and day 14. Encapsulated human adipose stem cells were stained with SYTO® 9(live) and Propidium Iodide (dead) viability staining kit (Life Technologies). Live cells were stained in green while dead cells were stained in red. (b) MTT assay of hASCs on keratin coating, glycol chitosan and polystyrene plates.

1. Results

Figure 1. The keratin used in this study was extracted from human hair based on Shindai method with slight modification. Hair was washed with detergent and reacted with chloroform/methanol to remove external lipid. The dry, de-oiled hair was pulverized with liquid nitrogen to get hair powder. The hair powder was mixed with extraction medium (25 mM Tris, pH 8.5, 2.6 M thiourea, 5 M urea, and 5% 2-mercaptoethanol) at 50°C for 72 h. The solution was filtered to remove hair sludge and the filtrate was storage at -20°C. The filtrate was thawed and centrifuged at 4500g to remove coarse aggregates. The Shindai extract was exhaustively dialyzed against demin-eralized water using a MWCO 10000 Da dialysis cassette for 12 h.

Figure 2. The result of Live/Dead Fluorescence assay and MTT assay showed that keratin biomaterials demon-strated a better ability of cell adhesion and proliferation with healthier morphological signs for hASCs than poly-styrene cell culture cluster.

2. onclusion

In conclusion, keratin biomaterials derived from human hair hold great potential serving as bioactive scaffolds for stem cells investigation. We deduce this composite matrix possibly can enhance host cell growth and may help tissue regeneration by differentiation of stem cells. Future study in vivo as well as human stem cell (both in vitro and in vivo) shall be carried out in order to bring not only scientific but also clinical significance.

Reference:

- [1] Nakamura, A., et al., Biol Pharm Bull, 2002. 25(5): p. 569-72.
- [2] Reichl, S., Biomaterials, 2009. 30(36): p. 6854-663.
- [3] Hill, P., H. Brantley, and Van Dyke, M., Biomaterials, 2010. 31(4): p. 585-93.
- [4] Anderson, J.M., A. Rodriguez, and D.T. Chang, Semin Immunol, 2008. 20(2): p. 86-100.

#4

All-Optical Physiology based on Fast Volumetric Imaging

Chiao Huang,¹ Kai-Ping Yang,¹ and Shi-Wei Chu^{1,2}

¹Department of Physics, National Taiwan University, 1, Sec 4, Roosevelt Rd, Taipei 10617, Taiwan

²Molecular Imaging Center, National Taiwan University, 1, Sec 4, Roosevelt Rd, Taipei 10617, Taiwan

Electrophysiology is widely used in neurosciences study, with major disadvantages of invasive operation, difficulty of recording multiple neurons in a very small volume and repetitive measurement of the same neuron. In contrast, all-optical physiology, which manipulates and records neuron signal with light, is a non-invasive tool with the advantages of high spatial resolution and potential multi-point recording capability¹. Because of the small size ($\sim\mu\text{m}$) and fast response ($\sim\text{ms}$) of neurons in complex 3D brain structures, it is necessary to develop suitable tools with high spatiotemporal resolution and fast volumetric recording ability. Volumetric imaging achieved by axial translation of sample or objectives is limited in the speed due to inertia. To increase scanning speed, it could be reached by partial sampling strategies such as random access microscopy² or spatial light modulators³. However, sample stability is highly demanded for these methods, which is very difficult for in vivo study. Other 3D imaging methods such as light-field microscopy⁴, light-sheet microscopy⁵ are also suffered from the limited penetrated depth and only applicable to transparent sample. For the requirement of full sampling and large penetration depth in opaque sample, fast axial scanning combined with multiphoton microscopy is desired. Compared to single-photon microscopy, multiphoton microscopy provides larger penetration depth due to less scattering of longer wavelength laser. Our system, which combined the two-photon microscopy and tunable acoustic gradient-index (TAG) lens, is most suitable for *Drosophila* in vivo neuron study. The principle of TAG lens is to change the refractive index distribution in lens by acoustic standing wave caused from resonance in lens media. Combined with objectives, the focus will move periodically in axial direction with high speed, providing fast axial scanning up to hundreds of kilohertz⁶. In addition to significantly reduced acquisition time of volume imaging, full sampling also tolerates the spatial instability of live *Drosophila*. Under monitoring through all-time, we can make sure every signal peak of neurons comes from neural firing but not sampling moving. By integrated with all-optical physiology, we can simultaneously stimulate and record the neurons. Our system provides fast volumetric dynamics of neuron response in several tens of micron depth, therefore it is more efficient compared to typical optical section imaging, which limits the observation in different depth of neuron structure.

Our results are shown in Fig. 1. With our system, we could observe the connectome in vivo with three-dimensional information of neuron response. In Fig. 1 (a), the dendrite response in focal plane was weak while without TAG lens. However, with TAG lens, as shown in Fig. 1 (b), the response got stronger, indicating that neuron dynamics was distributed over three dimension.

In conclusion, our technique, as a non-invasive method, allowed us to investigate 3D neural dynamics in live genetically-encoded *Drosophila* brain with fine spatiotemporal resolution, which is a powerful and innovative tool in neuron science research.

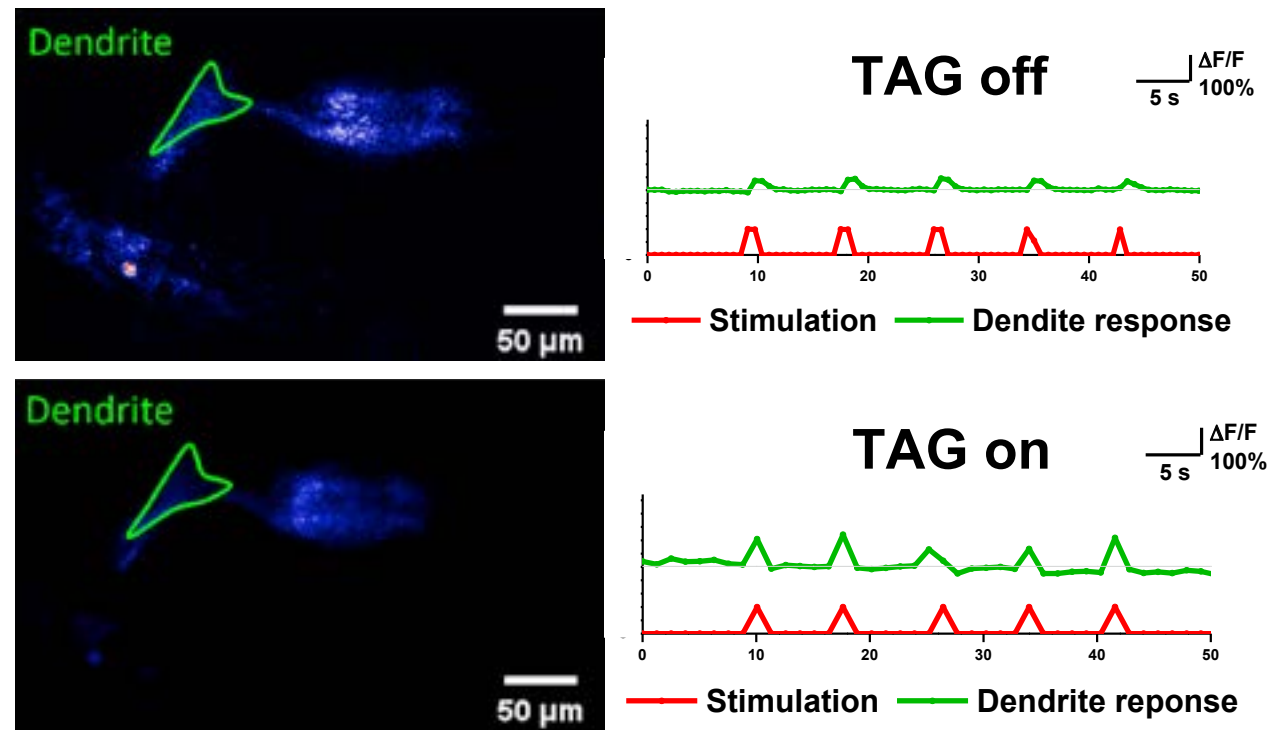


Fig. 1. All-optical functional imaging in vivo (a) Without TAG lens, the dendrite response in focal plane is weak. (b) With TAG lens, the dendrite response is strong, indicating that neuron dynamics was distributed over three dimension.

Reference:

- [1] Scanziani, M., et al. (2009). "Electrophysiology in the Age of Light." *Nature* 461(7266): 930-939.
- [2] Reddy, G.D., et al. (2008). "Three-Dimensional Random Access Multiphoton Microscopy for Functional Imaging of Neuronal Activity." *Nature Neuroscience* 11(6): 713-720.
- [3] Quirin, Sean, et al. (2014). "Simultaneous imaging of neural activity in three dimensions." *Frontiers in neural circuits* 8: 29.
- [4] Prevedel, R., et al. (2014). "Simultaneous Whole-Animal 3D Imaging of Neuronal Activity Using Light-Field Microscopy." *Nature Methods* 11(7): 727-730.
- [5] Ahrens, M.B., et al. (2013). "Whole-Brain Functional Imaging at Cellular Resolution Using Light-Sheet Microscopy." *Nature Methods* 10(5): 413-420.
- [6] Olivier, N., et al. (2009). "Two-Photon Microscopy with Simultaneous Standard and Extended Depth of Field Using a Tunable Acoustic Gradient-Index Lens." *Optics Letters* 34(11): 1684-1686.

#5

Neural Tissue Engineering through Modulated Magnetic Field and Aligned Neurotransmitted Scaffold

C-Y Lin¹, F. Kimura², T. Kimura², J-G Wu¹, S-C Luo¹ and W-F Su^{*1}

¹ *Department of Materials Science and Engineering, National Taiwan University, Taipei, Taiwan*

² *Graduate School of Agriculture, Kyoto University, Kitashirakawa Oiwake-cho, Sakyo-ku, Kyoto, Japan*

Abstract

Micropatterning of cells and pathfinding of neurites are two of the most essential issues in neural tissue engineering. 1) Although several biomaterials have shown to be promising as neural scaffolds, these two challenges are hard to overcome simultaneously. Here a novel method is developed to obtain desired tissue patterns and neurite outgrowth. Modulated magnetic field is firstly introduced to trap cells in the targeted pattern, 2) while aligned electrospun 3D scaffolds is then used to provide topographical and chemical cues guiding neurite outgrowth. PC12 cells are employed as a model neural system. A field modulator (400- μ m pitched line pattern) is set on a permanent magnet (0.52T) to produce a modulated magnetic field. Poly(glutamic acid)-co-poly(benzyl glutamate) is synthesized and electrospun into aligned 3D scaffolds. Cell viability, cell morphology, and scaffold topography are investigated through MTT assay, confocal microscopy, and scanning electron microscopy. This aligned neurotransmitted scaffold combined with modulated magnetic field is expected to fabricate engineered neural tissue.

Reference:

- [1] Zhu B. et al. (2014). "Large enhancement in neurite outgrowth on a cell membrane-mimicking conducting polymer." *Nature Comm.* 5, 4523
- [2] Kimura, T., et al. (2005). "Micropatterning of cells using modulated magnetic fields." *Langmuir* 21(3): 830-832.

Altered microstructural integrity in patients with tuberous sclerosis complex revealed by whole brain tract-specific analysis

Chien-Feng Huang¹, Pi-Chuan Fan², Isaac Wen-Yih Tseng^{1,3}

¹*Institute of Medical Device and Imaging, National Taiwan University College of Medicine, Taipei, Taiwan*

²*Department of Pediatrics, National Taiwan University Hospital and National Taiwan University College of Medicine, Taipei, Taiwan*

³*Molecular Imaging Center, National Taiwan University, Taipei, Taiwan*

1. Purpose

Tuberous sclerosis complex (TSC) is a systemic disease involving the central nervous system, skin, heart, eyes, kidneys, lungs, and liver [1]. It is an autosomal dominant neurocutaneous syndrome affecting about 1 in 6000 newborns and caused by a mutation in one of the two genes TSC1 and TSC2 [2]. About 85% of children and adolescents with tuberous sclerosis have CNS complications, including epilepsy, cognitive impairment, challenging behavioural problems, and autism [1]. Pathological studies indicated that neurons in TSC patients showed less integrity of myelination [3]. Wong et al. used Tract-based Spatial Statistical analysis and found a widespread decrease in cerebral white matter integrity in patients with TSC [4]. Based on previous studies, we hypothesized that diffusion indices of each individual tract bundle would also be changed in TSC. Therefore, we used tract-specific analysis of the whole brain to investigate the alteration of 76 major white matter tracts by diffusion spectrum image (DSI).

2. Methods

Subjects: A total of 44 patients with TSC were originally recruited in the study. Patients who had large intra-ventricular tumors and those younger than 5 years old were excluded from the analysis. Consequently, 27 patients (age: 23.2± 12.3 14 males and 13 females) and 27 age- and sex-matched healthy controls (age: 22.9± 12.7, 14 males and 13 females) were analyzed. The study was approved by the Institutional Review Board of the hospital and informed consent was obtained from all participants. **Imaging:** MRI scans were performed on a 3T MRI system (TIM Trio, Siemens, Erlangen) with a 32-channel phased array coil. T1-weighted imaging utilized a 3D magnetization-prepared rapid gradient echo pulse sequence: TR/TE = 2000/3 ms, flip angle = 9°, FOV = 256 × 192 × 208 mm³, matrix size = 256 × 192 × 208, and spatial resolution = 1 × 1 × 1 mm³. DSI used a twice-refocused balanced echo diffusion echo planar imaging sequence, TR/TE = 9600/130 ms, FOV = 200 × 200 mm², matrix size = 80 × 80, 56 slices, and slice thickness = 2.5 mm. A total of 102 diffusion encoding gradients with the maximum diffusion sensitivity $b_{max} = 4000 \text{ s/mm}^2$ were applied on the grid points in a half sphere of the 3D q-space with $|q| \leq 3.6$ units. **Analysis:** We used whole brain tract-based automatic analysis to obtain a 2D connectogram for each DSI dataset [5]. The connectogram provides generalized fractional anisotropy (GFA) profiles of 76 white matter tract bundles. We averaged the tract means over all participants within each group and calculated the signed differences between patients and controls for each tract bundle. We calculated the

effect size [6] to indicate the significance of the differences between the groups. Two sample t test was performed to investigate the difference of the mean GFA values between controls and patients. Bonferroni correction was used to account for multiple comparisons.

3. Results

As compared with healthy controls, patients with TSC showed significantly lower GFA in 13 tracts. These 13 tracts included the right arcuate fasciculus (AF), bilateral fornices (FX), the right perpendicular fasciculus, the left superior longitudinal fasciculus II (SLF II), the left stria terminalis, the left thalamic radiation (TR) of optic region, the callosal fibers (CF) of dorsal lateral prefrontal cortex, CF of ventral lateral prefrontal cortex, CF of paracentral cortex, CF of temporal pole, CF of hippocampus, and CF of amygdala; their effect sizes were 1.043, 1.230, 1.398, 1.426, 1.015, 1.087, 1.034, 1.091, 1.282, 0.992, 1.276, 1.114 and 1.312, respectively.

4. Discussion

This is the first study to use tract specific analysis to systematically investigate the microstructural alterations of white matter tracts in TSC. As mentioned before, TSC patients showed less integrity of myelination, which would probably result in generally decreasing GFA values of white matter tracts. Comparing to controls, 13 tracts were found to have significant differences. Lewis et al. [7] used a stochastic algorithm for tractography and found that TSC patients had lower FA than controls in AF. We confirm this conclusion with significant difference in AF. Patients with TSC would have high risk of epilepsy and ASD. In previous studies, patients with epilepsy had lower FA in fornix [8], and patients with autism had lower FA in AF, SLF II and CF of prefrontal cortex [9]. These altered tracts were found in the present study. It has been suggested that the biological basis of memory and emotion impairments may involve anatomical abnormalities in the amygdala and hippocampus [10]. This might be related to decreased GFA values in CF of amygdala and CF of hippocampus. In conclusion, the altered microstructural integrity of white matter tracts in TSC supports the hypothesis of underlying microstructural changes of brain in TSC, and is consistent with clinical symptoms.

Reference:

- [1] Curatolo P et al. (2008) *Lancet*.
- [2] O'Callaghan FJ et al. (1998) *Lancet*.
- [3] Lynsey M et al. (2007) *Neuroscience*.
- [4] A.M. Wong et al. (2013) *Neuroradiology*.
- [5] Chen Y et al. (2015) *Human Brain Mapping*.
- [6] Cohen J. (1988) *Hillsdale*.
- [7] Lewis et al. (2013) *Cerebral Cortex*.
- [8] Concha et al. (2005) *Neurology*.
- [9] Y.C. Lo et al. (2011) *Psychiatric Research: Neuroimaging*.
- [10] S. Baron-Cohen. (2000) *Neuroscience and Biobehavioral Reviews*.

3D Imaging of Hematoxylin and Eosin Stained Thick Tissues with a Sub-Femtometer Resolution by Using Cr:forsterite-laser-based Nonlinear Microscopy

Chien-Ting Kao¹, Ming-Liang Wei¹, Yi-Hua Liao² and Chi-Kuang Sun^{1,3}

¹ *Molecular Imaging Center, National Taiwan University, Taiwan*

² *Department of Dermatology, National Taiwan University Hospital and National Taiwan University College of Medicine, Taiwan*

³ *Department of Electrical Engineering and Graduate Institute of Photonics and Optoelectronics, National Taiwan University, Taiwan*

Abstract

In this paper, we demonstrate 3D imaging of hematoxylin-and-eosin stained thick tissues with sub-femtometer resolution using Cr:forsterite-laser-based nonlinear microscopy. Since the contrast is fully compatible with the current clinical practice, our demonstrated microscopy system can allow rapid intraoperative assessment of excision tissues before frozen pathology examination.

1. Introduction

Intraoperative assessment of excision tissues during cancer surgery is clinically important. The assessment is used to be guided by the examination for residual tumor with frozen pathology, while it is time consuming for preparation and is with low accuracy for diagnosis. Recently, reflection confocal microscopy (RCM) and nonlinear microscopy (NLM) were demonstrated to be promising methods for surgical border assessment. Intraoperative RCM imaging may enable detection of residual tumor directly on skin cancers patients during Mohs surgery. [1] The assessment of benign and malignant breast pathologies in fresh surgical specimens was demonstrated by NLM. [2] Without using hematoxylin and eosin (H&E) which are common dyes for histopathological diagnosis, RCM was proposed to image in vivo by using aluminum chloride for nuclear contrast on surgical wounds directly, while NLM was proposed to detect two photon fluorescence nuclear contrast from acridine orange staining. In this paper, we propose and demonstrate 3D imaging of H&E stained thick tissues with a sub-femtometer resolution by using Cr:forsterite-laser-based NLM. With a 1260 nm femtosecond Cr:forsterite laser as the excitation source, the hematoxylin will strongly enhance the third-harmonic generation (THG) signals [3], while eosin will illuminate strong fluorescence under three photon absorption. Compared with previous works, the 1260 nm excitation light provide high penetration and low photodamage to the exercised tissues so that the possibility to perform other follow-up examination will be preserved. [4] The THG and three-photon process provides high nonlinearity so that the super resolution in 3D is now possible. The staining and the contrast of the imaging is also fully compatible with the current clinical standard on frozen pathology thus facilitate the rapid intraoperative assessment of excision tissues.

2. Conclusion

In this talk, we will present our results with and without staining in human skin tissues. Without staining, the main contrast was provided by THG and SHG. The label-free THG provides endogenous contrast on melanin, lipid, and hemoglobin, while SHG provides endogenous contrast on collagen fibers. Without staining by hematoxylin, cell nucleus shows no contrast either through SHG or THG. After H&E staining, cell nucleus start to provide strong contrast under THG due to resonance effect [3] while the three-photon fluorescence channel will start to provide contrast under eosin, which stains all connective tissues including collagen fibers and cell cytoplasm. We will present spectroscopy study to confirm the three-photon nature of the fluorescence from eosin. Our resolution and penetration study indicates that the THG and three-photon process provides high nonlinearity so that the super resolution in 3D is now possible. The staining and the contrast of the imaging are also fully compatible with the current clinical standard on frozen pathology. Our study indicates that NLM plus H&E staining would be a promising and compatible method for rapid intraoperative assessment of excision tissues before frozen pathology.

3. Acknowledgement

This work is sponsored by National Health Research Institutes (NHRI-EX105-9936EI) and supported by National Taiwan University Hospital.

Reference:

- [1] E. S. Flores, M. Cordova, K. Kose, W. Phillips, A. Rossi, K. Nehal, and M. Rajadhyaksha, "Intraoperative imaging during Mohs surgery with reflectance confocal microscopy: initial clinical experience," *J. Biomed. Opt.*, vol. 20, no. 6, 061103, June 2015.
- [2] Y. K. Tao, D. Shen, Y. Sheikine, O. O. Ahsen, H. H. Wang, D. B. Schmolze, N. B. Johnson., J. S. Brooker, A. E. Cable, J. L. Connolly, and J. G. Fujimoto, "Assessment of breast pathologies using nonlinear microscopy," *P. Natl. Acad. Sci. USA*, vol. 111, no. 43, pp. 15304-15309, October 2014.
- [3] C. H. Yu, S. P. Tai, C. T. Kung, W. J. Lee, Y. F. Chan, H. L. Liu, J. Y. Lyu, and C. K. Sun, "Molecular third-harmonic-generation microscopy through resonance enhancement with absorbing dye," *Opt. Lett.*, vol. 33, no.4, pp. 387-389, February 2008.
- [4] R. R. Anderson, and J. A. Parrish. "The optics of human skin," *J. Invest. Dermatol.*, vol. 77, no. 1, pp. 13-19, 1981.

Altered microstructural integrity of the white matter tracts in children with aromatic L-amino acid decarboxylase deficiency: A systematic tract-specific analysis using diffusion MRI

Chih-Hsien Tseng^{1,2}, Wuh-Liang Hwu^{3,4}, Isaac Wen-Yih Tseng^{1,2,5,6}

¹ Institute of Medical Device and Imaging, National Taiwan University College of Medicine, Taipei, Taiwan

² Institute of Biomedical Engineering, National Taiwan University College of Medicine, Taipei, Taiwan

³ Department of Medical Genetics, National Taiwan University Hospital and National Taiwan University College of Medicine, Taipei, Taiwan

⁴ Department of Pediatrics, National Taiwan University Hospital and National Taiwan University College of Medicine, Taipei, Taiwan

⁵ Graduate Institute of Brain and Mind Sciences, National Taiwan University College of Medicine, Taipei, Taiwan ⁶ Molecular Imaging Center, National Taiwan University, Taipei, Taiwan

1. Purpose

Aromatic L-amino acid decarboxylase (AADC) deficiency is an inherited disorder that impairs synthesis of dopamine and serotonin. Children with AADC deficiency exhibit severe motor, behavioral, and autonomic dysfunctions. We hypothesized white matter integrity would be also altered in children with AADC deficiency. Therefore, a tract-specific analysis of the whole brain was performed to investigate the alteration of 76 major white matter tracts by diffusion tensor imaging (DTI).

2. Methods

The subjects consisted of 7 children with clinical diagnosis of AADC deficiency (gender: 3 males and 4 females, age: 4.86±2.48 years) and 7 age- and sex-matched healthy children controls. MR scanning was performed on a 1.5T MRI system (Signa HDx, GE). DTI was acquired using an echo planar imaging (EPI) sequence, TR/TE = 7000/105 ms, FOV = 110 × 110 mm, image matrix size 128 × 128, and 5 mm slice thick. A total of 42 diffusion encoding gradients with the maximum diffusion sensitivity $b_{max} = 1000$ s/mm² were applied to acquire diffusion dataset. T1-weighted imaging was performed using a 3D fast spoiled gradient echo (FSPGR) sequence: repetition time (TR) / echo time (TE) = 10 ms/4 ms, flip angle = 12°, FOV = 94 × 94 mm², acquisition matrix = 192 × 192, and 1 mm slice thick. Whole brain tractography was reconstructed by tract-based automatic analysis (TBAA). The procedure of TBAA method was briefly described as follows. 1) Study subjects were coregistered to create a study specific template (SST) using large deformation diffeomorphic metric mapping (LDDMM) [1]. 2) The SST was coregistered to the final template. 3) Sampling coordinates of 76 tracts were transformed from the final template to individual DTI datasets via the transformation matrix between final template and SST as well as the transformation between SST and individual DTI. 4) Fractional anisotropy (FA) values were sampled in the native

DTI space using the transformed sampling coordinates and a 2D array of FA profiles, named connectogram, was created for each subject. Two sample T-test was performed to investigate the difference of mean FA values between two groups. A threshold free cluster weighted (TFCW)

method was used following Smith's approach [2] to estimate weighted scores ($S(p) = \sum_{h=h_0}^{h_5} ep(h)$)

, where ep is the cluster extent level which survives at the given threshold h at step p) of effect size of each step between two groups. A 98% cut-point of the histogram of TFCW scores was then estimated to determine the most different clusters between these two groups. The most different clusters were then used to sample FA profiles and compare the difference between controls and patients.

3. Results

We found significant reduction of mean FA in the bilateral fibers of frontostriatal (FS) circuit of orbitofrontal cortex (OFC), and corpus callosum (CC) of dorsal lateral prefrontal cortex (DLPFC) ($p < 0.05$, uncorrected). In the TFCW estimation, the most different clusters were located in 15 fiber tracts including left arcuate fasciculus (AF), right cingulum bundle (main body part), left frontal aslant tract, bilateral inferior longitudinal fasciculus (ILF), right FS of ventral lateral prefrontal cortex (VLPFC), left FS of DLPFC, left FS of precentral gyrus, bilateral thalamic radiation (TR) of VLPFC, left TR of precentral gyrus, and CC of supplementary motor area (SMA). Spatial distribution of these tracts was mapped by three groups: association system (Figure 1a), projection system (Figure 1b) and commissure system (Figure 1c).

4. Discussion

This is the first study to use tract specific analysis to systematically investigate the microstructural alterations of white matter tracts in AADC deficiency. White matter tracts which had decreased FA values in patients were compatible with clinical diagnosis. FS circuit, the connection of striatum and frontal cortex, is dominated by dopaminergic and serotonergic systems. As mentioned previously, children with AADC deficiency would lose function of producing these two types of neurotransmitters, which might lead to decreased FA in several FS connections. We also found some tracts related to regions responsible for executive function (DLPFC and OFC) or regions regulating motor function (VLPFC and precentral gyrus) showing lower FA in patients. This might be related to developmental delay and motor dysfunction in AADC deficiency. In conclusion: the altered microstructural integrity of white matter tracts in AADC deficiency identified in our study is consistent with clinical symptoms.

5. Perspective

Dr. Hwu and his colleagues have been developing novel gene therapy for AADC deficiency [3]. Preliminary results of patients with one-year gene therapy indicated that there might be a recovery process in white matter integrity due to therapy. A longitudinal neuroimaging study with a sufficient sample size is warranted to clarify the effects of therapy on the microstructure of white matter tracts.

Reference:

- [1] Hsu, Y., Hsu, C. and Tseng, W. (2012). A large deformation diffeomorphic metric mapping solution for diffusion spectrum imaging datasets. *NeuroImage*, 63(2), pp.818-834.
- [2] SMITH, S. and NICHOLS, T. (2009). Threshold-free cluster enhancement: Addressing problems of smoothing, threshold dependence and localisation in cluster inference. *NeuroImage*, 44(1), pp.83-98.
- [3] Lee, N., Muramatsu, S., Chien, Y., Liu, W., Wang, W., Cheng, C., Hu, M., Chen, P., Tzen, K., Byrne, B. and Hwu, W. (2015). Benefits of Neuronal Preferential Systemic Gene Therapy for Neurotransmitter Deficiency. *Mol Ther*, 23(10), pp.1572-1581.

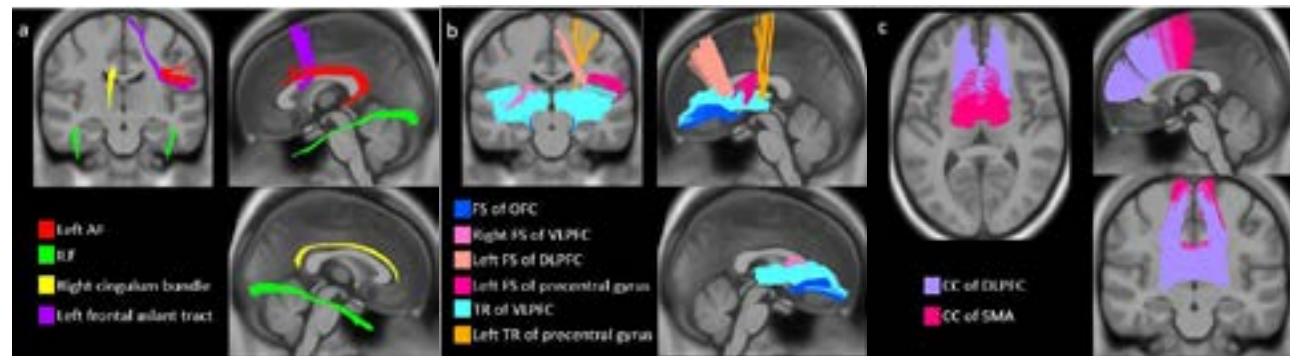


Fig. 1. White matter tracts which had clusters of lower FA in patients with AADC deficiency were showed respectively by associate system (a), projection system (b), and commissure system (c).

#9

Automated Analysis of Functional Connectome Images

Chi-Huan Chiang¹, Kuo-Jen Hsu^{1,2} and Shi-Wei Chu^{1,3}

¹ Department of Physics, National Taiwan University, No. 1, Sec. 4, Roosevelt Rd, Taipei 10617, Taiwan

² Brain Research Center, National Tsing Hua University, No. 101, Sec. 2, Kuang-Fu Rd, Hsinchu 30013, Taiwan

³ Molecular Imaging Center, National Taiwan University, No. 1, Sec. 4, Roosevelt Rd, Taipei 10617, Taiwan

Brain is probably the most mysterious organ in our body. By understanding our brain, we can better understand the mechanism behind consciousness. There is over 100-year history of studying individual neuron behaviors, but our understanding toward brain function is still very limited. One of the key reasons is that brain function is not dictated by a single neuron, but emerges from the sophisticated connections among neurons, i.e. connectome. Therefore, recently there are numerous efforts nowadays in the direction of unraveling the mystery behind the connectome.

To achieve that, the first step is to analyze connectivity among neurons in ex vivo brains and to construct an anatomical connectome. Then it is necessary to relate in vivo brain functions to anatomical connectivity¹, i.e. building up a functional connectome. The most important step toward the realization of functional connectome is the capability to observe every single action potential from every neuron in a brain, as specified in the BRAIN initiative of the USA. We have recently developed an imaging platform that is able to observe neuronal signal dynamics across the whole brain of drosophila. However, there are more than 100,000 neurons in drosophila brain² (1011 for human³), and thus manual analysis is nearly impossible for whole brain study. Here we develop a home-made program, based on the open-source software Python, for automated brain image analysis of individual neuron spatiotemporal dynamics images, eliminating the need of manually selecting pixels frame by frame. Moreover, by temporally fitting the neuron calcium signals at individual spatial pixel, various temporal dynamics such as signal flow direction, rising time variation, and signal length, can be mapped with micrometer spatial precision. Our result provides an unprecedented view of brain function and paves the way toward whole-brain functional connectome study.

Reference:

- [1] Koene R. A. Van Dijk et al., "Intrinsic Functional Connectivity As a Tool For Human Connectomics: Theory, Properties, and Optimization" *J Neurophysiol.*, Vol. 103, p.297-321, (2010).
- [2] A. Paul Alivisatos et al., "The Brain Activity Map Project and the Challenge of Functional Connectomics" *Neuron.*, Vol. 74, p.970-974, (2012).
- [3] Suzanaerculano-Houzel et al., "The human brain in numbers: a linearly scaled-up primate brain" *Front. Humx Neurosci.*, Vol. 3, Art. 31, (2009).

#10

Human Adipose Stem Cell Spheroid Forming on Glycol Chitosan and Gelatin Hydrogel

ChingCheng, Tsai¹, HsinYu, Chen¹ and Jiashing Yu¹

¹ Department of Chemical Engineering, National Taiwan University, No.1, Sec. 4, Roosevelt Rd., Da'an Dist., Taipei City 106, Taiwan

Abstract

The chitosan has a nice biocompatibility and degradability so that it is applied broadly in tissue engineering. Glycol chitosan which is soluble is a derivative of chitosan. In this study, the hydrogel was combined by glycol chitosan and gelatin which made cells able to attach on and its performance in cell culture was researched. This hydrogel could make the human adipose-derived stem cells (hASCs) form a sphere structure after culturing for several days. And the spheroids were observed by SEM and fluorescence. Due to the studies showing that the stem cells in spheroids were viable mostly and had better differentiation ability. Moreover, the material we used was usually studied for cartilage tissue engineering. In the future, we hope the glycol chitosan in hydrogel and formation of spheroids are able to promote the chondrogenic differentiation.

Reference:

- [1] "Co-delivery of Adipose-Derived Stem Cells and Growth Factor-Loaded Microspheres in RGD-Grafted N-Methacrylate Glycol Chitosan Gels for Focal Chondral Repair", Abby Sukarto, Claire Yu, Lauren E. Flynn, and Brain G. Amsden, 2012, Biomacromolecules.
- [2] "The influence of spheroid formation of human adipose-derived stem cells on chitosan films on stemness and differentiation capabilities", Nai-Chen Cheng, Shan Wang, Tai-Horng Young, 2012, Biomaterials.

#11

High Speed 3D Functional Imaging of Living Brain

Chih-Wei Liu¹, Wei-Kuan Lin¹, Chi-Huan Chiang,¹ Kuo-Jen Hsu,¹ and Shi-Wei Chu^{1,2}

¹ Department of Physics, National Taiwan University, No. 1, Sec. 4, Roosevelt Rd, Taipei 10617, Taiwan

² Molecular Imaging Center, National Taiwan University, No. 1, Sec. 4, Roosevelt Rd, Taipei 10617, Taiwan

Brain, which controls our behaviors, emotions, consciousness, memories and all other vital signs of human, is one of the most important organs in human body. Although the history of studying individual neuron behaviors is more than 100 years, our understanding toward brain function is still very limited. One of the key reasons is that brain function is not dictated by a single neuron, but emerges from the sophisticated connections among neurons, i.e. connectome. Therefore, recently there have been significant amount of researches toward the understanding of connectome¹). However, most current studies concentrate on "structural" connectome through anatomical approaches, while the development of "functional connectome", though much more informative, is limited by technical difficulties to map the brain with high enough spatiotemporal resolution throughout the whole volume. In order to study the way how functional connectome works in brain of living animals, the required tool should exhibit spatial resolution less than $\sim\mu\text{m}$, temporal imaging speed as high as $\sim\text{ms}$, and imaging size approaching millimeter cubic in volume.

Among current techniques, optical microscopy is the best candidate to match these specifications. Several schemes have been demonstrated recently to boost 3D imaging speed for functional connectome study of brain in vivo, including piezoelectric translator²), acousto-optic deflectors³), spatial light modulator⁴), light field microscopy⁵), light sheet microscopy⁶), liquid lens⁷), etc. However, most of these techniques cannot enhance imaging speed on both lateral and axial directions simultaneously. In addition, some of these suffer from scattering from tissue because of its wide-field illumination or can only use for transparent samples. To overcome these issues, we have reported, in the same conference last year, a powerful technique⁸) that combines high-speed axial scanning lens and multiphoton microscopy to increase scanning speed of 3D volumetric imaging down to sub-second scale.

However, in the earlier system, even though the axial scanning speed is more than 100 kHz, the 3D volume imaging speed is limited by the single point scanning on the lateral plane. In this work, we developed a 32-beam multifocal system to significantly enhance the lateral scanning speed with 1-2 orders of magnitude. Combined with the high-speed axial scanning lens, the volumetric imaging speed approaches milliseconds scale, that is adequate to probe dynamics of action potential among neurons. This powerful and innovative system is expected to greatly facilitate in vivo brain functional connectome studies in the near future.

Reference:

- [1] Oh, S.W. et al., "A mesoscale connectome of the mouse brain" *Nature* 508, 207–214 (2014)
- [2] Gobel, W. et al., "Imaging cellular network dynamics in three dimensions using fast 3D laser scanning" *Nature Methods*, 4, 79-79 (2007).
- [3] Reddy, G.D. et al., "Three-dimensional random access multiphoton microscopy for functional imaging of neuronal activity" *Nature Neuroscience* 11, 713-720 (2008).
- [4] Quirin, S. et al., "Simultaneous imaging of neural activity in three dimensions" *Front. Neural Circuits* 8, 29 (2014).
- [5] Prevedel, R. et al., "Simultaneous whole-animal 3D imaging of neuronal activity using light-field microscopy" *Nature Methods* 11, 727-730 (2014).
- [6] Ahrens, M.B. et al., "Whole-brain functional imaging at cellular resolution using light-sheet microscopy" *Nature Methods* 10, 413-420 (2013).
- [7] Oku, H. et al., "Variable-focus lens with 1-kHz bandwidth" *Optics Express* 12, 10 (2004).
- [8] Hsu, K.-J., "All-in-focus functional imaging system for drosophila brain activities study" in Department of Physics, National Taiwan Univ.: Taiwan (2014).

#12

Combining Magnetic Nanoparticles with Monocyte Chemoattractant Protein-1 (MCP-1) as the Targeting Tool for AtherosclerosisChung-Wei Kao¹, Che-Wei Lin¹, Wen-Yih Tseng² and Jiashing Yu¹¹ *Department of Chemical Engineering, National Taiwan University, No.1, Sec. 4, Roosevelt Rd., Da'an Dist., Taipei City 106, Taiwan*² *Center for Optoelectronic Medicine, National Taiwan University, No.1, Sec. 1, Ren'ai Rd., Zhongzheng Dist., Taipei City 100, Taiwan*

Myocardial infarction has accounted for much deaths compared to other diseases today. Commonly, atherosclerosis is a multifactorial inflammatory disease that would progress silently for long period and also widely accepted as the main cause of cardiovascular diseases. To prevent atherosclerotic plaques generating critically in early stage, imaging early molecular markers and quantifying the extent of disease progression are the effective ways. The objective of the work is to research monocyte-targeting magnetic nanoparticles which incorporate with the chemo kine receptor CCR2-binding motif of monocyte chemoattractant protein-1 (MCP-1) as diagnostic tools for atherosclerosis. We used amine-reactive dyes, Cyanine7 NHS ester, for labeling MCP-1 peptides and observed the binding circumstances. Because of superparamagnetism of magnetic nanoparticles, the particles are easily to separate with specific magnetic field. Also, magnetic nanoparticles can be intake and absorbed naturally by histones, such as ferritin, therefore it shows highly biocompatibility and degradability.

Reference:

- [1] CHUNG, E.J., MLINAR, L.B., NORD, K., SUGIMOTO, M.J., WONDER, E., ALENGHAT, F.J., FANG, Y., TIRRELL, M. 2015. Monocyte-targeting supramolecular micellar assemblies: a molecular diagnostic tool for atherosclerosis. *Adv Healthc Mater*, 4, 367-376
- [2] MLINAR, L.B., CHUNG, E.J., WONDER, E.A., TIRRELL, M. 2014. Active targeting of early and mid-stage atherosclerotic plaques using self-assembled peptide amphiphile micelles. *Biomaterials*, 35, 8678-8686
- [3] KUO, C.H., LEON, L., CHUNG, E.J., HUANG, R.T., SONTAG, T.J., REARDON, C.A., GETZ, G.S., TIRRELL, M., FANG, Y. 2014. Inhibition of atherosclerosis-promoting microRNAs via targeted polyelectrolyte complex micelles. *J Mater Chem B Mater Biol Med*, 2, 8142-8153
- [4] PETERS, D., KASTANTIN, M., KOTAMRAJU, V.R., KARMALI, P.P., GUJRATY, K., TIRRELL, M., RUOSLAHTI, E. 2009. Targeting atherosclerosis by using modular, multifunctional micelles. *Proc Natl Acad Sci U S A*, 106, 9815-9819

#13

Plasmonic SAX microscopy in deep tissue

Gitanjal Deka¹, Kuan-Yu Li¹, Shi Wei Chu^{1,2}

¹Department of Physics, National Taiwan University, No. 1, Sec. 4, Roosevelt Rd, Taipei 10617, Taiwan ROC

²Molecular Imaging Center, National Taiwan University, No. 1, Sec. 4, Roosevelt Rd, Taipei 10617, Taiwan ROC

Abstract

A major challenge in tissue imaging is the limited penetration depth, due to light scattering and absorption. By using near-infrared lasers, scattering and absorption can be minimized, thus improving penetration depth. However, the image resolution gets worse with increase in wavelength due to diffraction, which further degrades with increasing imaging depth. Several techniques such as stochastic optical reconstruction microscopy (STORM), photoactivated localization microscopy (PALM), structured illumination microscopy (SIM), and stimulated emission depletion (STED) have emerged to be useful for the purpose of resolution enhancement. However, these techniques are based on either wide-field imaging or laser scanning with spatial beam patterning, and thus are limited to surface observation [1].

In contrast, saturated excitation (SAX) microscopy, as a point scanning technique without spatial beam engineering [2], should be able to provide resolution enhancement for deep tissue imaging. However, SAX, as well as other above-mentioned high resolution techniques, uses fluorescence contrasts, thus are limited by photobleaching. Hence it is highly desirable to find a non-bleaching contrast agent, which is compatible with near-infrared excitation. Our group has recently demonstrated saturated scattering from a single gold nanoparticle [3]. Amalgamation of this finding with SAX microscopy, i.e. plasmonic SAX, provides a novel contrast mechanism to enhance spatial resolution below 100 nm, much better than fluorescence SAX [3]. Plasmonic nanoparticles have much larger scattering cross section than fluorescence, making them robust contrast agents, ideal for deep tissue imaging. Tunability of plasmonic resonance wavelength by manipulating the shape or size of the nanoparticles is yet another advantage of plasmonic SAX [4].

In this work, we explore saturation of different gold nanoparticles at different wavelengths. Those nanoparticles are adopted in observing resolution enhancement under animal tissue slices by plasmonic SAX microscopy. Our technique provides a novel non-bleaching contrast for future deep-tissue super resolution applications.

Reference:

- [1] B. Huang, M. Bates, and X. Zhuang, "Super resolution fluorescence microscopy," *Ann. Rev. Biochem* 78, 993-1016 (2009).
- [2] K. Fujita, M. Kobayashi, S. Kawano, M. Yamanaka, and S. Kawata, "High-resolution confocal microscopy by saturated excitation of fluorescence," *Phys. Rev. Lett.* 99, 228105 (2007).
- [3] S.-W. Chu, T.-Y. Su, R. Oketani, Y.-T. Huang, H.-Y. Wu, Y. Yonemaru, M. Yamanaka, H. Lee, G.-Y. Zhuo, and M.-Y. Lee, "Measurement of a saturated emission of optical radiation from gold nanoparticles: application to an ultrahigh resolution microscope," *Phys. Rev. Lett.* 112, 017402 (2014).
- [4] Y.-T. Chen, P.-H. Lee, P.-T. Shen, J. Launer, R. Oketani, K.-Y. Li, Y.-T. Huang, K. Masui, S. Shoji, and K. Fujita, "Study of Nonlinear Plasmonic Scattering in Metallic Nanoparticles," *ACS Photonics* 3, 1432-1439 (2016).

#14

Sub-20-nm spatial resolution based on saturation excitation (SAX) microscopy with an appropriate nonlinear response

Hou-Xian Ding¹, Kuan-Yu Li¹, Gitanjal Deka¹ and Shi-Wei Chu¹.

¹Department of Physics,
National Taiwan University, Taipei 10617, Taiwan R.O.C

Abstract

Contrast and resolution are two key factors in optical microscopy of biological samples. For century, fluorescence has provided rich variety of contrasts for imaging those samples. Since the last decade high resolution imaging with fluorescence contrasts are in the forefront of optical imaging by achieving nanoscale resolution. Most common techniques such as stimulated emission depletion (STED) microscopy, structured illumination microscopy (SIM), photoactivated localization microscopy (PALM) and stochastic optical reconstruction microscopy (STORM) achieve resolution enhancement either by switching or saturation of fluorescence species. Saturation excitation (SAX) of fluorescence is another emerging superresolution imaging techniques with optical section capability and without beam manipulation [1]. However, all the above mentioned techniques require high laser intensity for resolution enhancement and hence limited by photobleaching. Specially, in case of fluorescence SAX microscopy, resolution improvement beyond 100 nm is difficult due to increase in photo bleaching while detecting high harmonic signals.

The strong scattering from plasmonic nanoparticles can be a possible nonbleaching and robust contrast mechanism. According to our recent discovery, the scattering from individual plasmonic nanoparticles are also saturable, making it possible for SAX detection. With 2f and 3f harmonic demodulation, plasmonic SAX achieve better resolution than the traditional fluorescence SAX microscopy [2]. However, the requirement of large excitation intensity for higher order (>3f) demodulation may hinder further resolution enhancement. For a fluorescence dye, high power excitation can cause photobleaching and for metallic nanoparticle, it can heat up the surrounding making it less suitable for biological application.

In this report, we found that with a suitable nonlinear intensity response, the spatial resolution of SAX can be as low as sub-20-nm, even with only the 2f demodulation at a relatively low excitation intensity. Fig. 1 compares the simulation image of a 2f demodulation signal of fluorescence saturation curve, and artificial response curve, based on SAX microscopy. By extracting lower order (2f/3f) demodulation at low excitation intensity, the dilemma of photobleaching or the photoburning can be omitted in achieving high resolution by SAX microscopy. Our study innovates a novel technique for superresolution imaging with a laser-scanning system.

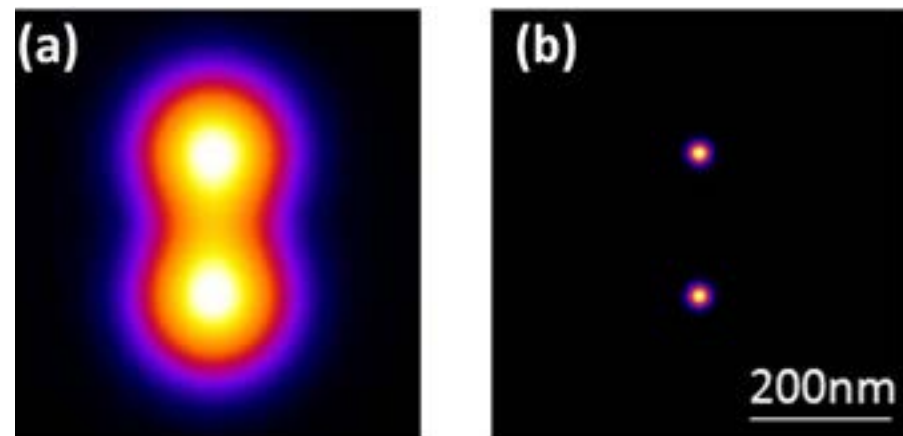


Fig. 1. The simulation image of (a) 2f demodulation signal of fluorescence saturation curve, and (b) artificial response curve, based on SAX microscopy. The FWHM of (a) and (b) are 160-nm and 20-nm respectively.

Reference:

- [1] Fujita, K., Kobayashi, M., Kawano, S., Yamanaka, M. & Kawata, S. "High-resolution confocal microscopy by saturated excitation of fluorescence." *Phys. Rev. Lett.* 99, 228105 (2007).
- [2] S. W. Chu, T. Y. Su, R. Oketani, Y. T. Huang, H. Y. Wu, Y. Yonemaru, M. Yamanaka, H. Lee, G. Y. Zhuo, M. Y. Lee, S. Kawata, and K. Fujita, "Measurement of a saturated emission of optical radiation from gold nanoparticles: application to an ultrahigh resolution microscope," *Phys. Rev. Lett.* 112(1), 017402 (2014)

#15

To Reveal the Recognition between C-Reactive Protein and Phosphorylcholine by Quartz Crystal Microbalance

Jhih-Guang Wu, Shyh-Chyang Luo

Department of Materials Science and Engineering, National Taiwan University

No. 1, Sec. 4, Roosevelt Road, Taipei, 10617, Taiwan

1. Introduction

Quartz crystal microbalance (QCM) is a sensitive and real-time method to reveal the mass change of adsorption on the surface. The quartz crystal, a piezoelectric material, owns their special overtone when we applying an alternating current. The frequency of quartz crystal will change after something adsorbs to the surface or leaves the surface. According to the Sauerbrey equation (shown below), we can use the change of quartz frequency (ΔF) to estimate the change of mass (Δm).

$$\Delta m = -C \times \Delta F$$

The human C-reactive protein (CRP) is a common biomarker for acute inflammation and tissue damage. According to the prior work, the phosphorylcholine (PC) functional groups can specific interact with the CRP. To evaluate the interaction between CRP and PC, we synthesized a poly(3,4-ethylenedioxythiophene) with PC functional groups by electropolymerization method. Through QCM, we were able to observe the amount of protein binding and discuss the mechanism of this phenomenon.

2. Results and Discussion

By changing the composition of monomer solution for electropolymerization, we can fine tune the density of PC groups on surfaces. We found the monomer solution which contain 100% EDOT-PC provided the best specific binding of CRP and can prevent the non-specific binding of bovine serum albumin (BSA). The amount of protein adsorption is monitored by QCM (Fig. 1a). Then, we changed the concentration of CRP (from 20 nM to 320 nM) for binding tests. (Fig. 1b).

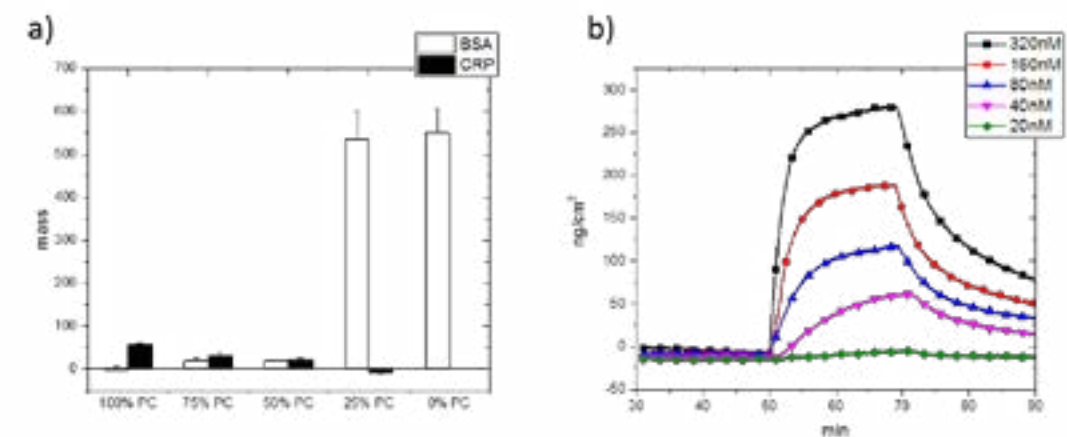


Fig. 1. (a) The amount of BSA and CRP binding based on QCM results; (b) The binding profile of CRP binding at different concentration of CRP.

#16

A new method for synapse capture by electrostatic interaction for epifluorescence and super-resolution microscopy

YJia-Fong Jhou¹, Yun-Huan Chen¹, Shu-Wei Lin¹, Fan-Ching Chien², Hwan-Ching Tai¹

¹Department of Chemistry, National Taiwan University, Taipei, Taiwan

²Department of Optics and Photonics, National Central University, Taoyuan, Taiwan

Alzheimer's disease (AD), a protein-misfolding disorder characterized by abnormal aggregation of beta amyloid (A β) and tau, accounts for more than 50% of senile dementia cases. AD is also characterized by the loss of neurons and synapses in the neocortex and limbic system, which strongly correlate with cognitive impairment. Consequently, we are using enriched preparations of synaptic terminals (synaptosomes) to study synaptic dysfunction and its relationship with AD.

To visualize protein changes in isolated synaptosomes, they need to be immobilized over glass surfaces for immunofluorescence staining. However, traditional fixation and immobilization methods using formaldehyde often generate aggregation artifacts. To resolve this issue, we invented a new way to capture synaptosomes by electrostatic attraction. Synaptosomes carry negative surface charges due to membrane lipids and glycans, with Zeta potential around -16 mV. Instead of formaldehyde, we introduced EGS (ethylene glycol bis(succinimidyl succinate)) as a fixative to make the surface even more negative and to prevent aggregation by electrostatic repulsion. On the other hand, we functionalized glass surfaces by (3-aminopropyl) triethoxysilane (APTES) to introduce positive charges. The electrostatic attraction between synaptosomes and amine-coated glass is very strong and resistant to mild sonication. Thus we achieved synaptosome fixation and immobilization via simple procedures and gentle conditions, and improved the image quality of immunofluorescence imaging. Importantly, we were able to apply direct stochastic optical reconstruction microscopy (dSTORM) to visualize tau protein at mouse synaptic terminals at 30 nm resolution. This technique will be further applied to AD patient-derived synaptosomes to examine presynaptic and postsynaptic pathologies associated with tau protein.

#17

Comparison of Cell Behaviour on Nanofibrous Surface with Different Orientation Properties

Tang Kao Chun¹, Li Shing Tak¹ and Jiashing Yu¹

¹Department of Chemical Engineering, National Taiwan University, No.1, Sec. 4, Roosevelt Rd., Da'an Dist., Taipei City 106, Taiwan

Abstract

There is a lot of research discussing about the utilization of the electrospinning fiber for scaffold construction in tissue engineering. However, the discussion is much less about the effect on cell behaviour with different orientation properties. Therefore, several examinations like alamar blue assay, SEM and others are done to compare more thoroughly among the difference between different orientation properties of electrospun nanofiber. We categorized different orientation as aligned orientation and randomly-distributed orientation and the cells we used are human adipose stem cells (hASC). It is found out that there are some differences between different orientation properties. From the observation of SEM image, it can be found that morphology between aligned and randomly-distributed orientation is rather different. The cells on the aligned orientation nanofibers adhered and grew along with the same direction of the electrospun nanofibers, while the cells on the randomly-distributed nanofibers tended to grow widely spread among several nanofibers. From alamar blue assay, it is found that there exists cell proliferation rate difference and the aligned orientation had higher proliferation rate than the randomly-distributed one. We concluded that it is the environment that affected the proliferation rate and morphology of hASC cells. The finding will advance our understanding about better orientation properties for cell-growing environment, and thus facilitate enhanced nanofibrous scaffolds for tissue engineering applications.

Reference:

[1] Shuo Wang, Shaoping Zhong, Chewee Teck Lim. Effects of fiber alignment on stem cells-fibrous scaffold interactions. *Journal of Materials Chemistry B*; 2015, p. 3358-3366

Fabrication of Uniform Pore Size Scaffolds And Its Influence Toward Adipose-Derived Stem Cells Chondrogenic Ability

Kuan-Han, Wu¹ and Jia-Shing, Yu¹

¹ Department of chemical engineering,
National Taiwan University, Taipei, Taiwan

Abstract

3D scaffolds that were manufactured with former techniques perform a non-uniform pore size, which results in many factors that might affect cell behaviors. In this research, we apply microfluidic techniques to fabricate a uniform pore size 3D gelatin scaffold. First, there are several factor that affects the pore size of the scaffold, the fluid flow rate, gas pressure and microfluid channel radius. Therefore, we manipulate these factors and fabricate scaffolds with two pore sizes, 50 μm and 100 μm . With these scaffolds, we start to compare the morphology of human adipose stem cells (hASC) under different pore sizes. As we know, a single hASC cell is around 50 μm , so it can stretch among adjacent bubbles in both scaffolds. But among the larger pore size scaffolds, more hASC can grow in a single bubble. Furthermore, we compare the chondrogenic differentiation ability of hASC in these scaffolds applying differential medium. First, cell morphology was observed to assure that cells grew in the z-axis, which makes 3D reasonable. Furthermore, several tests and staining that can prove the existence of chondrogenic differentiation are made and to compare the differentiation ability among the two different scaffolds. As a result, both scaffolds result in a better differentiation ability of hASC compared to 2D situation. For clearer observation, cryosectioning and immunofluorescence staining are used to reassure the differentiation. The 100 μm scaffold shows a significant effect of chondrogenesis differentiation.



Fig. 1. 1 Image of scaffolds. (Start from the left, 50 μm , 100 μm and SEM image of 100 μm y).

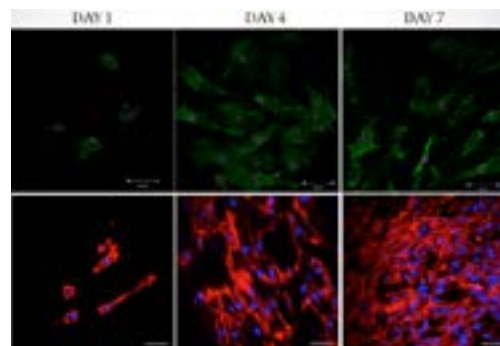


Fig. 2. Cell morphology. (Green indicates F-actin, pink indicates DAPI, upper row is 100 μm scaffolds, bottom row is 50 μm scaffolds)

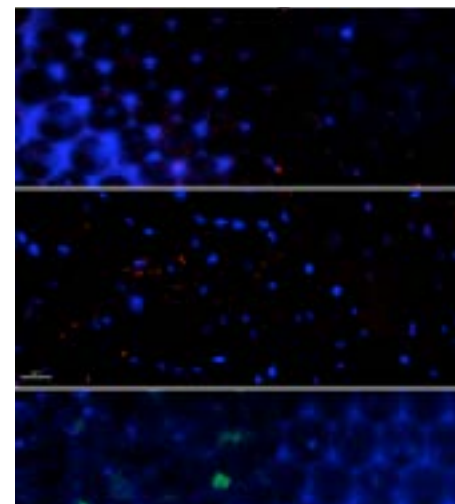


Fig. 3. Cimmunofluorescence staining. (Green indicates SOX9, blue indicates DAPI, red indicates COLII. First and third rows: 14days. Second row: 21days. Left section: 100 μm . Right section: 50 μm)

1.Results

Figure 1 shows the SEM image and optical microscope image of the scaffolds. They are totally uniformed in pore size. Also the sizes are at either 50 or 100 μm , as mentioned.

Figure 2 shows the morphology of cells in scaffolds. From first day to seventh day, there is a clearly stretching of cell. Also, the cell number increases significantly, shows that the scaffold has a great cell proliferation ability.

Figure 3 shows the immunofluorescence staining for SOX9 and COLII. There is a significant better expres-sion of COLII in 100 μm scaffolds, which the red spot (COLII) were more widespreaded among the scaffolds.

2.Discussion

Among the two different pore size discussed, there are several topics to be investigated. First of all, the mor-phology of cells that grows among interconnected pores. With the phalloidin staining, it is cleared that cells stretched and must have live across different bubbles, which can assure that the scaffold is comprised of inter-connected bubbles. Second, in both size scaffolds, cells can be fully stretched only after 4 days of growing. Third, among chondrogenesis, there is clearly a significant better ability for larger pore size scaffolds to express better chondrogenesis by observing both SOX9 and COLII expression. Also, 21 days of chondrogenesis has a better expression compare to 14 days.

3.Conclusion

It is clear that pore size does have a significant effect toward cell behavior. Not so clearly in cell morphology but significant in differentiation. Due to the space needed for cell aggregation during chondrogenesis, it is be-lieved that a proper amount of space improves the ability for cells to differentiate.

Reference:

- [1] Anderson H and A. van den Berg (2004) Microfabrication and Microfluidics for tissue engineering, 4(2):98-103.
- [2] McCoy RJ, Jungreuthmayer C and O'Brian FJ (2012) Biotechnol Bioeng, 109(6):1583-1594.
- [3] Oh, S.H., et al. (2007) Biomaterials, 28(9):1664-1671.
- [4] Dhandayuthapani B (2011) International Journal of Polymer Science, 19.
- [5] Drury JL and Mooney DJ (2003) Biomaterials., 24:4337-51.
- [6] Madl CM, Mehta M, Duda GN, Heilshorn SC, and Mooney DJ (2014) Biomacromolecules., 15:445-55.
- [7] Locke M, Feisst V, and Dunbar PR (2011) Stem Cells., 29:404-11.

Deep brain imaging in Drosophila by 3-photon excitation

RKuo-Jen Hsu^{1,2}, Tianyu Wang³, Chris Xu³, Yen-Yin Lin², Shi-Wei Chu^{1,4} and Ann-Shyn Chiang^{2,5,6,7}

¹*Department of Physics, National Taiwan University, No. 1, Sec. 4, Roosevelt Rd, Taipei 10617, Taiwan*

²*Brain Research Center, National Tsing Hua University, No. 101, Sec. 2, Kuang-Fu Rd, Hsinchu 30013, Taiwan*

³*School of Applied and Engineering Physics, Cornell University, Ithaca, NY 14853, U. S. A.*

⁴*Molecular Imaging Center, National Taiwan University, No. 1, Sec. 4, Roosevelt Rd, Taipei 10617, Taiwan*

⁵*Institute of Biotechnology, National Tsing Hua University, No. 101, Sec. 2, Kuang-Fu Rd, Hsinchu 30013, Taiwan*

⁶*Genomics Research Center, Academia Sinica, No. 128, Sec. 2, Academia Rd, Taipei 11529, Taiwan*

⁷*Kavli Institute for Brain and Mind, University of California, San Diego, La-Jolla, CA 92093-0526, U. S. A.*

Brain study is the most important scientific issue nowadays. However, our understanding toward it is still very limited. Currently, scientists are using model animals such as *C. elegans*, *Drosophila*, zebrafish and mouse to study brain functions. Among them, *Drosophila* is the best choice for the well-established structural map¹. To study brain functions, it is required to imaging every spike from every neuron² even in deep brain. However, two-photon microscope cannot image through the whole *Drosophila* brain in vivo when combined with GCaMP³, the most widely used fluorescent probe nowadays. Therefore, deep brain imaging modalities is highly desired. For example, adaptive optics (AO) can correct wavefront distortion to enhance image contrast at depth⁴. Photo-activatable fluorophores (PAFs) also improves image contrast by switching off out-of-focus fluorescence⁵. High-energy laser increase ballistic photon numbers at depth to improve excitation efficiency⁶. Long wavelength excitation around 1300 and 1700-nm reduces scattering to improve penetration depth⁷ when water absorption is avoided. However, current AO reports always emphasizing improved image contrast but not significantly improved imaging depth. Long converting time is required for PAFs that is not favorable to brain functional study. High-energy laser is harmful to brain due to tissue heating and multiphoton ionization. Comparing the above, long wavelength excitation is the most suitable choice to achieve deep brain imaging in *Drosophila*. Moreover, three-photon excitation offers better excitation localization compare to two-photon excitation, so the out-of-focus fluorescence can be further suppressed⁷. Combined with GFP, the best excitation wavelength should be around 1300-nm⁸. In this report, we are using 1300-nm excitation to image GFP-labeled *Drosophila* brain. As a result, the whole *Drosophila* brain can be imaged with single cell resolution. This imaging modality will be invaluable for brain functional study in the near future.

Reference:

- [1] A. - S. Chiang et al., “Three-dimensional reconstruction of brain-wide wiring networks in *Drosophila* at single-cell resolution” *Curr. Biol.*, vol. 21, p.1-11, (2011).
- [2] A. P. Alivisatos et al., “The brain activity map project and the challenge of functional connectomics” *Neuron*, vol. 74, p.970-974, (2012).
- [3] T. - W. Chen et al., “Ultra-sensitive fluorescent proteins for imaging neuronal activities” *Nature*, vol. 499, p.295-300, (2013).
- [4] K. Wang et al., “Direct wavefront sensing for high-resolution in vivo imaging in scattering tissue” *Nat. Commun.* xeer et al., “Two-photon imaging to a depth of 1000 μm in living brains by use of a Ti: Al₂O₃ regenerative amplifier” *Opt. Lett.*, vol. 28, p.1022-1024, (2003).
- [7] N. G. Horton et al., “In vivo three-photon microscopy of subcortical structures within an intact mouse brain” *Nat. Photon.*, vol. 7, p.205-209, (2013).
- [8] L. - C. Cheng et al., “Measurements of multiphoton action cross sections for multiphoton microscopy” *Biomed. Opt. Express*, vol. 5, p.3427-3433, (2014).

#20

Optical Biopsy of Melasma for Diagnosis Decision Using in Vivo Non-invasive Harmonic Generation Microscopy

Ming-Liang Wei¹, Yu-Hsiang Su², Wei-Hung Weng¹, Yuan-Ta Shih¹, Guan-Liang Lin¹, Yi-Hua Liao³ and Chi-Kuang Sun^{1,2}

¹ Molecular Imaging Center, National Taiwan University, Taipei, Taiwan

² Graduate Institute of Photonics and Optoelectronics, National Taiwan University, Taipei, Taiwan

³ Department of Dermatology, College of Medicine, National Taiwan University and National Taiwan University Hospital, Taipei, Taiwan

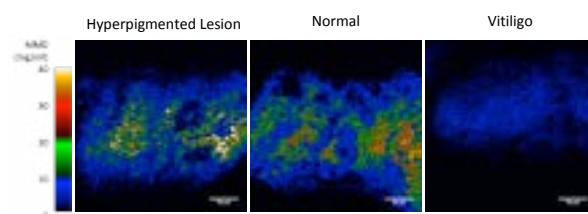
Melasma is a common skin disease on the face of hyperpigmentation disorder of melanin and has been the great concern for mid-aged women for the sake of unsightliness. Melasma is often a therapeutically challenging disease because there is a great variance concerning efficacy of depigmenting treatments from person to person. Since the distribution and quantity of melanin are the main factors of the therapeutic decision and outcome of melasma, dermatologists desire the information of melanin in skin in order to better assess the responses of treatments and to finally eke out their cure.

Harmonic generation microscopy (HGM) is a nonlinear optical microscopy for in vivo label-free optical virtual biopsy of human skin [1, 2]. HGM obtains the desired information from epidermis to dermis for dermatologists, and the enhanced contrast induced by melanin in HGM makes it a valuable technique to realize long-term tracking of melanocytes, melanophages and melanin distributions in living human skin.

In this research, thirty Asian women, between 30 to 65 years old and having symmetrically distributed melasma on the cheeks, were recruited, and we propose a method using HGM to long-term track melanocytes, melanophages and melanin distributions for the therapy of melasma and to help the dermatologists to improve their curing strategy. This work is sponsored by NHRI Taiwan under project of NHRI-EX105-9936EI and MOST of Taiwan under project of MOST 103-2221-E-002-137-MY3.

Reference:

- [1] Chen SY, Chen SU, Wu HY, Lee WJ, Liao YH, and Sun CK., "In vivo virtual biopsy of human skin by using noninvasive higher harmonic generation microscopy," *IEEE Journal of Selected Topics in Quantum Electronics*, 16 (3), pp. 478-492. (2010)
- [2] Tsai MR, Lin CY, Liao YH and Sun CK., "Applying tattoo dye as a third-harmonic generation contrast agent for in vivo optical virtual biopsy of human skin," *J. Biomed. Opt.* 18(2):026012 (2012).



#21

Polyimide/amino-silica mixed matrix membranes for gas separation

Po-Hsiu Cheng^{1,3}, Chien-Chieh Hu¹, Shang-Chih Chou², Chun-Hung Chen², Jia-Shing Yu³, Kueir-Rarn Lee¹ and Juin-Yih Lai¹

¹ Department of Chemical Engineering and R&D Center for Membrane Technology, Chung Yuan Christian University, Chung-Li 32023, Taiwan 200 (R.O.C.)

² Taiwan Textile Research Institute, No.6, Chengtian Rd., Tucheng Dist., New Taipei City 23674, Taiwan (R.O.C.)

³ Department of Chemical Engineering, National Taiwan University, No. 1, Sec. 4, Roosevelt Rd., Taipei 10617, Taiwan (R.O.C.)

In the past decades, mixed matrix membranes were developed to improve gas separation performance of polymeric membranes. High performance mixed matrix membranes for gas separation was investigated in this work. Different amount of amino-silica were added into polyimide to enhance the gas separation performance of MMMs.

CO₂ permeation data and SEM images of the MMMs suggested that the amino-silica and polymer matrix well adhered. SEM-EDX mapping of the MMMs confirmed the good dispersion of the fillers within the polymer matrix. Experimental results showed thermal degradation temperature decreased but glass transition temperature increased with increasing amino-silica loading.

Compared with the traditional silica, the amino-silica could enhance the CO₂ permeability and diffusivity of MMMs due to the facilitated transport of amine groups in amino-silica. For 12wt% amino-silica loading, significantly improved separation results for the CO₂ separation from N₂ was observed, CO₂ permeability increased 141% combined with the gas selectivity remained effectively unchanged versus pure polyimide membrane.

Reference:

- [1] C. Y. Wu, C. C. Hu, L. K. Lin, J. Y. Lai, Y. L. Liu, Liberation of small molecules in polyimide membrane formation: An effect on gas separation properties, *J. Membr. Sci.*, 499 (2016) 20–27.
- [2] B. Zornoza, C. Téllez, J. Coronas, Mixed matrix membranes comprising glassy polymers and dispersed mesoporous silica spheres for gas separation, *J. Membr. Sci.*, 368 (2011) 100–109.
- [3] M. Moaddeb, W. J. Koros, Gas transport properties of thin polymeric membranes in the presence of silicon dioxide particles, *J. Membr. Sci.*, 125 (1997) 143–163.
- [4] T. S. Chung, L. Y. Jiang, Y. Li, S. Kulprathipanja, Mixed matrix membranes (MMM) comprising organic polymers with dispersed inorganic fillers for gas separation, *Prog. Polym. Sci.*, 32 (2007) 483–507.

Cu@polymer Nano-template for the Preparation of Drug Nano-vesicle as a Promising Photodynamic Therapeutic Agent

Po-Ting Wu¹, Chen Lin¹, Yu-Wei Tai¹, Chih-Chia Huang² and Jiashing Yu¹

¹ Department of Chemical Engineering, National Taiwan University, Taipei, Taiwan

² Department of Photonics, National Cheng Kung University, Tainan, Taiwan

Abstract

Copper nanoparticles (CuNPs) are now widely used in many fields, including biomedical aspects. However, CuNPs are not commonly applied as drug carriers due to the high toxicity and accumulation.

In this work, we used poly(styrene-alt-maleic acid)(PSMA) as facile protection agent to synthesize Cu-polymer core-shell nanostructure via one-step hydrothermal reaction, whereas PSMA is a commercially available polymer. To reduce toxicity, we remove the copper core by reacting with HCl to remove the Cu interior and form hollow-shaped PSMA nano-vesicle. Zeta potential measurement was utilized to determine the negatively charged surface structure of PSMA nano-vesicle in the solution (pH=6). Our demonstration showed that the PSMA nano-vesicle could absorb aromatic and positively charged drugs (methylene blue (MB) because of its carboxyl and aromatic functional groups, offering electrostatic and π - π stacking interactions, respectively. The loading efficiency of the MB drug in the PSMA nano-vesicle was estimated to be 15 %. Optical, chemical, and biological stability, and ability to delivery into the cell body the MB-loaded PSMA nano-vesicles will be tested for the treatment of photodynamic therapy.

1. Results

2.1 Characteristics of Cu@polymer NPs

The color of Cu@polymer NPs is dark purple due to the nano size of copper core (Figure 1(a)). To confirm the structure, TEM photo is shown in Figure 1(b). The diameter of NPs is about 80 nm. We can tell that MB is successfully loaded on NPs via the spectra in Figure 1(c). There is a 580 nm peak representing Cu and an obvious peak at 660 nm which is the absorption peak of MB.

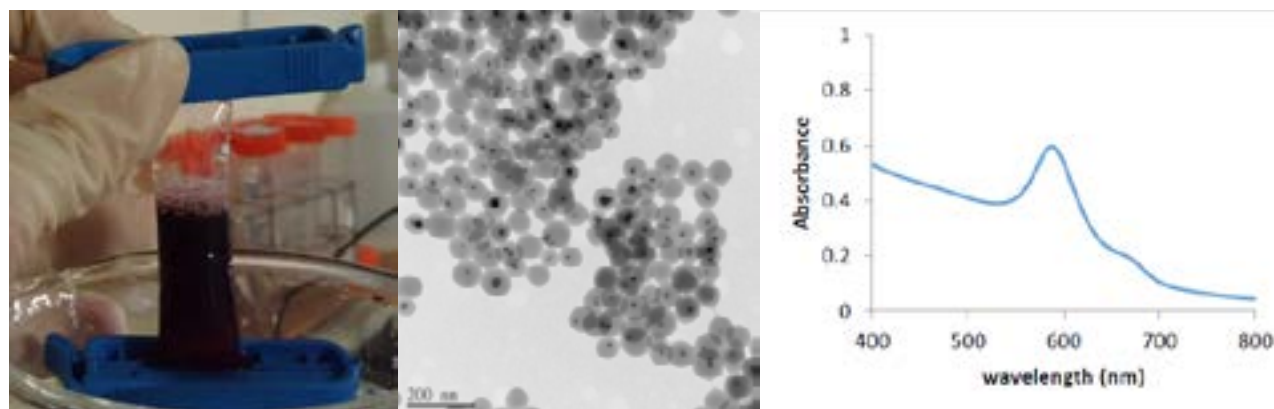


Fig. 1. (a)The photo of Cu@polymer (b)TEM of Cu@polymer (c)Spectra of Cu@polymer 2.2 Characteristics of hollow-shaped PSMA nano-vesicles

When the color become transparently blue which means MB is still loaded on carriers, the nano-vesicles were readily prepared (Figure 2(a)). TEM photo confirms that copper core is removed (Figure 2(b)). Also, the spectra tells that MB is still loaded on nano-vesicles since the 660 nm peak is remained (Figure 2(c)). Zeta potential of nano-vesicles was also analyzed. The average zeta potential is -42 mV, which shows that electrostatic repulsion force between nano-vesicles is enough for well-dispersed in water.

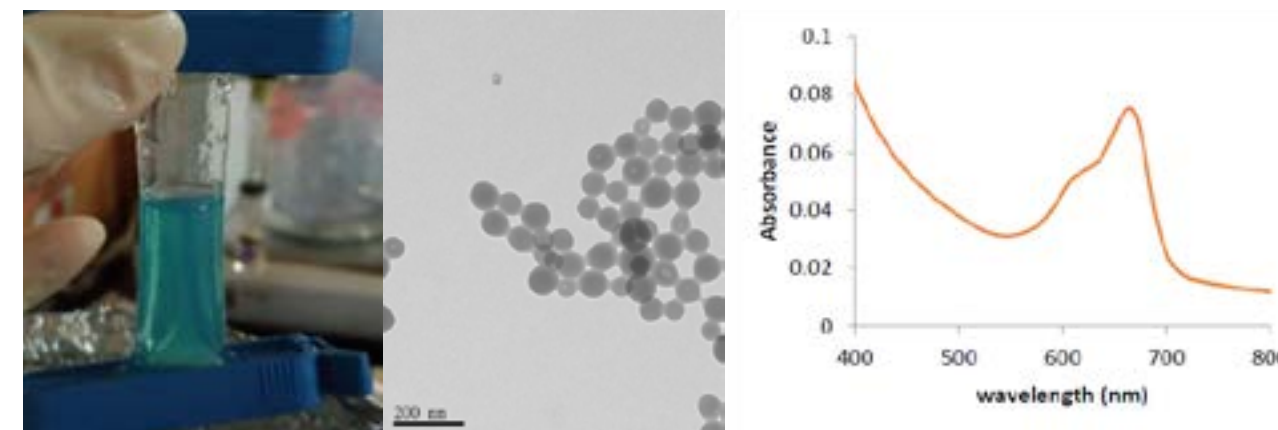


Fig. 2. (a)The photo of nano-vesicle (b)TEM of nano-vesicle (c)Spectra of nano-vesicle

2. Discussion

The robust stability and high biocompatibility of PSMA nanostructure has been proved by other research, and that is what we have to test in further work. Though PSMA nano-vesicles were prepared successfully, there are some problems to be solved. The copper remains in the solution may raise the cytotoxicity. Though there is no obvious aggregation of nano-vesicles in photos, nano-vesicles still link together under TEM. The solving method we are working on is adding surfactant such as sodium dodecyl sulfate and chelating agent such as EDTA, and this is the direction of the research.

Reference:

- [1] Liu, T. M., J. S. Yu, C. A. Chang, A. Chiou, H. K. Chiang, Y. C. Chuang, C. H. Wu, C. H. Hsu, P. A. Chen and C. C. Huang (2014). "One-step shell polymerization of inorganic nanoparticles and their applications in SERS/nonlinear optical imaging, drug delivery, and catalysis." *Scientific Reports* 4: 5593

CREATION OF CELL-DERIVED EXTRACELLULAR MATRIX OF BOTH RANDOM AND ALIGN ECM SCAFFOLD AS A TEMPLATE FOR VASCULAR TISSUE ENGINEERING

Shing Tak Li¹ and Jiashing Yu¹

¹Department of Chemical Engineering, National Taiwan University, Taipei, Taiwan

Abstract

Biomedical researchers found great interest in extracellular matrix (ECM) scaffolds derived from cultured cells for tissue engineering applications. ECM scaffolds can be prepared from autologous cells to generate autologous ECM (aECM) scaffolds. It can avoid the undesired host-responses that may be induced by allogenic or xenogenic materials and circumvents the limited supply of autologous tissues.

In this study, we first fabricate random and align PLGA meshes as a template for cell culturing using PLGA electro-spun fibres. Afterward, Human adipose stem cells (hASCs) were seeded onto the PLGA template with endothelial differentiation induction medium. Cell-ECM-PLGA constructs were formed by the culturing cells in the PLGA mesh for five to six days. Finally, the whole product was decellularized by freeze-thaw cycling and NH₄OH aqueous solution treatment to remove the undesired PLGA template. The ECM left behind will be freeze-dried and sterilized.

Finally, hASCs were seeded onto the ECM scaffold and tested in vivo by using Chick Chorioallantoic Membrane (CAM) assay. The results showed that the ECM scaffold provided wonderful effort in angiogenesis. And the ECM scaffold fabricated in the align PLGA mesh showed a better result compare to the random PLGA meshes.

1. Experimental

PLGA solution in HFP is fed at a rate of 4 mL/h using a syringe pump and subjected to a high voltage (10-22 kV) for electrospinning. The PLGA electrospun fibrous membranes are collected on a dual-drum rotating collector. The collected electrospun fibrous membranes are placed in an oven to remove any residual solvent.

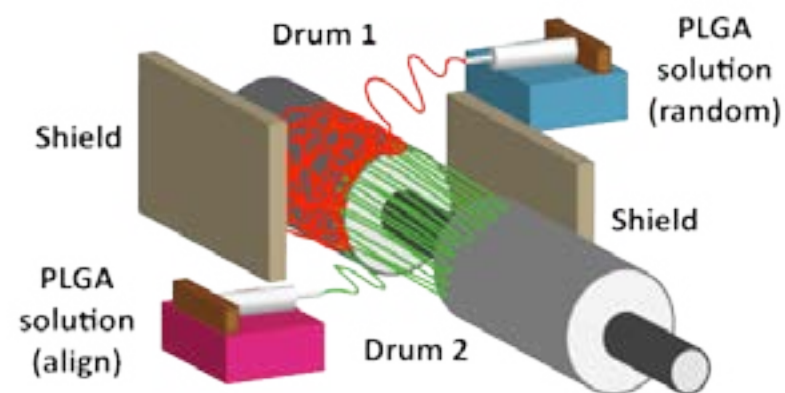


Fig. 1. – Figure 1 showed the methods to fabricate random PLGA meshes and align PLGA meshes by using a rotating drum.

Human adipose stem cell (hASCs) will be seeded to a random and align electrospun PLGA fibrous membrane. After being cultured for a certain period of time, the cell-ECM-PLGA constructs will be decellularized by freeze-thaw cycling in NH₄OH aqueous solution. The constructs will be then immersed sequentially in aqueous solutions of ammonia and trisodium phosphate in order to remove the PLGA template. The ECM scaffolds are obtained after being washed with MilliQ water and freeze-dried.

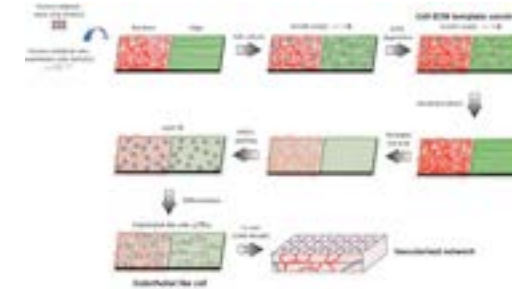


Fig. 2. – Figure 2 showed the protocol to fabricate ECM scaffold by culturing hASC cells.

2. Result

The ECM scaffold showed significant increase of angiogenesis in CAM assay. Comparison between the ECM secreted by the same hASCs and HUVEC cells cultured on the random / align region of the PLGA meshes, hASCs cultured on align region shows higher cell density and more endothelial cell differentiation. As a result, the ECM scaffold fabricated by the align PLGA meshes had a better performance in angiogenesis, in other words, it can play an important role in vascular tissue engineering.

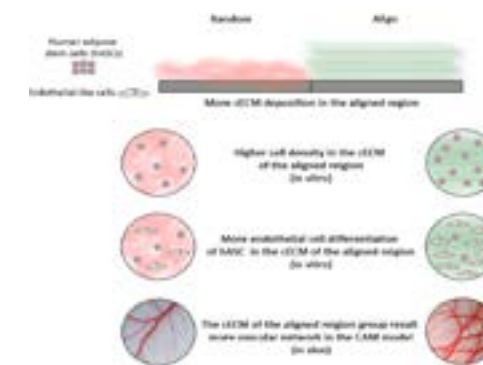


Fig. 5. – Figure 5 showed the comparison of the results between the ECM scaffolds fabricated in random and align PLGA meshes.

Reference:

- [1] Choi JS, Kim BS, Kim JY, Kim JD, Choi YC, Yang HJ, Park K, Lee HY, Cho YW. J Biomed Mater Res A. 2011 Jun 1;97(3):292-9.
- [2] Lu H, Hoshiba T, Kawazoe N, Chen G. Biomaterials. 2011 Apr;32(10):2489-99.
- [3] Jin CZ, Choi BH, Park SR, Min BH. J Biomed Mater Res A. 2010 Mar 15;92(4):1567-77.

Whole brain tract-based automatic analysis of white matter changes in anisometropic amblyopia

Hsien-Te Su¹, Tzu-Hsun Tsai², Yao-Chia Shih³, Yu-Shiang Tseng⁴, Chien-Chung Chen⁴ and Wen-Yih Isaac Tseng¹

¹ Institute of Medical Device and Imaging, National Taiwan University College of Medicine, No.1, Sec. 1, Jen Ai Rd., Taipei, 100, Taiwan

² Department of Ophthalmology, National Taiwan University Hospital, No.1, Changde St., Taipei 10048, Taiwan

³ Institute of Biomedical Engineering, National Taiwan University, No. 1, Sec. 4, Roosevelt Rd., Taipei 10617, Taiwan

⁴ Department of Psychology, National Taiwan University College of Science, No. 1, Sec. 4, Roosevelt Rd., Taipei 10617, Taiwan

1. Purpose

Brain structure deficit has been implicated in the genesis of anisometropic amblyopia. Previous studies have reported multiple functional or structural cortical alterations.¹ Although white matter change has also been studied,² it is still unclear which fasciculus is most affected by amblyopia. In this study, whole brain tract-based analysis was adopted to investigate the microstructural changes of neural tracts in patients with anisometropic amblyopia.

2. Methods: Subjects

11 patients with anisometropic amblyopia (age: 36± 10.4 years, 5 males and 6 females) and 22 age-matched neurotypical controls (age: 37.2± 9.5 years, 12 males and 10 females) were recruited in the study. The amblyopic patients were all anisometropic amblyopia. They completed a series of exams, including visual acuity tests and MRI scans. Imaging: MRI scans were performed on a 3T MRI system (TIM Trio, Siemens, Erlangen) with a 32-channel phased array coil. Diffusion spectrum imaging (DSI) used a twice-refocused balanced echo diffusion echo planar imaging sequence, TR/TE = 9600/130 ms, FOV = 200 x 200 mm², matrix size = 80 x 80, 39 slices, and 2.5 mm in slice thickness. A total of 102 diffusion encoding gradients with the maximum diffusion sensitivity $b_{max} = 4000 \text{ s/mm}^2$ were sampled on the grid points in a half sphere of the 3D q-space with $|q| \leq 3.6$ units. Analysis: Whole brain tract-based automatic analysis (TBAA) was performed to obtain a 2D connectogram for each DSI dataset.³ The connectogram provides generalized fractional anisotropy (GFA) profiles of 74 white matter tract bundles. To obtain a summary of the tract profile data, we averaged the GFA values over each tract to obtain a tract mean and compare the mean GFA values of the 74 white matter tracts between the two groups, two sample T-tests were performed. To correct for multiple comparisons, the Benjamini–Hochberg method for false discovery rate (FDR) control⁴ was used due to the dependency among white matter tracts.⁵ The significance level for the analyses was defined as 0.05.

3. Results

The amblyopic patients showed lower GFA values in several white matter tracts than the normal sighted controls. There was significant difference in ten white matter tracts. The GFA values significantly decreased in bilateral superior longitudinal fasciculi I (SLF I), bilateral corticospinal tracts of hand components (CST of hand), bilateral corticospinal tracts of trunk components (CST of trunk), left corticospinal tracts of toe components (CST of toe), left frontal-striatum of the orbitofrontal cortex (FS of OFC) and bilateral thalamic radiations of the precentral gyrus (TR of precentral gyrus) in patients with anisometropic amblyopia. (Table 1)

4. Discussions

The altered white matter tracts might be related to motor control (bilateral TR of precentral gyrus and corticospinal tracts in several components), visuospatial processing (bilateral SLF I) and integration abilities (left FS of OFC). Consistent with previous studies, Webber et al. proposed that fine motor skills were reduced in children with amblyopia compared with normal sighted subjects.⁶ In another fMRI resting-state study, patients with anisometropic amblyopia show decreased regional homogeneity in orbitofrontal cortex compared to normal control, which may reflect decreased integration abilities in amblyopia.⁷ Adults with a history of unilateral amblyopia show deficits in planning and controlling the grasp and many of deficits in motion.⁸ Consequently, stereoscopic vision is obviously impaired in amblyopia. This may lead to decreased GFA of the SLF I which is crucial for visuospatial processing.⁹

Table 1:

	GFA Value Mean ± SD		P-value
	Controls	Patients	
Left SLF I	0.313 ± 0.011	0.299 ± 0.012	0.000481
Right SLF I	0.332 ± 0.015	0.308 ± 0.016	0.000689
Left CST of hand	0.197 ± 0.008	0.188 ± 0.006	0.001004
Right CST of hand	0.227 ± 0.006	0.220 ± 0.004	0.000151
Left CST of trunk	0.258 ± 0.007	0.249 ± 0.007	0.002322
Right CST of trunk	0.242 ± 0.01	0.232 ± 0.008	0.004056
Left CST of toe	0.253 ± 0.008	0.243 ± 0.01	0.000371
Left FS of OFC	0.264 ± 0.023	0.237 ± 0.025	0.005980
Left TR of precentral gyrus	0.306 ± 0.017	0.288 ± 0.018	0.000672
Right TR of precentral gyrus	0.307 ± 0.018	0.293 ± 0.012	0.000099

References:

- [1] Mendola, J., et al., Human Brain Mapping 2005;25: 222-236.
- [2] Allen B., et al., Vision Research 2015;114: 48-55.
- [3] Chen Y, et al., Human Brain Mapping 2015;36(9): 3441-3458.
- [4] Benjamini, et al., Annals of statistics 2001; 1165-1188.
- [5] Wahl M, et al., NeuroImage 2010;51(2): 531-541.
- [6] Webber A, et al., Investigative Ophthalmology & Visual Science. 2008;49(2): 594.
- [7] Lin X, et al. PLoS ONE 2012;7(8): e43373.
- [8] Giaschi D, et al. Vision Research 2015;114: 122-134.
- [9] Li Q, et al. Neuroscience Letters 2015;597: 7-12.

In Vivo Deep-tissue Super-resolution Imaging of Motor Axon with Two-Photon SAX Microscopy

Tian-You Cheng¹, Cheng-Yung Lin², Ryosuke Oketani³, Szu-Yu Lee⁴, Jia-Hong Lai⁴, Huai-Jen Tsai², Katasumasa Fujita³ and Chi-Kuang Sun^{1,4,5,6}

¹Molecular Imaging Center, National Taiwan University, Taipei, Taiwan

²Institute of Biomedical Science, Mackay Medical College, New Taipei City, Taiwan

³Department of Applied Physics, Osaka University, Osaka, Japan

⁴Graduate Institute of Photonics and Optoelectronics, National Taiwan University, Taipei, Taiwan

⁵Department of Electrical Engineering, National Taiwan University, Taipei, Taiwan

⁶Institute of Physics and Research Center for Applied Sciences, Academia Sinica, Taipei, Taiwan

1. Introduction

Two-photon fluorescence microscopy (TPFM) is widely used to reveal cell structures and molecular distribution in deep tissues. TPFM, relying on the two-photon absorption of fluorophores, is capable of optically selecting an axially isolated plane of tissues [1] and has become a powerful tool for three-dimensional imaging of neurons. The strong interaction between the fluorophore and short-pulse laser beam results in the saturation effect. Under the saturation condition, the fluorescence intensity is not linear proportional to the square of the excitation intensity, so that the point-spread function (PSF) contains even higher order (than the second order) spatial frequency components. Namely, the resolution can be further improved by extracting the higher-order spatial frequency components [2]. In this talk, we present in vivo deep-tissue super-resolution two-photon fluorescence microscopy of neurons based on the fluorescence saturation effect and the extraction of the higher order spatial frequency components. A factor more than 6 improvement in the spatial resolution will be presented for green fluorescent protein (GFP) based super-resolution TPFM.

2. Principle of s-TPFM

The resolution improvement in two-photon saturated-excitation (SAX) microscopy (here we call it s-TPFM) is based on the utilization of the nonlinear fluorescence response, which is induced when the strong interaction between the fluorophore and excitation laser light results in the saturation effect due to the non-zero fluorescence lifetime and limited molecular concentration in the focal volume of the laser light. Therefore, higher order spatial frequencies appear at the center of PSF due to the strong nonlinearity from fluorescence saturation. These higher spatial frequencies represent smaller PSF and could be extracted by demodulating the saturated fluorescence induced by an intensity-modulated laser light [2]. Consequently, extraction of the high spatial frequency components can improve the resolution.

3. Results and conclusions

In this presentation, we will present the first ever in vivo s-TPFM experiments by using green fluorescence protein as our contrast agent. Deep tissue super-resolution imaging will be demonstrated

while the resolution improvement will be discussed. In our experiment, we used the Tg (mnx:gfp) zebrafish line, in which motor axons are labeled by GFP to study the improvement on spatial resolution. As exemplified in Figure 1, in vivo two-photon fluorescence images of zebrafish were obtained by demodulation at the fundamental (Fig. 1(a)) and 3th-harmonic frequencies (Fig. 1(b)) at a penetration depth of 171 μm beneath the zebrafish skin. Fig. 1(c) and Fig. 1(d) indicate intensity profiles extracted from the Fig. 1(a) and Fig. 1(b) at marked lines, respectively. Fig. 1(c) displays the profile of the TPFM intensity featuring a full-width half-maximum (FWHM) of 730 ± 75 nm. This should be contrasted with the profile of Fig. 1(d) displaying a FWHM of 108 ± 13 nm. A 6-7 times resolution improvement can be achieved compared to traditional TPFM. Recently we have shown the neuron imaging inside a mouse whole brain, with a penetration depth ~ 3 mm [3]. Comparing with other super-resolution technique, our demonstrated s-TPFM has the best resolution at the penetration depth deeper than 150 μm [4]. Our study thus show that s-TPFM can be a powerful tool for deep-tissue super-resolution imaging of neuron. This work is sponsored by NTU Molecular Imaging Center and the Ministry of Science and Technology of Taiwan.

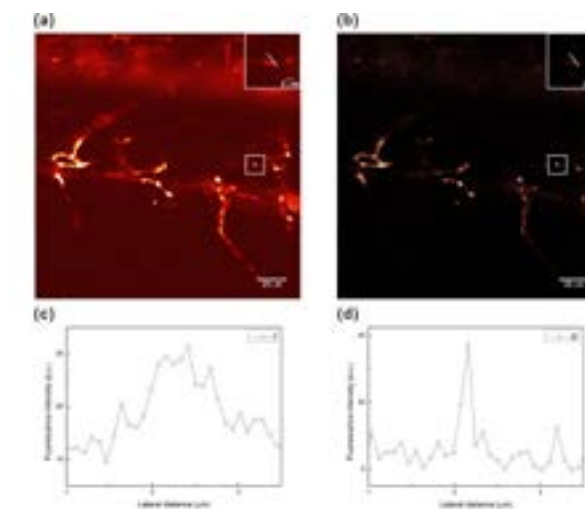


Fig. 1. In vivo (a) TPFM and (b) s-TPFM images of GFP zebrafish motor axon ~ 171 μm below the skin surface. The excitation wavelength was 940 nm. (c), (d) show line profiles of the images as indicated by white line in (a) and (b), respectively. Much improved resolution on the order 150 nm can be achieved for synapse imaging. A 4-5 times resolution improvement can be achieved compared to traditional TPFM. Bars = 20 μm .

Reference:

- [1] W. Kenk, J. H. Strickler, and W. W. Webb, "Two-photon laser scanning fluorescence microscopy," *Science* 248, 73-76 (1990).
- [2] K. Fujita, M. Kobayashi, S. Kawano, M. Yamanaka, and S. Kawata, "High-resolution confocal microscopy by saturated excitation of fluorescence," *Phys. Rev. Lett.*, 99, 228105 (2007).
- [3] T.-Y. Cheng, S.-Y. Lee, R. Oketani, J.-C. Lee, C.-Y. Lin, C.-T. Yen, H.-J. Tsai, K. Fujita, S. Kawata, and C.-K. Sun, "Super-resolution two-photon fluorescence microscopy through fluorescence saturation," *Focus on Microscopy 2016 (FOM2016)*, P2-B/19 (2016).
- [4] S. Berning, K. I. Willig, H. Steffens, P. Dibaj, and S. W. Hell, "Nanoscopy in a Living Mouse Brain," *Science* 335, 551 (2012).

#26

Endoscopy Embedded with Focus Tunable Dielectric Liquid Lens

Wei Min Cheng¹, Chen Yen Lin^{2,3}, Yuan Luo^{3,4}, J. Andrew Yeh¹

¹*Institute of NanoEngineering and MicroSystems, National Tsing Hua University, Hsinchu, 300, Taiwan*

²*Department of Electrical Engineering and Graduate Institute of Photonics and Optoelectronics, National Taiwan University, Taipei 10617, Taiwan*

³*Institute of Medical Device and Imaging, National Taiwan University, Taipei, 10051, Taiwan*

⁴*Molecular Imaging Center, National Taiwan University, Taipei, 10051, Taiwan*

Abstract

Endoscopic systems can provide wide-field image of the target inside a cavity, such as a tumor, during a surgery. Due to limited depth of field and no axial scanning capability, physicians need to move an endoscope back and forth to acquire images at different depths within a target. Instead of changing distance between endoscopic tip and the target, an endoscope using dielectric liquid lens with variable focal length by controlling the input voltage to shift focal plane across the sample. Tunable-focus liquid lens [1] offers short response time by adjusting shape of the liquid inside a miniaturized optical system [2]. The structure of the liquid lens is shown in Fig.1. Multi-plane images of USAF1931 target in Fig.2 at different focal planes are acquired by applying different voltages to the dielectric liquid lens. In our work, the dielectric liquid lens places next to the eye lens of the commercial available endoscope before the CCD camera, and the endoscope system with tunable lens shows images at different depths without sacrificing the resolution. We demonstrate that the liquid lens can be implemented with a commercial endoscope to conduct an axial scanning to extend depth of field without losing resolving power through simulation and experimental measurements.

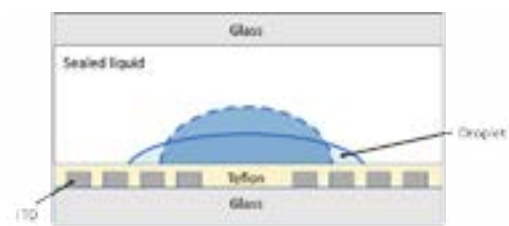


Fig. 1. Schematic side-view of dielectric liquid lens. When the applied voltage into the liquid through the ITO electrode, the dielectric force is produced to form variable droplet.

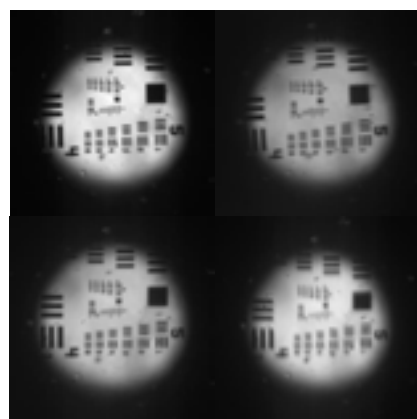


Fig. 2. Using a uniform white light as illumination, images of a USAF target is shown in (a) without liquid lens applied into the endoscope system. (b) Resultant images with liquid lens set into the system as no applied voltage, (c)(d) Resultant images with two different steps applied into the dielectric liquid lens.

Reference:

- [1] Chih-Cheng Cheng, C. Alex Chang, and J. Andrew Yeh, "Variable focus dielectric liquid droplet lens," *Opt. Express* 14, 4101-4106 (2006)
- [2] Kuiper, S. and Hendriks, B. H. W., "Variable-focus liquid lens for miniature cameras," *Applied Physics Letters*, 85, 1128-1130 (2004)

#27

Biomaterial Scaffolds for Neurogenesis

Yen-Yu Chang¹, Ying-Shan Lee², Chen-Hua Wang¹, Jhih-Guang Wu¹, Wei-Fang Su^{1*}, and Tang K. Tang^{2*}, Shyh-Chyang Luo^{1*}

¹*Department of Materials Science and Engineering, National Taiwan University, Taipei 10617, Taiwan*

²*Institute of Biomedical Sciences, Academia Sinica, Taipei 11529, Taiwan.*

Abstract

Brain diseases usually are caused by neuropathy that leads to neuronal cell death or reduction of synapses. Clinical treatment, such as medicine treatment, surgical treatment, or behavior treatment, are widely used, but most of them aren't effective because damaged neurons are unable to regenerate. An insight understanding of brain development will provide us better treatments of brain diseases. Therefore, there is clearly a need for further research on neurogenesis. Many studies have shown that neural stem cells would gradually grow into multiple brain layers during the development. As guidance by radial glia, juvenile neural stem cells would move from ventricular zone to cortical plate and differentiate into various types of neuronal cells, forming different layers of brain ultimately. Here, we aim to produce various types of biocompatible polymeric scaffolds that is biomimic extracellular matrix (ECM). These scaffolds are used to test their abilities to support neural stem cell proliferation and differentiation in vitro. Furthermore, the neural cell differentiation and movement along the fibers to build the various layers of the brain. The ultimate goal is that we can grow a mini brain, guided by fibers to form multiple layers, in an artificial cultured condition. We design and synthesize poly(γ -benzyl-L-glutamate) and poly(γ -benzyl-L-glutamate)-co-poly(glutamic acid) for study because glutamic acid is one of the chemical cues for signal transport between axons and dendrites. The electro-spinning technique is used to fabricate 3D fibrous scaffolds which have high porosity to promote nutrition transport and cell proliferation. The scaffolds are tested to find the viability to guide the growth and differentiation of neural stem cells. Poly(γ -benzyl-L-glutamate) and poly(γ -benzyl-L-glutamate)-co-poly(glutamic acid) scaffolds have successfully been used for differentiation of PC12 cell lines and Retinal ganglion progenitor cells in our lab. Now, we are testing the culture conditions of neural stem cells on these scaffolds. The preliminary results regarding the viability and morphology of neural stem cells on these scaffolds will be presented.

#28

High Spatio-Temporal-Resolution Detection of CF Dynamics from a Single Chloroplast with Confocal Imaging Fluorometer

Yi-Chin Tseng¹ and Shi-Wei, Chu^{1,2}¹ Department of Physics, National Taiwan University, Taipei City, 10617, Taiwan² Molecular Imaging Center, National Taiwan University, Taipei City, 10617, Taiwan

Chlorophyll fluorescence (CF) is known to be a useful indicator to study plant physiology or photosynthesis efficiency since it has been proven to be strongly associated with photosynthesis efficiency. Conventionally, fluorometers provide a convenient approach to characterize CF. In principle, it should be possible to derive photosynthetic efficiency of a plant, a leaf, a cell or even a single chloroplast with given CF yield information. However, current fluorometers are limited to large-area studies since they rely on wide-field imaging modality, and do not provide optical section with high spatio-temporal resolution down to micrometer or millisecond level. In this work, we proposed a novel confocal imaging fluorometer, which not only provides high resolution/contrast images, but also allows high-speed CF measurement within a single chloroplast.

Our results demonstrate that the confocal imaging fluorometer exhibits micrometer spatial resolution, and is able to map CF distribution from a single chloroplast, as shown in Fig. 1. Furthermore, the temporal resolution reaches the order of millisecond, so for the first time, intensity dependent CF transients (i.e., Kautsky effect) are achieved by laser scanning imaging as shown in Fig. 2. The results indicate that confocal imaging fluorometry is a promising novel tool for future CF associated studies especially for photosynthetic performance on the scale of organelle.

1. Keywords

chlorophyll fluorescence; confocal microscopy; Kautsky effect; photosynthesis efficiency

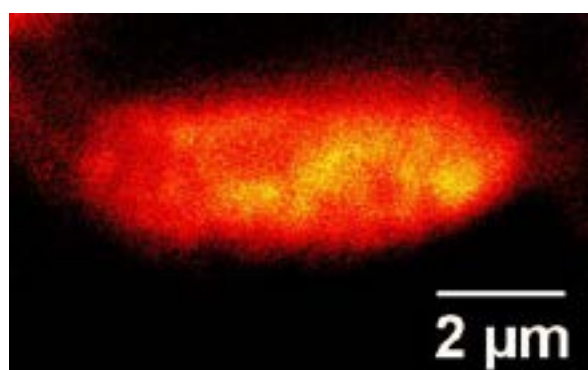


Fig. 1. CF signal from a single chloroplast captured by confocal imaging fluorometer.

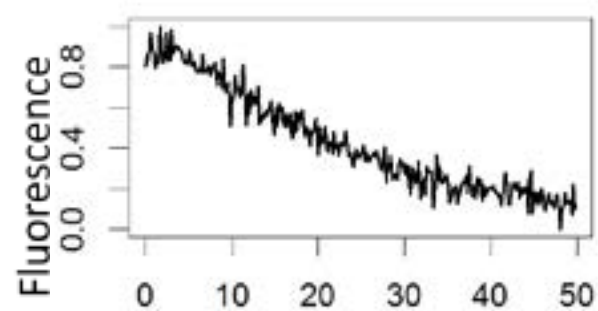


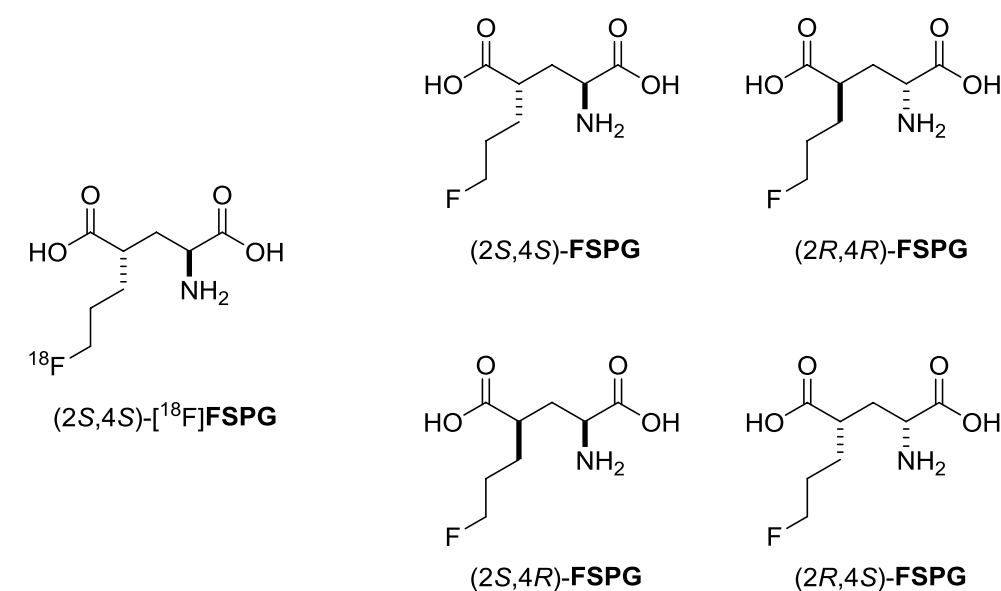
Fig. 2. Normalized CF transients from a single chloroplast.

#29

Synthesis of Four Stereoisomers of 4-(3-Fluoropropyl)-glutamate for Quality control of ¹⁸F-FSPG in Clinical Trials

Yun-Ning Tseng (曾韻寧)¹, Kai-Ting Shih (施凱庭)¹, Ling-Wei Hsin (忻凌偉)^{1,2,3}¹ School of Pharmacy,² Molecular Probes Development Core, Molecular Imaging Center, and³ Center for Innovative Therapeutics Discovery, National Taiwan University, 17, Xuzhou Road, Room 936, Taipei 10055, Taiwan

(4S)-4-(3-[¹⁸F]Fluoropropyl)-L-glutamate (BAY 94-9392, or ¹⁸F-FSPG) is a potential tumor-imaging molecular probe to assess system xc⁻ transporter activity with positron emission tomography (PET). There are four stereoisomers of FSPG, and therefore synthesis and establishment of the analytic methods for these isomers are essential for the quality control of the production of ¹⁸F-FSPG for clinical uses. Direct alkylation of protected L- and D-glutamates yielded the (2S,4S)- and (2R,4R)-FSPG, respectively. Treatment of protected L and D-pyroglutamates with fluoropropyl triflate provided the (2S,4R)- and (2R,4S)-FSPG as the major products, respectively. With these reference standards and analytical methods for the chemical and optical purities, the human clinical trials have been approved by Taiwan Food and Drug Administration (TFDA), and currently are in progress at National Taiwan University Hospital (NTUH).



Faculty Positions Opening

The College of Photonics at the National Chiao Tung University invites applications for tenure-track faculty positions at all levels in Tainan Campus. We are seeking highly qualified candidates committed to a career in teaching and research in the areas of optics and photonic systems, novel laser systems and applications, optical metrology, sensing, imaging, optical information processing, storage, and displays using non-traditional technologies, solar energy systems, green energy technology and systems, optical systems for bio-medical and agriculture, optical designs and system integration.

Applicants are encouraged to apply by December 31, 2016, but applications will be accepted continuously until the positions are filled.

Instructions for Applicants

1. Website: http://www.cop.nctu.edu.tw/menu02_05_ii.html?nid=158

2. Submit the following Documents (e-mail is preferable):

- Filled Application form;
- Curriculum vita; includes research statement, teaching statement, and key publications
- 3 reference letters

3. Submit the following Documents (e-mail is preferable):

Contact person:

Professor Ken Y. Hsu ken@cc.nctu.edu.tw or

Ms. Lingching Chen (陳伶青小姐) lingching@nctu.edu.tw

Faculty Search Committee

College of Photonics

No. 301, Gaofa 3rd Road., Guiren District

Tainan City 71150

Taiwan